Advances in Active Resonator based Planar Microwave Sensors for Material Characterization

By

Mohammad Abdolrazzaghi

A thesis submitted in partial fulfillment of the requirements for the degree of

Master of Science

in

Electromagnetics and Microwave

Department of Electrical and Computer Engineering

University of Alberta

© Mohammad Abdolrazzaghi, 2017

Abstract

Microwave planar resonators have been used for material characterizations for the past two decades. Among the many advantages from planar sensors, some of the main drawbacks are discussed and the relevant methods are provided to tackle them through this thesis. Generally, unique characteristics of microwave sensors such as the ability to perform non-intrusive real-time measurements makes them very appealing for chemical characterization. This becomes more interesting for harsh environment as it has very simple interface. Inherent associated challenges in microwave resonant based sensing are sensitivity and selectivity. Recently, the sensitivity issue has been addressed in our group to eliminate such problem by developing high resolution microwave sensors. In this thesis, we focus on advancing such sensors and further investigating their sensitivity and selectivity related challenges.

To design high resolution sensor a passive microwave resonator is embedded within a regenerative circuit to provide negative resistance and remove the loss of the system. The resultant high-quality factor sensor is able to track highly sensitive measurements such as Nano-particles, e.g. Asphaltene based model-oils. In this study, precipitation and deposition of the Asphaltene at 1.2 GHz is measured and showed that it is concentration-dependent when mixed with a precipitant element, e.g. *n*-Heptane here.

In the second step, two pairs of ultra-wideband high gain slot bow-tie antenna are exploited to accompany the sensor and remove any wired connection with the

measuring device. Single-layered antennas are designed to offer 5dB gain over the bandwidth of 1.35-2 GHz, with whose installation, the quality factor of the sensor becomes Q ≈22000. Common chemicals such as IPA, acetone, ethanol, methanol, and water are analyzed with wireless communication. Salt-water wall with concentration of 0.003125 g/ml – 0.1 g/ml is used as the lossy medium, and the sensor's bare response could also be captured.

In the next step, the unwanted environmental impacts on sensing are considered as erroneous factors needed to be removed for robust measurements. Hence the single active resonator is developed into dual active sensor with enhanced functionality in tracking environmental effects. Dual uncoupled active Split Ring Resonators (SRRs), are enhanced in Q-factor from 51 and 54 up to 150k and 210k at 1.365 GHz and 1.6 GHz, respectively. The effect of humidity in sensing material under test (MUT) is calibrated out and more reliable sensing characteristics can be evaluated regardless of the uncontrollable ambient conditions. Based on the proposed technique, root of mean-square-error of processed results of measuring water in humid air was significantly reduced from 169k down to 27k. Common liquids are detected within moist sand environment successfully and the material impact is completely distinguished from that of the moist sand.

It is also shown that the dual active resonator can be used in unique configuration for other applications, for instance to analyze the dispersion coefficient (k) of Nano-particle suspensions inside solutions. The measured k for Asphaltene in Heptane is consistent with the values reported in the literature.

Dispersion of Asphaltene Nano-Particles in n-Heptane is measured in wide range of 0.000625-0.625 (%wt) Asphaltene : Toluene. Dual active resonator is designed at independent frequencies of 1.03 GHz (f_L) and 1.149 GHz (f_H). With the frequency shifts (Δf_L, Δf_H), average flow rate, and the inner diameter of the tube, the molecular diffusion coefficient, and then the dispersion coefficient can be rapidly derived according to two-window solution of Taylor-Aris dispersion analysis. Samples with higher concentration of Asphaltene are shown to have faster spread and larger dispersion in the flow. Dispersion coefficients of the samples cover the range of $5.2^{-7} \times 10^{-4} mm^2/s$ in great agreement with conventional methods.

In the last impactful attempt to improve the sensitivity of the sensor, mixing behavior of the sensor in its oscillatory mode is exploited, where it's output combined with an additional signal is shown to produce intermodulation products. Intermodulation (IM) of the sensor's two independent sources in this configuration magnifies the variations in the sensing element arbitrarily and commensurately with IM product order. The resulting structure, then provides sensitivity much larger than the primary signal. The improvements are all into effect in the final design of mixer-based sensor where wireless communication is also applied. Common fluids such as Toluene, IPA, Methanol, and Water are tested in fluidic channel and demonstrated that the sensitivity for intermodulation products are significantly increased.

Preface

This thesis presents advances made to high resolution microwave sensors that has been recently developed in Dr. Daneshmand's group. In all the subjects presented in this thesis, Mohammad Abdolrazzaghi is the main student contributor. The work is performed individually or in collaboration which are explained as follows.

In chapter 3, the design and fabrication of the active sensors used for Asphaltene concentration sensing [1] as well as the sensor used for wireless communication [2] are in collaboration and help from Dr. Mohammad H. Zarifi, a postdoctoral fellow in the group. Mohammad Abdolrazzaghi is the main student contributor on this subject. Sample preparation for sample model-oils was a joint practice of the student and Cedric Floquet, employee of Slumburger, Edmonton, Canada. In design and analysis of the active resonator sensor, extensive technical discussions were put forward with Dr. Mohammad H. Zarifi. The results for this chapter are published in ACS Energy and Fuels Journal.

Chapter 4 is the work of the writer to advance single active resonator in to double platform to enable new sets of tests and measurements. The results of this chapter are published in International Microwave Symposium (IMS 2016) conference and IEEE Sensors Journal. The author is the main contribute of the work.

Chapter 5 is presented in International Microwave Symposium (IMS 2017) conference. The author is the main contributor of the work.

Dedication

To my *lovely* **parents**,

without whom,

this amount of hope for the life,

love for the work,

and persistence through the hardships

would never be possible.

Acknowledgements

First of all, I would like to acknowledge Dr. Mojgan Daneshmand, my exceptionally supportive supervisor, and most importantly, my life-long friend, who helped me a lot more than I really deserved during my stay at University of Alberta. She was a great company and had encouraged me in despair and downfalls such that many accomplishments of the thesis will not be achievable without her insightful and on-time support and care. Secondly, I would thank wholeheartedly from Dr. Mohammad H. Zarifi, former Post. Doc. of our group and currently Assistant Professor of University of British Columbia for his relentless care for my progress and development beside technical discussions and training on the lab-equipment. He is truly more that an intimate friend to me and has backed me in many occasions of tumultuous moments of my studies at this university.

My sincere appreciation goes to Prof. Witold Pedrycz for his unstoppable support of the idea I had proposed in the Fuzzy Logic class and helped in cultivating it such that our endeavor resulted in a prestigious and novel paper. I have got learned more than a prof-student relationship from him, as he helped me grow more spiritually in terms of academic conduct and communication to a new level.

Dr. Ashwin K. Iyer, has always been a role model for many engineering students in terms of being committed to ethical issues and also great teaching capabilities. I'm grateful for the chance of working with him on a side project (not included in thesis for brevity) and helped me improve my technical discussions in

research language. He was supportive in harsh periods of the research and charming enough in social behavior.

I would like to, deeply, thank Cedric Floquet, the direct contact of us with the oil/sand company, Slumburger in Edmonton, Canada, who trusted me in taking up the project related to model-oil analysis that resulted in publishing some novel techniques for extracted oil quality monitoring.

I would like to extend my gratitude to my sincerely respectful friend, Dear Elham Baladi, who helped me from the scratch as a great support in technical discussions and also pushed me up to develop in more personal and social aspects, without whose kind attitude it would be a lot more difficult for me to keep up. Never can be ignored, the effective and instructive discussions of my colleagues, my friends, in microwave-to-millimeter (M2M) group, including Thomas Jones, Sameir Deif, and Niloofar Sharifadinzadeh during the past 3 years at the University of Alberta.

I would like to thank my friends, whose insightful discussions with me helped me improve in my knowledge and experience including Prof. Pedram Mousavi, Rezvan Rafiei Alavi, Telnaz Zarifi Dizaji, Ali Kiaee, Pooya Shariati, Waleed El-Halwagy, Hirad Soltani, and Justin Pollack.

Along the continuous effort many colleagues had in my career at the University of Alberta, I am thankful to Natural Sciences and Engineering Research Council of Canada (NSERC), Alberta Innovative and Technology Futures (AITF), Canada Research Chair (CRC), for providing research funding, and Canada Microsystem Center (CMC), for providing lab-equipment. Besides, I'm

appreciative to Rogers company, CoilCraft, American Technical Ceramics (ATC) for their generous free sample offers for, respectively, substrates, inductors, and capacitors to expedite the research.

Support and fast replies of the staff at the Electrical and Computer Engineering Department of University of Alberta, are undeniable part of my accommodation at the department, and also my deep thanks go to my all instructors including Witold Krzymien and Steven Dew for their rich lectures. Also, respectful examiners, Prof. Vien Van, and Prof. Masum Hossain, have graciously accepted our request in a short time, which helped me a lot, are acknowledgeable in both academic record and professional conduct towards my final days of research at U of A. Thank you.

The last but not the least, all of these struggles were doomed to failure without the hearty and inexpressible support and care from thousands of kilometers away, from my family members, especially my lovely Father and Mother, whose day and night wishes were my success, prosperity, and happiness.

Table of Contents

List of Tables

List of Acronyms

IPA	Isopropyl Alcohol
MUT	Material Under Test
IM	Intermodulation
SRR	Split Ring Resonator
RF	Radiofrequency
NRW	Nicholson-Ross-Weir
ANN	Artificial Neural Network
CPW	Co-Planar Waveguide
BE	2-Butoxyethanol
NIR	Near Infrared
UV	Ultraviolet
UV-Vis	Ultraviolet–visible
CMOS	Complementary Metal-Oxide-Semiconductor
HPLC	High-Performance Liquid Chromatography
PTFE	Polytetrafluoroethylene
VNA	Vector Network Analyzer
FEM	Finite Element Method
HFSS	High Frequency Structural Simulator
VSWR	Voltage Standing Wave Ratio

DC	Direct Current
RH	Relative Humidity
TL	Transmission Line
GC	Gain Controller
LF	Low Frequency
HF	High Frequency
MSE	Mean Square Error
PCS	Photon Correlation Spectroscopy
DNA	Deoxyribonucleic Acid
ADS	Advanced Design System
DSRR	Double Split Ring Resonator

List of symbols

Z_0	Characteristic Impedance
d	Sample Thickness
b	Outer cylinder's radius in coaxial cable
ε_r	permittivity
μ_r	permeability
S_{ij}	S-Parameters from port: j to port i
Y_0	Characteristic Admittance
k	Boltzman Constant
T	Room temperature
B	measured bandwidth
R	the resistivity of the device
V_{omax}	maximum amplitude of the resonance profile
η	solvent viscosity
C	*S*olute concentration
k	dispersion coefficient
D	diffusion coefficient
R_h	hydrodynamic radius

t	Time
x	Location
t_0	Resident time
p	polarization per unit volume
ϕ	the volume fraction of solids
K^{∞}	dielectric constant and DC conductivity
C_1	real induced dipole coefficient
C_2	imaginary induced dipole coefficient
x_i	mole fraction of component
P_i	polarization of pure component

Chapter 1

Introduction

1.1 Motivation

Sensing the presence of a substance in an environment, whether the substance or the host medium would be in solid, liquid, or gas phase, is the matter of importance in wide range of applications. For example, the presence and the level of DNA cells in a biological tissue is needed to be known to recognize some diseases. The dose of drugs for healing a patient suffering from heart stroke requires accurate understanding of the combination of its ingredients. In agriculture, modernized machineries require instantaneous information about the soil moist level to inject needed water for optimum and efficient growth of the plants. Another expensive example is about the type and density of the extracted oil down the well, which can be categorized based on the type of Asphaltene and its concentration in different levels of extraction with variant high pressure and temperature. Factories, responsible for their exhaust and global warming would need to pay attention, continuously, to the level of their pollutant emissions. Moreover, the quality of water at the refineries at large scale is under constant monitoring for the existence and the level of harmful suspensions. These, plus many more other examples, are the daily practice of various industries in order to keep their level of production ina

healthy state and control the possible abnormal production conditions with proper knowledge of their process. Highly accurate and reliable sensors are required to be employed in each section to monitor the variations in the material under test (MUT) to ensure the quality of the outcome. Expensively installed sensing devices with labour intensive performance are some of the limiting factors, based on which, the continuous and widespread inspection of the expected products are at risk. Hence, the desire for novel sensors that could be applied in the industrial conditions and still offer the same performance of the prevailing sensors with lower production cost, is required.

Microwave planar sensors, used for material characterization, have attracted the attention of researchers, during the past two decades, because of their low-cost and still highly accurate sensing capabilities. In addition, since the planar sensor is not in direct contact with the MUT, it is called a non-contact-/contactless-/non-invasive-/proximity-/remote-, *etc*. sensor_ terms that can be used interchangeably. Using the contactless feature, one can ensure neither the sensor nor the MUT would be contaminated in a sensing scheme. This combined with the small size of the planar sensors, especially in resonant mode using metamaterial induced elements, promotes them to be the candidate for highly sensitive measurements in harsh environment (high temperature, high pressure), and also on materials with limited accessibility (explosive, corrosive, toxic, etc.). All are a result of the fact that electromagnetic power can interact with the MUT in free space without the need for direct wired-connection. Another suitable condition for the planar sensors to be used is geometrically non-planar surfaces; these sensors can be easily patterned on

flexible substrates and then wrapped around 3-D objects (e.g. cylindrical) to be used in more practical applications, where close monitoring distance enhances the sensitivity. Wearable sensing for human-centric applications and most of industrial applications, especially in oil/sand are the result of their potential to be conformably mapped.

The prevailing sensors are mostly labor-intensive, expensive, time-consuming in preparation, and need maintenance for proper performance over a long time. The planar design of microstrip sensor are proven in comparable performance and is in high-demand during the past decade in material characterization.

1.2 Objective

Despite of many applications and needs to for planar sensors. There several shortcomings that must be addressed. In this thesis, we investigate on microwave sensor resolution, sensitivity and selectivity enhancements.

First of all, the poor resolution of the passive sensor is not enough to resolve the small variations in the readout circuit due to the amplitude noise. The low-to-moderate quality factor of microstrip resonators, e.g. SRR, is the limiting factor in sensitive readouts. Improving the quality factor is an asset for the sensor to go for lower concentration detection in liquid-mixtures and gaseous medium.

Secondly, nowadays all of the electronic apparatuses are connected to each other in a large network to have a universal control over them from single station, a concept, commercially, denoted as Internet of Things (IoT). The passive resonators are of no capability to transmit their data without being combined with

a transmitter as a separate RF circuit that adds to the complexity of the design and is not cost effective. This challenge is noticed carefully and is required to be solved for wireless communication.

Thirdly, environmental effects of temperature and humidity impacts the final readout of the planar sensor since it is open to environment beside the MUT. These extraneous elements should be removed from the sensing data to have reasonable and repeatable report of the MUT analysis. Part of this thesis is devoted to presenting the methods to remove the environmental unwanted effects.

Moreover, although the open side of the planar sensor is in proximity of the MUT and it provides a non-contact sensing scheme, this would reduce the sensitivity of the resonator since MUT is not fully enclosed by the sensor and only part of the MUT is interacted electromagnetically. Hence, a great effort has always been in effect to increase the sensitivity of planar sensor, yet extensive study is required. The main purpose of the thesis is to have an impactful and significant enhancement on sensitivity and selectivity while preserving a high resolution non-contact design as the basic.

1.3 Thesis Outline

The thesis is prepared as follows:

The first chapter is for introduction of the microwave planar resonators and the benefits they have for material characterization, the current challenges and the proposed methods for its improvement.

Second chapter is for an extensive literature review on microwave sensors, with special attention to planar sensors.

Third chapter discusses the advancements on ultra high quality factor resonators and the experiments that is enabled and proposed in this thesis. This section constructs the backbone of the rest of the thesis. Later, this active sensor is incorporated in a unique configuration for wireless communication to be connected to wireless sensor network nodes.

Forth chapter focuses on improving the single active sensor into dual active sensor with main advantages in using one of resonators as the reference and the other as the main sensing resonator. From proper calibration, the extraneous effect of environment is removed from the sensor's readout. Another application of solid suspension's dispersion coefficient in solvent is also studied using the dual active resonator as an application.

Fifth chapter is devoted to the main improvement of the sensitivity in the sensor that utilizes the intermodulation products of a mixer designed combined with sensing element. It is shown that the questionable elements of intermodulation, especially in communication, can be so much beneficial in sensing application, as a mean of magnifier for smaller changes. It is shown with experimental results that the mixer-sensor combination can be used as a sensor with much larger frequency shift compare to its main tone for a given effective permittivity variaion.

The last chapter, sixth, is devoted to conclusion of the thesis that summarizes this thesis achievements and outlines some future study directions .

Chapter 2

Literature Review: Microwave Planar Sensors for Material Characterization

Chemical and Material characterization has gained so many applications and hence significant importance during the past 2 decades. Apparatus and tools are developed to monitor the physical and chemical properties of these materials which resulted in many types of sensors for food quality, water quality, biosensing, chemical sensing, etc. Microwave near-field sensors can be used to evaluate the changes of the MUTs close to them such as soil moisture sensing, and this proximity to the MUT controls its sensitivity.

Sensors in microwave region were developed into various industries including remote sensing [3], medicine[4], and material sensing [5]–[13], studying nanotube structures [14]–[16]. Material characterization methods can fall into many different categories of analyzing the capacitance [17], [18], resistance [19], [20], resonance profile [21], [22], perturbation of cavity [23]–[25], and employing the MUT in reflectometry [26]–[28], cyclic voltammetry (electrochemical method) [29], [30], *etc*. Many of which lack sensitivity, due to single parameter dependency, and low precision, in very complicated and phased dependent methodologies. Moreover, the contact between MUT and the sensor is problematic in corrosion, maintenance,

MUT wastage, contamination of MUT, and the hard access to toxic or explosive MUT. Hence, resonant based sensors that incorporate non contact complex permittivity sensing of the MUT are superior choice.

Planar sensors also offer more advantages compared to the microwave cavities. They are much smaller in size and can be conformal to any surface. The thin substrates of planar sensors enable their application for round cylinders or similar structures such as oil/sand pipeline or human wrist. On the other hand, resonant based structures are suitable for single frequency or discrete multiple frequencies in accuracy compared with most of the broadband methods of wide band spectroscopy. Moreover, the complexities and the challenges in measurement and post processing of broadband techniques such as reflection method of dielectric probe technique or transmission method of coplanar waveguide transmission lines are more than simple resonant based test setup for industrial applications. Due to advantages of planar microwave sensors, this thesis will focus on advancements in this field.

In general, microwave sensors can be categorized into passive and active, resonant and non-resonant, reflection or transmission techniques, and open-ended or closed sensing environment. The following sections review few existing techniques in planar microwave sensors, divided into passive and active sensors with consideration on the type of resonance-based or non-resonance based devices.

2.1 Passive Planar Sensors

2.1.1 Passive Non-Resonant Sensors

Planar transmission lines have been in use for many liquid characterization purposes for a long time [31]–[36]. In this method, a transmission line is being used to analyze the liquid/solid MUT as the substrate or superstrate. External MUT covers the whole transmission line (Fig. 2-1(a-b)) that changes its effective permittivity and the resultant characteristic impedance of the line (Z_0). Then, the measured transmission coefficient and phase variation in reflection/transmission responses is related to the dielectric permittivity and loss factor according to the well-known expressions [31]. It should be noted that this method can be used both for solid and liquid MUTs as of convenience.

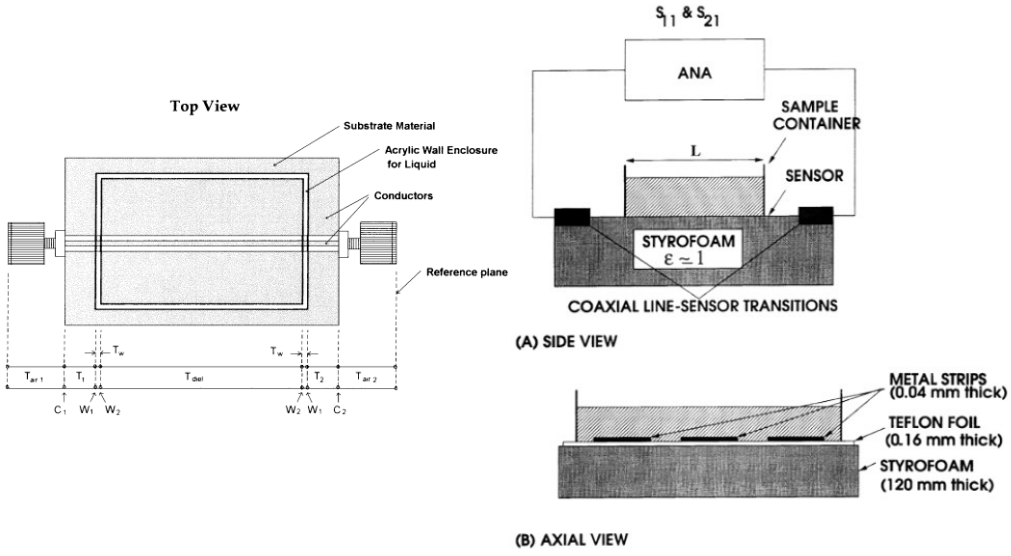

(a) (b)

Fig. 2-1, (a) Schematic of wide bandwidth measurement cell [35], (b) The experimental arrangement in the frequency domain with the automatic network analyzer (ANA) side view and axial view [36]

2.1.2 Passive Resonant Sensors

Resonance based sensors are found more high resolution in their performance compared with wide-band non-resonant structures, even though limited in monitoring discrete finite frequencies. This encourages the researchers to incorporate resonators in sensing behavior, mostly at single frequency, and elicit the characterization of MUT using the behavioral variation of the resonator in various environments. Below is several types of sensors, whose resonance profile is analyzed in sensing.

2.1.2.1 Substrate Integrated Waveguides

Moving to resonant methods that offer more accurate results in single or limited number of discrete frequencies, resonance frequency of the resonators are related to the MUT as a perturbing element and will undergo changes due to the variation in the environment (MUT). In this regard, substrate integrated waveguide cavity resonators are suitable for their higher unloaded quality factor. Solid or liquids can fill the cavities and the resonating waveguide changes its frequency according to permittivity of introduced MUT. The frequency of the resonator is linked inversely to its size, hence higher frequencies are preferred for size convenience. Coaxial cavity resonators are also used for MUT with moderate and high loss content [37]. The complex permittivity measurement is done using the perturbation theory [38], [39].

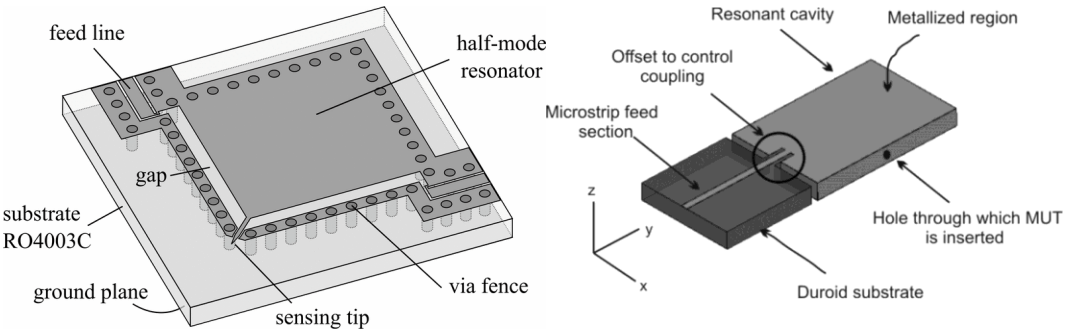

(a) (b)

Fig. 2-2, (a) "Geometry of the substrate-integrated half-mode near-field sensor" taken from [40], (b) Layout of substrate integrated waveguide cavity resonator with microstrip feed section and hole within the cavity through which the MUT is inserted" taken from [41]

Ref.[40] introduced a very sensitive half-mode substrate integrated waveguide near field sensor at 5 GHz with bare sensor's quality factor of around 100, could distinguish the concentrations less than 1% of liquid mixtures such as saline, ethanol, salt, sugar and water solutions. Measurement criteria was based on the quality factor shift, where in presence of aqueous environment would drop to about 16 (Fig. 2-2(a)).

Integration of waveguide cavity resonator with planar feed line using microstrip transmission lines are presented in Ref. [41] (Fig. 2-2(b)). Resonant cavities at 8 GHz are injected with capillaries carrying MUT so that the variations in the content of MUT are reflected in effective dielectric property of cavity and hence the resonant frequency.

2.1.2.2 Free-Space Method of Sensing

Another type of sensors are free-space based methods that are useful for high frequencies (above 10 GHz) [42] with no preparation time, and can be used for high temperature-based measurements. These can fall into two main category of non-

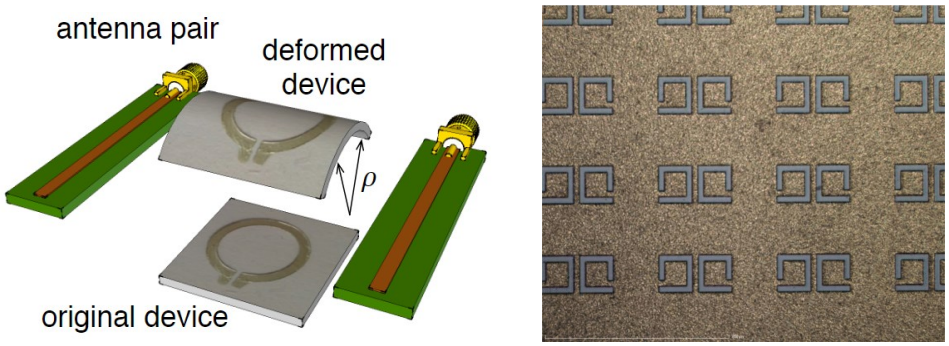

(a) (b)

Fig. 2-3, free-space resonant-bases methods for sensing (a) using a pair of monopole, and (b) at terahertz frequencies.

resonant and resonant based sensors. In the former type, a set of antennas are used as a transceiver and receiver such that the MUT would be between the two antennas and based on the magnitude and phase variation in the transmitted signal at special frequency/frequency band one can determine the electrical characteristics of the MUT. The accuracy of this method depends on several parameters as the incident wave on MUT is assumed to be plane wave, and the MUT is homogeneous in texture and extends to infinity laterally to avoid diffraction effects on the edges.

The resonant based sensor in free space are those resonating elements, such as SRRS, excited with the incoming plane waves from external pair of antennas. It has been shown that such methods are sensitive enough to help diagnose glaucoma with printed SRRs on flexible substrates excited by a pair of monopole antennas [43] and also MUT characterization at terahertz frequencies [44] (see Fig. 2-3).

2.1.2.3 Microstrip Resonators: $\frac{\lambda}{2}$, Split Ring Resonator, etc.

Planar microwave sensors are privileged of small size, ease of fabrication, low-cost, and lightweight properties compared to different microwave cavity resonators

and micro-cantilever-based sensors [8]–[10]. Open ended half-wavelength resonators are modified as SRR and widely used as sensing elements due to their high quality factor and small size [45]–[47]. Planar sensors were used in microfluidic devices for the label-free biomolecule and concentration detection [48]–[53]. In order to increase the accuracy and minimum detectable-limit in liquid medium, complimentary structures of SRRs were exploited [54]–[56].

A few examples of the complex permittivity (dielectric constant and the loss factor) measurement using resonant based sensors are for substrate permittivity extraction, since it plays a detrimental role in the design of RF and microwave circuits, especially at high frequencies [57]–[60]. Ref. [57] has designed a cross-shaped microstrip ring at 880 MHz for substrate sensing of Teflon, R4003, FR4, RF35 and glass. A post-processing step is used for inversion of the measured data to the actual values using Artificial Neural Network (ANN). The compact design brings about less expensive cost for the mass-production. Ref. [59] introduces a quarter-wavelength resonator on planar substrate coupled to input/output of a 2-port network working at 656.6 MHz. This method is applicable to powder moisture content detection with a low cost planar design. In Ref.[60], a ring resonator at 2.4 GHz is used to sense the moisture content of concrete or sand grains. Compact size and high accuracy of the sensor are some of features of this highly sensitive sensor.

Numerous applications of sensor are reported in literature that are able to efficiently combine with liquids and flowing media using micro-channels or larger tubes. The only interfacial material between the MUT and the sensor is the wall of

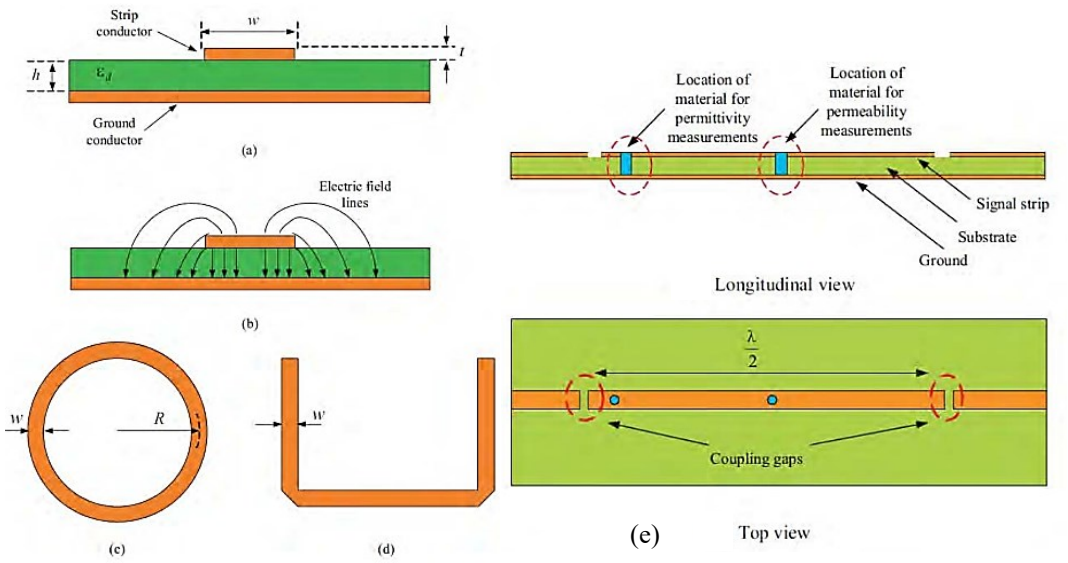

Fig. 2-4, (a) cross section of the microstrip design, (b) fringing E-field distribution in microstrip, (c) Ring and (d) Split ring structures as microstrip resonators, taken from [61], (e) Microstrip straight SRR as sensor for resonant perturbation measurements on liquid samples, taken from [62]

tube. Several typical examples are given below with introductory information about their design and advantages.

These resonators are among integral part of many microwave circuits such as filters or oscillators. The resonant microstrip section of these sensors are open-/short-ended quarter-/half-/full-wavelength in size (Fig. 2-4(a-d)). Multiple harmonics of the fundamental frequency of resonance can also be found in transmission response of the sensors due to their accommodation in the same ring/split-ring. The half wavelength sized sensors are governed by the following expression for their resonance frequency [61]:

$$l = \frac{nc}{2f\sqrt{\varepsilon_{eff}}} \tag{1}$$

where c is the speed of light, f is the frequency and ε_{eff} is the effective permittivity of the substrate and the surrounding medium.

The end tips of the resonator are highly concentrated in E-field and hence sensitive to capacitive variations. Fig. 2-4(e) shows a planar straight ribbon of microstrip that is used for dielectric material sensing [37], [62].

Since the MUT requires full contact with the sensor and its corrosive/contaminating effects are not desirable for repetitive and long terms measurements. In an attempt to avoid direct contact of sensor and the MUT, planar sensors are found helpful since they are open from a side that allows them to be in proximity of the MUT. Using planar microstrip design, one can perform the measurements in non-invasive manner using the propagation of the electromagnetic waves into free space and its interaction with the MUT around it. With proper control and manipulation of the electric fields, one can reach the desired sensitivity, the more localized E-fields around the MUT, the more variations observed at the output. This method can be used for both solids and liquids. As the sample for test is not required to be large in volume and only is needed to cover the sensitive part, this method is used for very small amount of sample, especially in pharmaceutical and biomedical applications, where accurate characterization of analytes for minute sample sizes (less than few microliters) are vital.

Dielectric resonator based split ring resonator (SRRs) have shown much better quality factors in microwave regime that brings about better resolution in the readout circuit and increasing detection limit [63] (Fig. 2-5(a)). The quality factor of about 10 at resonance frequency of 8.25 GHz was enhanced up to 300 at 11.3 GHz. In another work of [64] (Fig. 2-5(b)) a simple split ring resonator at 2 GHz is

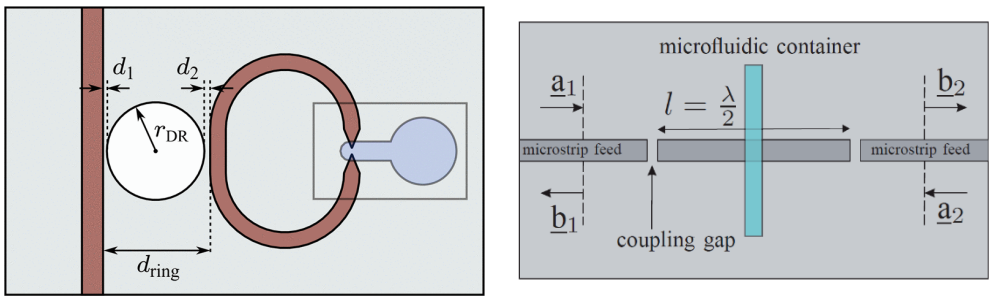

(a) (b)

Fig. 2-5, (a) "Geometry of liquid sensor with an SRR coupled to a DR" taken from [63], (b) "Schematic view of the λ/2 microstrip resonator and microfluidic container" taken from [64]

shown to provide highly sensitive region that is exploited in detecting small concentrations of glucose (as of 0.01 %) in water.

A type of ring resonators that are perturbed with the existence of the external material is presented in [65] (Fig. 2-6(a)). The resonator, operating at 3 GHz, is tested using common liquids of hexane, chloroform, ethanol, methanol and water. The compact sensor is suitable for on-chip applications. Another planar microfluidic sensor based on quarter wavelength resonator in a co-planar

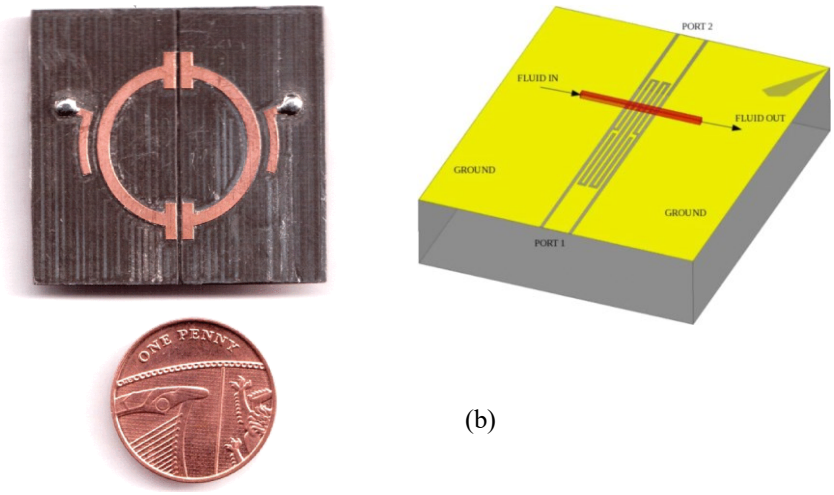

(a) (b)

Fig. 2-6, (a) "Photograph of the DSSR sensor, realized using a microstrip structure." taken from [65], "Schematic view of the RF coplanar resonator with a microfluidic channel on top" taken from [66]

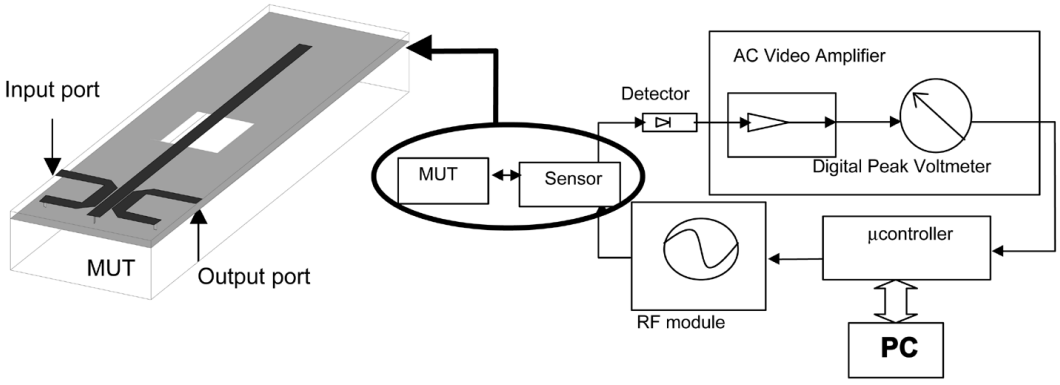

Fig. 2-7, "Block diagram of the measurement system and detail of the geometry of the planar sensing head" taken from [58]

waveguide (CPW) structure is shown in Ref. [66] (Fig. 2-6(b)) working at 20 GHz. It is used for detecting the concentration of ethanol/de-ionized water mixture (0-20 %) and accurate complex permittivity measurement is achieved.

In low-cost and easy-to-fabricate designs, planar microstrip rings/split-rings are among favorable resonators [58], [62], [67], [68]. In Ref.[58], a square-wave modulated RF signal is fed into the resonator, and the transmitted signal is demodulated. The detected voltage is proportional to $|S_{21}|^2$ (see Fig. 2-7).

2.2 Active Planar Sensors

In this section, a literature review of active sensors will be presented. Initially, active resonators are explained and then active sensors based on these structures are reviewed.

2.2.1 Active Resonators

An important indicator of the performance of a resonator is the quality factor (Q-factor). The Q-factor is defined as the ratio of the resonant frequency to the bandwidth of the resonator. It can also be expressed in terms of the ratio of energy

stored over the power loss of the system. The Q-factor plays a critical role in the resolution of the sensor and in the electric field concentration in the sensing medium.[1], [2], [12], [69]–[71]. It has been shown that by adding parallel positive feedback, the resonator's quality factor can be enhanced (see Fig. 2-8 (a)) In such configuration, it can be used as the receiver front-end with a sharp filter to help selectivity in receiving section (see Fig. 2-8 (b)). This characteristic was in favor of first types of regenerative receivers, developed and invented by Edwin Armstrong in the late 1920s [72]. Regenerative amplifiers have been previously

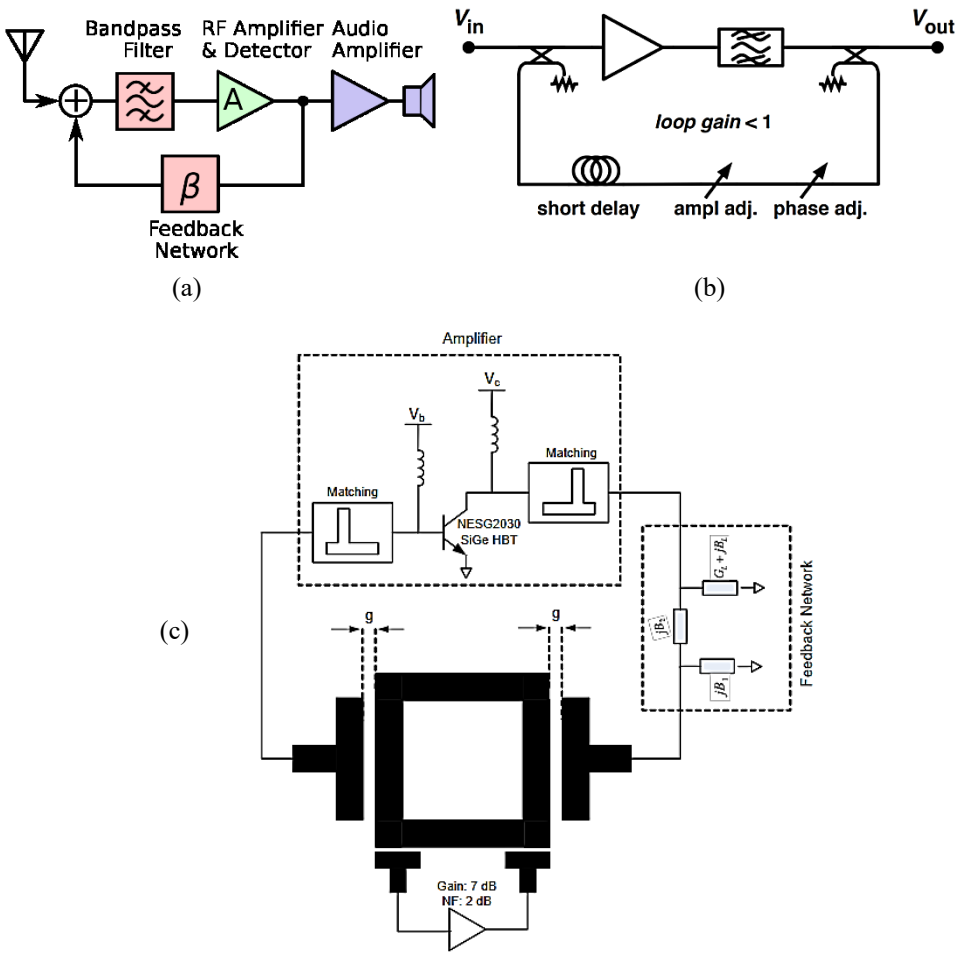

Fig. 2-8, Regenerative (a) receiver [157] and (b) amplifier's [73] general schematic, (c) The regenerative amplifier in oscillator design (taken from [158])

studied for communication transceiver applications; structures that consist of passive microwave resonators combined with active circuitry to enhance their performance. The key factor in their design is to keep the loop gain less than 1 to suppress any unwanted oscillations. In a complementary design of oscillators, the passive tanks have also been armed with positive feedback to compensate their loss and hence increase the Q-factor of the oscillator tank, consequently, lower the phase noise (see Fig. 2-8(c)).

2.2.2 Basics of Active Sensors

Our group has shown pioneering work in implementing such resonators as sensors and proving its enabling application as microwave sensors. High quality factors, a translation of low electromagnetic losses, can increase the resolution of the microstrip resonator sensor and relax the requirement for close physical distance of the medium and the sensor, therefore, enabling contactless measurements. This becomes more important noting that in chemical sensing era, MUT generates considerable amount of loss that should be compensated in the sensor.

Such improvements in the system were from the fact that a positive feedback loop [73] as shown in Fig. 2-9(a) is added to the system and regenerates the lost signal. The equivalent electrical model of the active sensor is demonstrated in Fig. 2-9(b), where a negative conductance ($G_{NR} < 0$) acts as the positive feedback. The Q-factor of this system can be derived as follows:

$$Q = \frac{\omega C}{G_i + G_{MUT} + G_e - G_{NR}} \tag{2}$$

(a)

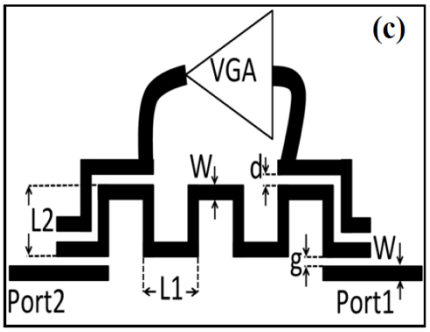

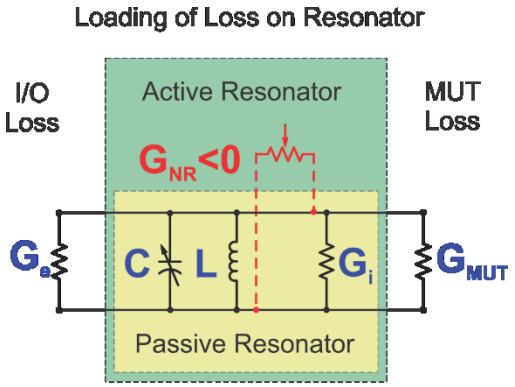

(b)

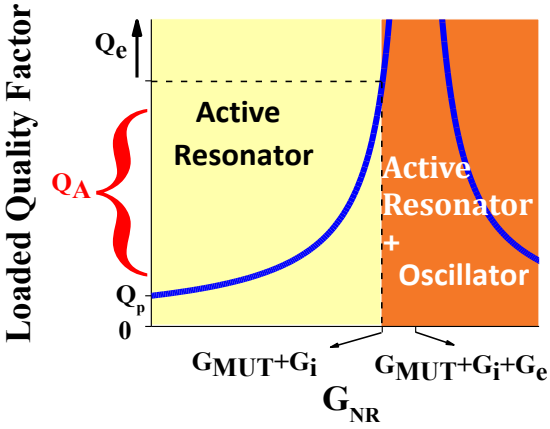

(c)

Fig. 2-9, (a) Schematic of the active sensor, taken from [80], (b) Negative Resistance equivalence of feedback loop in regenerative amplifiers, (c) Active resonator and oscillation regions of the sensor

where G is used to represent the conductance and easier calculations. The denumerator is under influence of the feedback network and its smaller value, due to compensation of the losses with positive feedback, would result in higher quality factors, up to a region where the internal losses are fully compensated ($G_{NR} = G_{MUT} + G_i$). After this point, the oscillations happening inside the resonator can (not necessarily) be captured at the output based on the level of loaded conductance from the input/output transmission lines. Full description of this phenomenon lies in digging into Eq (2).

The gain compensation is considered to be in line with phase compensation of the passive filter to optimally improve the frequency performance. When the loop gain is less than one, quality factor is enhanced by amplifying the input signal and compensating the generated loss of the resonator. As the gain is increased, an oscillating tone is added and the sensor will generate a signal tone at the resonant frequency of the tank.

It has been shown that the resonance (Gaussian) profile of SRRs as a permittivity sensor is amplified and the resultant resonator is called active resonator or regenerative amplifier with positive feedback [1], [2], [12], [13], [70], [74], [75]. Hence the resolution of the output is enhanced strongly to help resolving the peak of the sensor easily and the additive amplitude noise would be less. Therefore, the resonance frequency detection would be much easier and smaller shifts of the sensor can also be readily interpreted, which can be transferred as "enhanced readout resolution".

It has been shown that the active compensation resulted in Q-factors improving from 200 to over 10k typically [1], [2], [12], [70], [71]. The method can potentially compensate the environmental losses and enable high performance sensing in lossy mediums such as liquid. [2], [12], [76], [77]. Many applications are enabled due to the high resolution sensing that brings about lower concentrations in mixtures, smaller changes in gaseous mixture concentrations, and the minute environmental variations can be easily tracked.

"Enhancing the Q-factor lowers the minimum detectable changes in effective permittivity as suggested in [78], [79] as follows:

$$|\Delta\varepsilon_r| \propto \frac{\varepsilon_r}{V_{0max}Q}\sqrt{4KTBR} \quad (3)$$

where $\Delta\varepsilon_r$ is the minimum detectable permittivity change, k is equal to 1.38×10^{-23} J/K, T is the room temperature in Kelvin, B is the measured bandwidth, R is the resistivity of the resonator, α is a compensation constant which relates to the size and the volume of a test material detected by the sensor, and V_{omax} is the maximum amplitude of the resonance profile. It is evident from the equation that by increasing Q, the minimum detectable permittivity is expected to decrease, which leads to enhanced resolution in permittivity sensing. Additionally, increasing the quality factor of a planar resonator strengthens the electric field around the sensor, which consequently increases the field of view for the sensor and enables the non-contact high resolution permittivity sensing. As it can be seen from Fig. 2-9(a), the meandered type microstrip resonator is embedded in a regenerative feedback network such that proper gain is provided by the transistor (Cell: NE68033) at frequency of about 1.4 GHz and the resolution in transmission response of the active sensor is enhanced dramatically (Fig. 2-10 (b))" [80]. The gain of the amplifier is controlled with the bias voltage of the transistor and can be as low as the off-stage of the transistor which would show no improvement over the passive

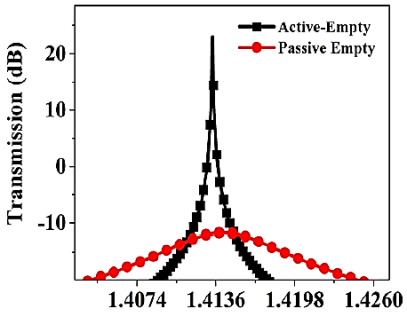

Fig. 2-10, improvement in quality factor in active sensor compared with its passive counterpart circuit.

2.2.3 Active Sensor Applications

Highly sensitive measurements are now plausible using the abovementioned method with ultra-high resolution sensor, when the concentrations in liquid mixtures are minute and even extremely tiny ppm-levels of gases can be captured in an environment. In this section two main applications of high-resolution material characterization is discussed in liquid and gas phases.

2.2.3.1 Liquid Sensing

Lossy medium including the liquids absorb the electromagnetic signals as they pass through. In that, the transmission and reflection coefficients would be noisy and not distinct enough to gain information about MUT. Hence, the characterization will be deteriorated for sensitive measurements, such as concentrations of a MUT inside a lossy medium. Active sensors help overcome the loss of the propagation in the system and the signatures of the medium are retrieved with no attenuation. The

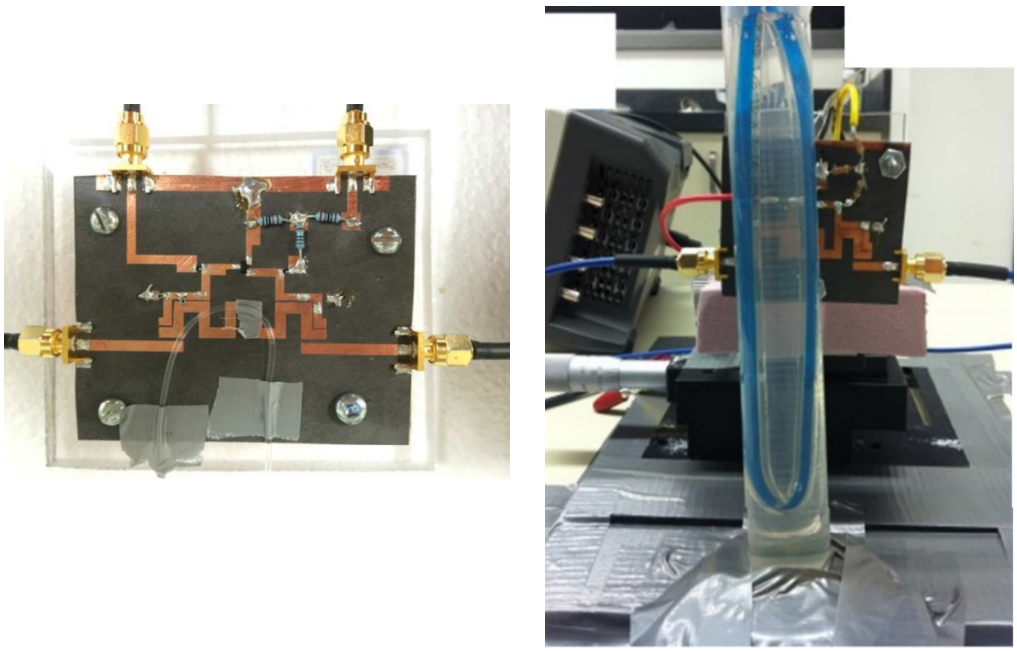

(a) (b)

Fig. 2-11, (a) Lossy liquid sensing, (taken from [129])(b) Lossy liquid inside lossy medium sensing using active resonator (taken from [76])

following examples are to illustrate only some of the applications in aqueous solutions.

Simplest form of the characterization is shown to be with the configuration of Fig. 2-11 (a), where the tube is located in the hot-spot of the resonator at 1.4 GHz. Common liquids of IPA, ethanol, methanol, and water are tested to verify the performance and distinct responses are obtained for each material. Moreover, dilutions of KOH within the range of 0.1-100 mM in water are tested and the frequency variations as well as Q-factor changes are used to detect the concentrations of the mixtures.

In another more complex form of experiment, the medium inside which the material should be characterized is set to be also lossy liquid, as water as shown in Fig. 2-11(b). An active sensor, in this case resonating at 1.52 GHz, is located 12 cm

away from the outer container of the samples and penetrates deeply inside the medium in free space. Interestingly, still correct assigning of the output of the sensor to distinct materials of the same common liquids, as the previous experiment, was achieved with proper loss compensation from the active sensor.

2.2.3.2 Gas Sensing

In a highly sensitive measurement of gas detection, the concentration are so small that the regular planar sensor can not observe any change due to exposure to gas. Instead, beads, as the porous spheres are developed to capture the gas inside their holes and the dimeter of the hole depends on the type of bead. The sensor, working at 1.42 GHz, can resolve particle size range of 40-400 μm within 3 MHz when these petroleum coke beads are suspended in air. The adjustably of the gain allows to compensate for the excessive loss from the external MUT on the sensor's system as well and this empowers the sensor in many fields that require dealing with highly lossy medium such as water. Adjusting the quality factor when confronted with water, as the host medium, the range of frequency shifts for beads immersed in water (ε_r'=78 and $tan\delta$=0.15) are within 500 kHz using beads as a test material.

It is already been shown in highly sensitive measurements that deals with the concentration of gaseous exhausts in the air, which for sure is not in the capability of passive sensor to follow. In Ref. [75] a micro-bead assisted sensor is used for organic vapor sensing of 2-Butoxyethanol (BE). Two types of beads are used for capturing the gas and magnify the resultant variation in effective permittivity of the environment using their continuous collection in the holes of the spherical porous

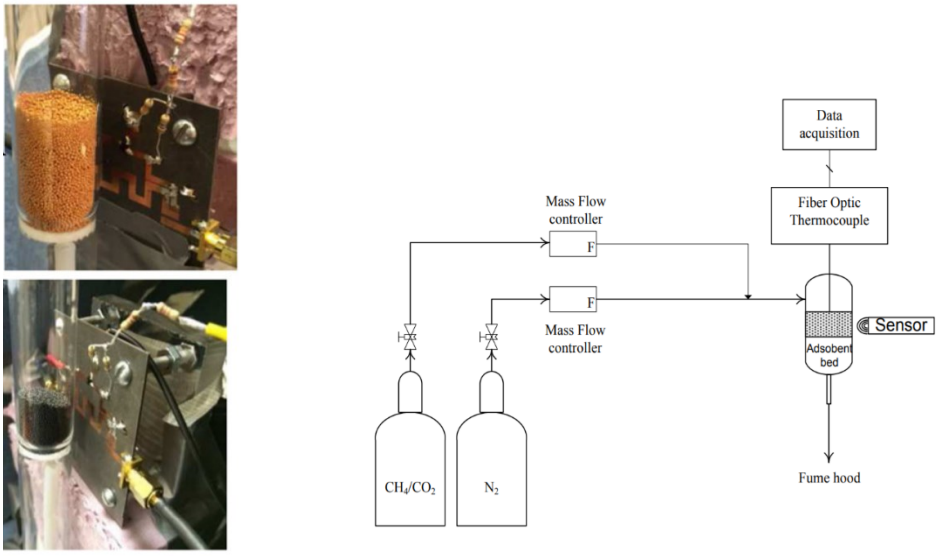

(a) (b)

Fig. 2-12, (a) Gas sensing using BE and polymer beads, (b) comparison of the Zeolite 13X selectivity towards CO_2 compared with CH_4. (taken from [81])

media. Carbon beads could demonstrate frequency shift of 10 kHz for exposure to a 35 ppm concentration of BE and polymer based adsorbents show 160 kHz for the same concentration (see Fig. 2-12(a)).

In another example [81], the interaction of Zeolite 13X with CO_2 and CH_4 in gaseous streams are discussed as shown in Fig. 2-12(b). The mixture of the CH_4/CO_2 with N_2 as the balance gas, was pumped into the container full of porous beads, which is in front of the sensing region of the active sensor, resonating at 1.55 GHz. Concentrations of 1-50 % of CO_2 and CH_4 are examined and comparing the frequency shifts of the two materials, show larger tendency of the Zeolite 13X beads to absorb CO_2 compared to CH_4, which is an indicator of an enhanced selectivity of the sensor with respect to CO_2.

Chapter 3

Nano-Particle Sensing and Wireless Communication Using Active Resonator

In the first part of the following chapter, development of passive core resonator into active resonator is shown to deliver much higher quality factor in the transmission response, a feature suitable for extremely small Nano-Particles in a solvent liquid, and is explained thoroughly in a paper entitled "**Contactless Asphaltene Detection Using an Active Planar Microwave Resonator Sensor**" [1]. Two main methods are discussed regarding the Asphaltene concentration, one is for individual injections of the samples and the other is to use another reference element, e.g. n-heptane here, for its more accurate practical measurement.

Then, the microwave active sensor is enhanced in its communication with the measuring device using two pairs of ultra-wideband high-gain antennas, excerpted from a paper entitled "**Wireless communication in feedback-assisted active sensors**" [2]. It is shown that transmitted data through loss-less and also lossy medium can be processed, where stable and precise measurements can be performed.

3.1 Nano-Particle Detection Using Microwave Planar Sensor [1]

Asphaltene precipitation and deposition during production, or transportation of crude oil is a critical issue for the oil and gas industry.[82], [83] This type of organic scaling can cause plugging of wells or flow lines, reservoir impairment, and more generally, fouling issues necessitating costly remedial maintenance.

The Asphaltene fraction is the most polar fraction of crude oil and is defined as a solubility class.[84] Asphaltenes is soluble in aromatic hydrocarbons, yet, insoluble in alkanes such as heptane or pentane. Pressure, temperature, or chemical composition change in the environment can initiate precipitation. Successful prevention of scaling issues requires the analysis of the Asphaltene fraction of a crude oil, as well as a theoretical and practical understanding of the environmental parameters affecting the Asphaltene stability. In particular, knowledge of the Asphaltene content of the crude oil and pressure onset precipitation can be crucial [82].

Traditionally, Asphaltene content is determined with a wet chemistry method [84]. Onset (precipitation) determination can be performed using a wide range of techniques: gravimetric, acoustic resonance, or near infrared (NIR) scattering [85]. These methods are resource intensive, and operator dependent. VIS-NIR spectrum based techniques study the optical absorption spectrum of the materials and are based on correlations between the sample coloration and the Asphaltene concentration in Asphaltene/toluene solutions [86], [87]. Samples ranging between

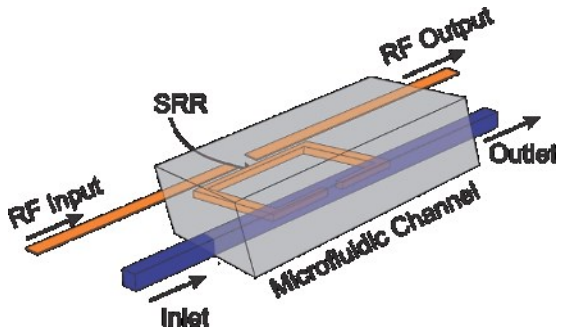

Fig. 3-1. Schematic of microfluidic sensing paradigm

0.5-15 g/L have been tested with optical spectroscopy techniques [88]. While new UV-Vis spectroscopic techniques address some of these issues [89], the nature of the measurement still requires optical access to the sample: optical windows can be prone to fouling and may require tailored engineering solutions and materials to survive exposure to oilfield fluids. A robust and contactless technique, where the optical transparency of the test vessel is not necessary, is sought after.

Sensing using microwave resonators is a promising approach to address these challenges (Fig. 3-1). Such sensors rely on measuring changes in their resonant frequency when the environmental dielectric properties vary. Different resonant cavity designs exist with planar systems offering a small size, embedded solution. Planar microwave resonator sensors demonstrated reliable performance in industrial, biomedical and environmental applications [13], [90]–[93]. Recently, passive microstrip resonators, as dielectric property sensors, attracted attention due to their compact size, non-contact sensing capabilities, simplicity, and CMOS (complementary metal oxide semiconductor) and lab-on-a-chip compatibility,[2], [11], [75], [94]–[98]. SRR has been reported as the core of sensing device for

material, humidity, temperature, and Nano-structures analyzers [99]–[103]. Lossy dielectric media can also be monitored using SRRs [12], [76].

In this feasibility study, we investigate the use of an active microwave resonator sensor to detect, measure and monitor dissolved and precipitating Asphaltenes. A model oil composed of extracted Asphaltenes re-dissolved in toluene is used. We first propose two different schemes to measure the Asphaltene content of model oil samples within a wide range of concentrations 0.00125-10 % (v:v). First, individual injections of samples inside a fixed tube are tested, and then a diffusivity based method using a reference liquid is implemented to improve the performance. We next demonstrate an active resonator based technique to monitor precipitation and deposition. We present our findings as a proof of principle, a first step towards the development of an instrument capable of replacing optically based measurements. Compared to passive schemes, active sensors, with their loss-compensated resonance and sharp sensing profile, present improved performance: better accuracy for detecting resonance frequencies and, increased resolution allowing the sensing of minute differences between model oils. The proposed sensors with the configurations described in this manuscript is designed to operate at laboratory conditions and could be used for applications such as Asphaltene inhibitor screening and selection.

3.1.1 Method and materials

3.1.1.1 Model oil preparation

We used model oils to affranchise ourselves from any potential matrix interference, and to ensure a wide high resolution measurement range. Asphaltene is extracted from a heavy crude oil following a simplified ASTM D6560 protocol3, where only one rinsing stage is implemented. The stock solution of model oil is prepared by dissolving the extracted Asphaltene in HPLC grade toluene to generate a 25% (w:w) solution. A range of model oils is prepared by volumetric dilution in toluene. To enable direct comparison with existing optical methods, each model oil is diluted again in toluene by a factor 40 and its concentration is expressed in % (v:v) of the initial solution.

Prepared solutions were kept in a 5 mL borosilicate glass vial (εr=4.3, $\tan(\delta)$=0.0047) with a PTFE seal lid.

HPLC grade heptane (n-C7) was used as a precipitant with a volume ratio of 1:10 (model oil : n-C7) for the precipitation experiments.

3.1.1.2 Data acquisition

The vector network analyzer (VNA) is used to compute the scattering parameters of the sensor as a device with two ports. Transmission profiles (S21) are collected from a R&S-ZVL VNA (Rohde and Schwarz, Germany) and recorded with LabView (National Instruments, US) at a rate of 1 sample/10sec. The data is then post processed to extract the S21 resonance frequency and amplitude. In cases

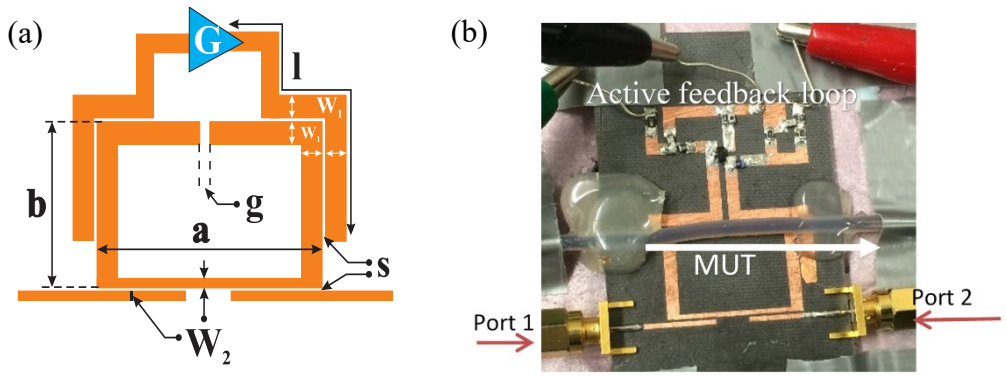

Fig. 3-2. (a) Schematic of the active sensor. (b) Photograph of the sensing setup (MUT stands for material under test)

Table 3-1

Critical dimensions of the sensor

Parameter	a	b	I	g	W_1	W_2	S
Dimension (mm)	26.0	17.0	44.0	2.0	2.1	1.0	0.4

of mapping the extracted variations in amplitude and frequency over time with specific profiles, MATLAB is used for feature extraction.

The resonator was kept in a temperature controlled sealed box purged with dried nitrogen gas to prevent the effect of temperature and humidity to interfere with the signal.

3.1.2 Implementations and Results

3.1.2.1 Resonator schematic and design

The concept of the resonator is similar to that of published in previous work [70]. Here, the planar resonator sensor is a half wavelength ring resonator magnetically coupled to an input and transmission lines, resulting in a Gaussian peak signal at the frequency of resonance. A schematic of a typical sensor used for

this study is shown in Fig. 3-2(a). Its critical dimensions are summarized in Table 3-1. The strong electric field concentration at the gap 'g' of the ring resonator provides the sensitive region for sensing. For a passive resonator, the typical quality factor of less than 300 is limited by losses in transmission. By adding a negative resistor with a feedback loop control to compensate for electromagnetic losses [70], the passive resonator becomes an active sensor with enhanced performance. A NE68033 (manufacturer, country) transistor with a 3 GHz gain cut-off frequency is used as an amplifier. To achieve optimum high frequency stability and loss compensation capability, we followed the manufacturer recommendations and operated the transistor at frequencies around 1.2 GHz. Fig. 3-2 shows a model of the sensor simulated using Finite Element Method (FEM) in ANSYS HFSS (ANSYS Inc. US[104]) with microstrip traces of 35um thickness on Rogers 5880 substrates ($\varepsilon_r = 2.2, tan(\delta) = 0.0009$). The active circuit is modeled as a negative resistance in parallel with the resonator. The resonance frequency is designed to consider the parasitic effects of the resonator as a shunt capacitance (as small as 50 fF) with the ground that is due to imperfections in fabrication and soldering errors as loading effects. Fine tuning negative resistance creates a resonant profile in good agreement with the measured data. For the S21 transmission parameter at a resonance frequency of 1.19135 GHz, a good agreement between simulation and measured response is achieved. The quality factor improves from 120 to 10,000 for a passive and active resonator respectively, resulting in an extremely sharp resonant profile.

3.1.2.2 Benefits of an active resonator

The active resonator used in the sensor provides a very sharp resonance S_{21} transmission profile such that a high resolution is achievable as shown in Fig. 3-3(a). The figure presents two different profiles which have 1MHz difference. Because of its high quality factor and high roll-off in the skirt of the resonance frequency peak, tracking small changes is possible. On the other hand, the relatively low quality factor of the passive resonator does not allow for a clear distinction in 1 MHz span. The low-quality factor of 120 is prone to amplitude noise, resulting in a high uncertainty in recognizing the S_{21} resonance frequency. To further demonstrate the improvements brought by the active scheme, the resonant frequencies of the passive and active sensors were measured over 1000 s and plotted in Fig. 3-3(b). A scatter of ± 300 kHz in passive mode compared with less than 10 kHz in active mode were recorded, demonstrating the superior capabilities of the active scheme.

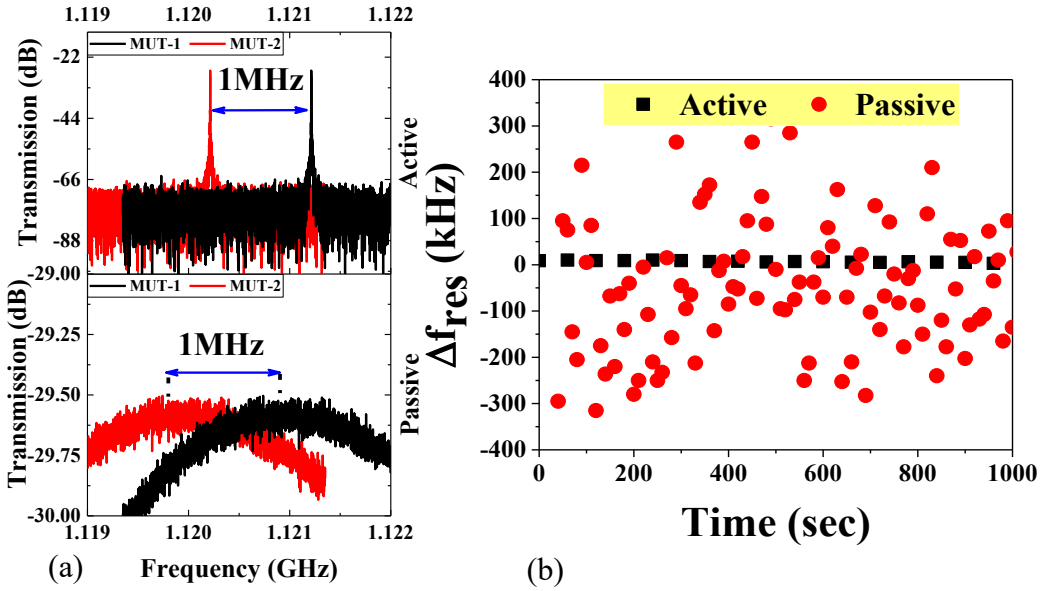

Fig. 3-3, (a) Illustrative example of the difference of resolution between a passive and an active sensor. MUT: material under test. (b) Impact of the active scheme on the precision of the

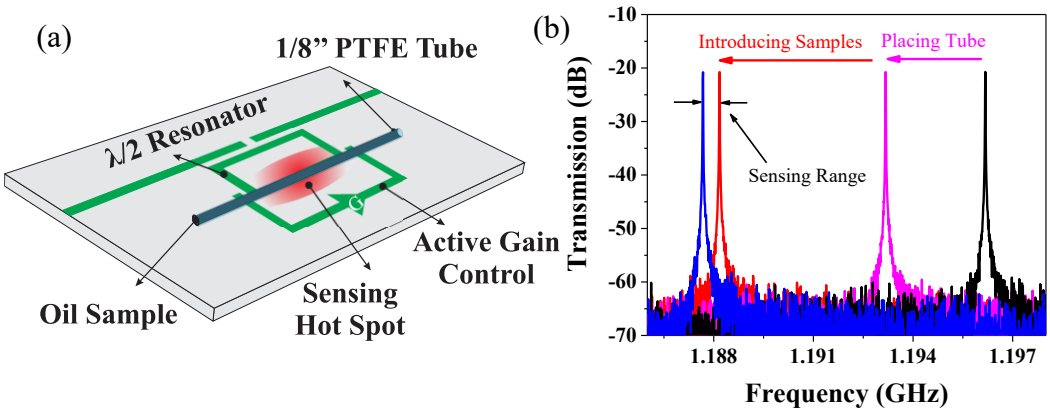

Fig. 3-4, (a) Graphical representation of the concentration measurement scheme. (b) Measurement principle.

3.1.3 Concentration measurements

3.1.3.1 Test setup

A schematic of the active sensor and measurement setup is found in Fig. 3-4. A 1/8’’ PTFE tube is placed horizontally touching the sensor surface such that it fully covers the hotspot. The position of the tube is kept fixed to the sensor’s surface throughout the entire experiment so that it can be considered as a reference for different MUTs. The resonator can be modelled as a parallel RLC circuit with Resistance R, Inductance L, and capacitance C, which resonates at $f_r = 1/\sqrt{2\pi LC}$. Its behavior depends on the effective permittivity of the sensor environment ($\varepsilon_{r\text{-}eff}$), which can be projected into a capacitance in the circuit model. The bare sensor resonant profile demonstrates a frequency downshift, due to capacitive loading of the tube on the resonator, as illustrated in Fig. 3-4(b). When the MUT affects the

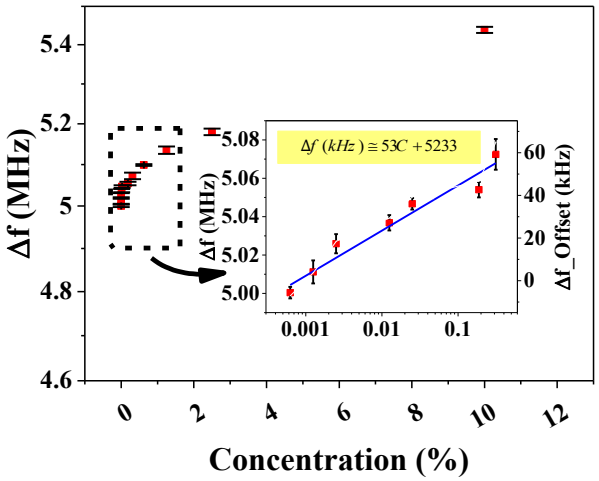

Fig. 3-5, Resonance frequency shifts obtained at different concentrations.

($\varepsilon_{r\text{-}eff}$), the resonant profile varies accordingly, such that higher dielectric constants shift the frequency to lower values, whereas existence of loss in the MUT would tend to shift it upwards.

3.1.3.2 Direct concentration measurements

A view of the setup is shown in Fig. 3-4(a). A volume of 200-µL of model oil at concentrations of 0.00125, 0.0025, 0.0125, 0.025, 0.1875, 0.3125, 0.625, 1.25, 2.5, and 10 % (v:v) was injected sequentially. In this test, heptane is used as reference material to create a reference data point and eliminate possible environmental and user error from the measurement. Model oils of different Asphaltene concentrations are then injected.

The measurements are performed in triplicate with the error bar representing the standard deviation of the average is given. As the permittivity of Asphaltenes (~5)[105] is larger than toluene (~2), an increasing shift in the resonance frequency with increasing Asphaltene concentration is observed. The full set of data is plotted

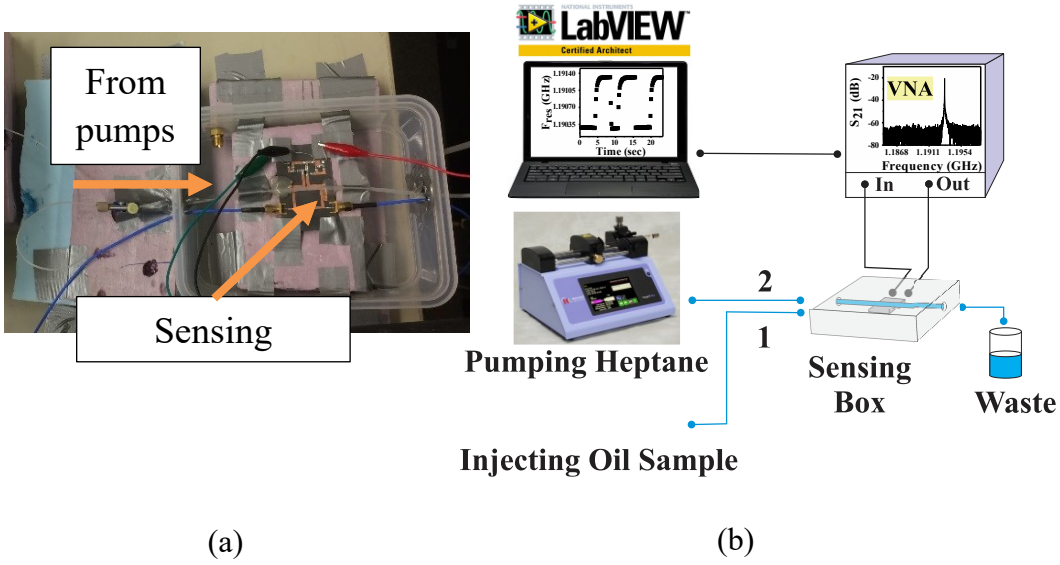

(a) (b)

Fig. 3-6, (a) sensing setup for viscosity measurements and (b) schematic of the test for viscosity

in Fig. 3-5, where the logarithmic scale is used to zoom in the low range of concentrations in inset. The resonance frequency varies from 5.0 MHz to 5.4 MHz for the full range of concentrations. A linear fitting function is employed to interpolate the intermediate values as shown in Fig. 3-5. Resolving these frequency shifts is only possible because of the active resonator. As shown before, a passive resonator has a precision of around ±0.3 MHz, and would bury the measured signal and information into the noise.

3.1.3.3 Concentration measurement with a diffusivity based method

In this section, the reference is chosen to be “n-Heptane” which fills the tube while acting as a reference. We used the Taylor-Aris dispersion effect to our advantage. Each plug of model oil injected in the tube was followed by a plug of heptane at a flow rate of 0.5 mL min-1. The enhanced diffusivity induced by the

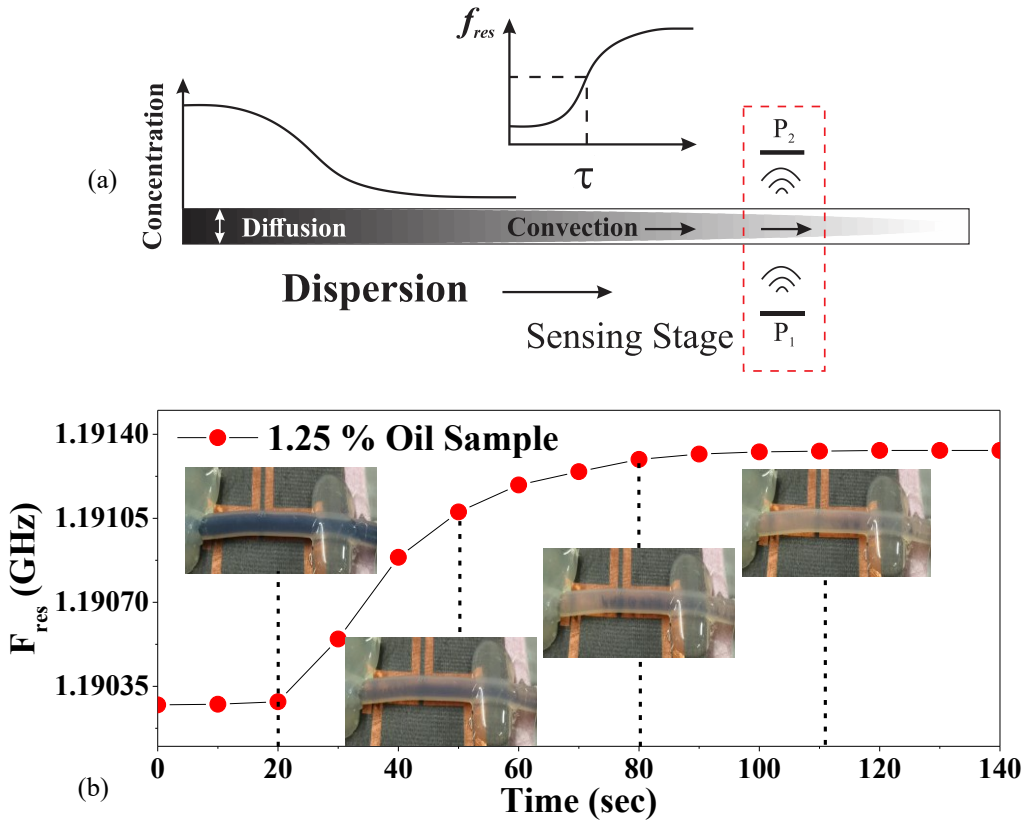

Fig. 3-7, (a) Dispersion flow of oil sample in combination with n-Heptane (not to scale, exaggerated to exemplify the measurement principle), (b) Frequency shift recorded when pushing a plug of 1.25% (v:v) model oil with HPLC grade heptane.

shear flow in the tube generated a tail of precipitating Asphaltene. Fig. 3-6(a-b) shows the test setup, where a slug a model oil is swapped for a plug of heptane in front of the hotspot of the sensor. Continuous recording of the data is done by LabView [106] with a rate of sample/10 sec.

Fig. 3-7(a) depicts the dispersion of the flow from a complete oil sample as it transits to heptane. Each concentration of model oil has specific dispersion rate, meaning that each concentration will have a different transition time (defined as time constant). Fig. 3-7(b) shows the typical frequency shift when a slug of a model

Table 3-2,

Fitting parameters

Parameter	P_{00}	P_{01}	P_{02}
Value	92.12	-3.2	-0.008
Parameter	P_{10}	P_{11}	P_{20}, P_{12}, P_{21}, P_{22}
Value	-0.12	0.004	0

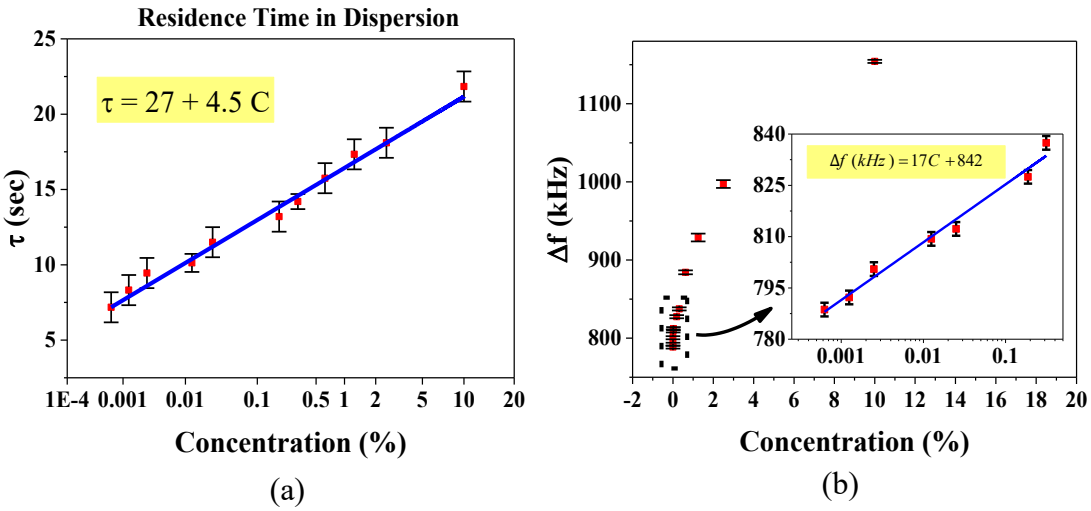

Fig. 3-8, (a) Transition time versus model oil concentration. (b) Frequency shift versus model oil concentration

oil is swapped for a plug of heptane in front of the hotspot of the sensor. A time series of photographs in Fig. 3-7(b) illustrates the process.

The transition phase between both fluids can be seen at the inflection point of the sigmoidal graph for resonant frequency's time-based trend, which is called the residence time (τ), and extracted for each model oil samples. Each value is then plotted as shown in Fig. 3-8(a). For comparison, the resonance frequency shifts are also plotted in Fig. 3-8(b). With the diffusivity based method, the full range of Asphaltene model oil concentration, from 0.00125 to 10% (v:v), can be measured.

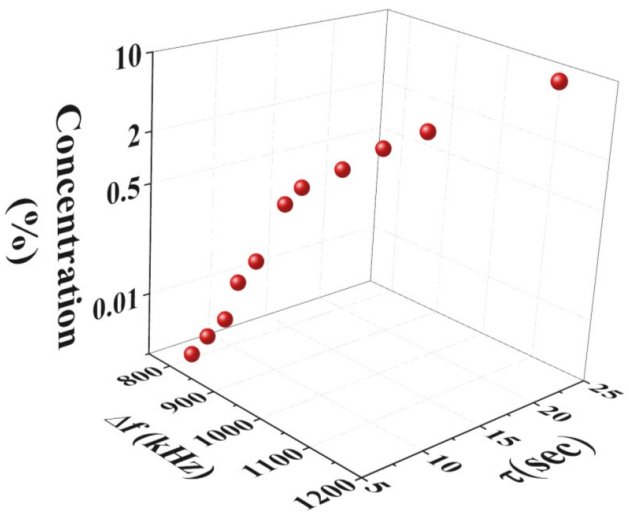

Fig. 3-9 Relationship between concentration, resonant frequency shifts and their time constants

3.1.3.4 Dual parameter analysis

In order to fully exploit the extracted information in characterizing the diffusion process, a combination of the measured data is presented in Fig. 3-9, where the logarithmic scale for concentration is assumed to be a function of both measured Δf and τ. A polynomial function (spatial surface) is pursued to be used as a mathematical formula in predicting intermediate values as follows:

$$C = \sum_{\substack{i=0,\\ j=0}}^{2} P_{ij} \Delta f^{i} \tau^{j} \tag{4}$$

where $P_{ij|i,j}$=0,1,2 are parameters given in Table 3-2. after optimizing the fitting in MATLAB, which yielded a great agreement of R^2=0.99 with the experimental data. A 2nd order polynomial function is the simplest case for the analysis to cover all the data, and still include the individual/mutual impact of extracted features of the diffusion process. The two datasets, Δf and τ, are independent from each other. They

convey useful characteristics of the model oils such as the Asphaltene concentration and corresponding diffusion rate. Combining the two datasets consolidates the measurement method and reduces the error bars associated with the measurement since it considers a more robust set of information about the sample and not only frequency variations.

3.1.4 Precipitation detection

3.1.4.1 Permittivity analysis of suspensions

Electromagnetic waves in microwave region interact with materials with respect to their electrical signatures, such as permittivity and conductivity. Mixture of several species (solutions, suspensions, electrolyte, etc.) represents mixed properties of all of its individual constituents according to their volume fractions. As a first order approximation, Asphaltene can be considered as colloids suspended in crude oil and solvable in toluene. Based on DeLacey and White theory [107], the real and imaginary parts of the dielectric constant of a suspension can be calculated if the induced dipole of the suspended inclusion is known:

$$\varepsilon'(\omega) = \varepsilon'_S + 3\varphi\varepsilon'_S\left[C_1(\omega) - \frac{K^\infty}{\omega\varepsilon_0\varepsilon'_S}C_2(\omega)\right] \tag{5}$$

$$\varepsilon''(\omega) = 3\varphi\varepsilon'_S\left[\frac{K^\infty}{\omega\varepsilon_0\varepsilon'_S}(C_1(\omega) - C_1(0)) + C_2(\omega)\right] \tag{6}$$

where ϕ is the volume fraction of solids, ε_r' and K^∞ are dielectric constant and DC conductivity of the host medium, and C_1 and C_2 are the real and imaginary parts of induced dipole coefficient[108]. Here, not only the permittivity of the inclusions

and the host medium should be considered separately, but also the volume of liquid that is being substituted by solid particulates is of great importance. Reducing the external inclusion in the mixture with high ε_r' decreases the effective and inhomogeneous permittivity of the mixture. Therefore, it is expected that by monitoring the permittivity variation in the liquid, one can characterize the mixture, and its precipitation status with regards to time and quantity.

3.1.4.2 Sensor design and simulation

In this occurrence, the sensor is a meandered shape half-wavelength resonator on microstrip that is coupled to an active gain-controlling section to enhance its quality factor from ~270 up to ~10 k. The operating concept is very similar to the one explained in section 3.1. Details are given in the reference [75] and a schematic can be found in Fig. 3-10(a).

The resonator has two main hotspots at both of its end parts where maximum electric fields are confined. For the ANSYS HFSS simulation, a cylindrical sample with dimensions of D_2 = 6 mm, h = 20 mm is placed 1 mm off the left hotspot with ε_r=2, $tan(\delta)$=0.01 (representing the host medium). To simulate the precipitation, an external material is put inside the host cylinder (ε'_r=5, $tan(\delta)$=0.1) of variable diameter D1 to represent precipitating materials. The precipitated Asphaltene model gets larger in diameter and shorter in height to mimic the deposition process (Fig. 3-10(b)). Results computed using the finite-element method in ANSYS HFSS are shown in Fig. 3-10(c). The top section of the sample is the main part for the sensor. Change in effective permittivity of the environment is represented by deposition where the extracted material (high ε'_r) is moving away from the hotspot

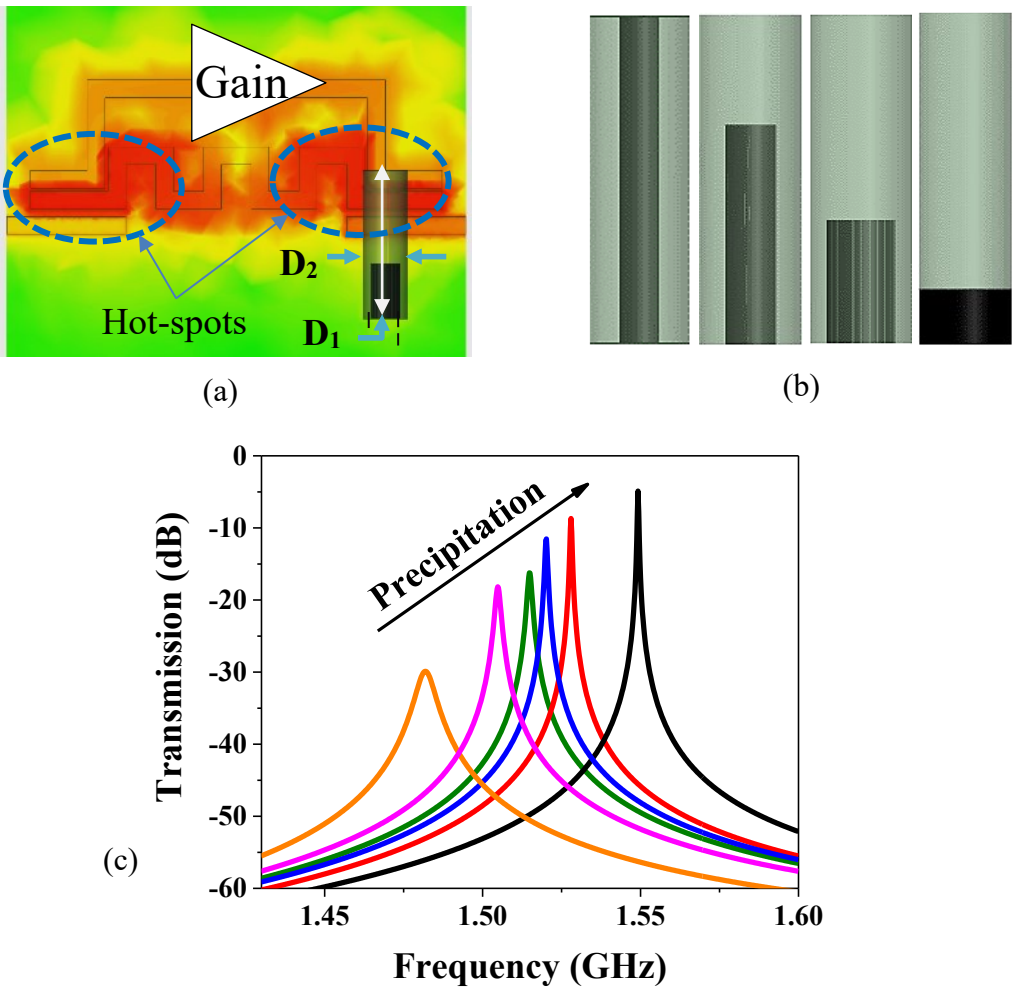

Fig. 3-10, (a) Schematics of the modelled sensor with dimensions of D_2 = 6 mm, h = 20 mm, and variable D_1, (b) Details of the precipitation model used for the simulation. (c) Simulated signal output from HFSS

and settling down at the bottom of the cylinder. Thus, the high permittivity of the solute is affecting less and less the resonant frequency (f_r) over time resulting in an increasing f_r.

3.1.4.3 Precipitation detection

The experimental setup is shown in Fig. 3-11(b). The active sensor is mounted vertically in order to monitor the precipitation inside a 5 mL borosilicate glass vial containing the mixture of model oil and heptane. The vial is mounted 5 mm away from the sensor, and the glass thickness is approx. 1 mm. Three samples with concentrations of 0.1875% (v:v), 0.6250% (v:v) and 1.25% (v:v) and a toluene blank were all mixed with heptane as the precipitant element. A 6-minute time lapse of the deposition of the precipitated Asphaltene for the 0.625% sample is shown in Fig. 3-11(b). Conceptual variation of the size and volume of the aggregated molecules is presented in Fig. 3-11(c), where first nanoparticles start being precipitated. Next, their collection brings about nanoaggregates, in smaller scale,

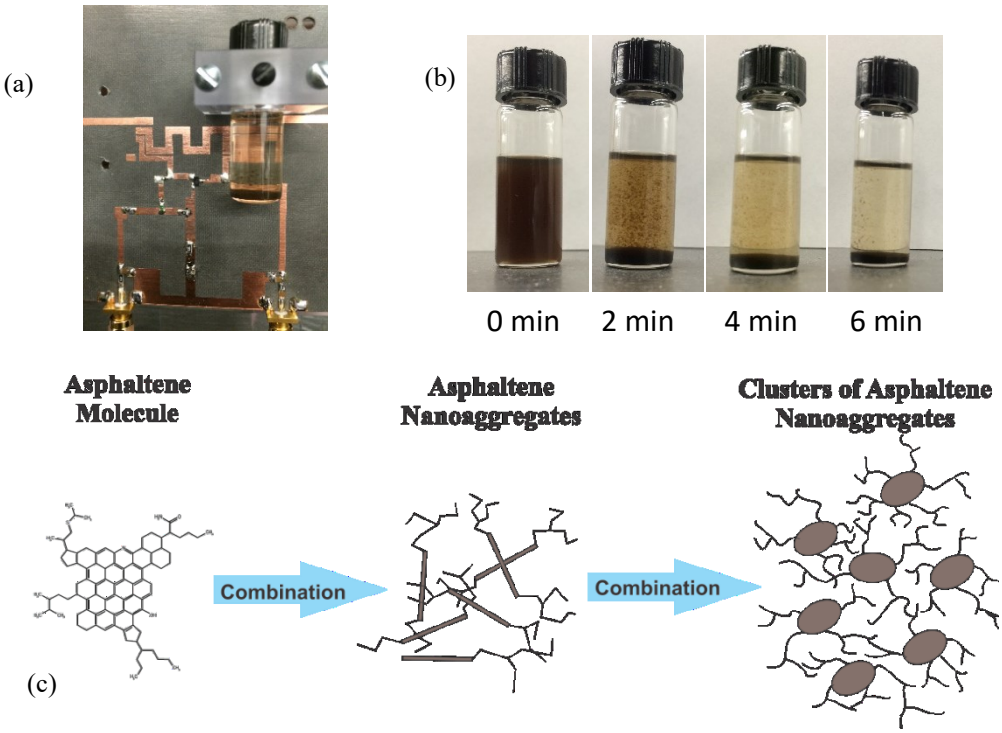

Fig. 3-11, (a) Experimental setup for time-based monitoring of deposition. (b) Evolution of the precipitation and deposition over time for the 0.625%-sample (ratio 1:10). (c) Conceptually demonstrating precipitation and aggregation

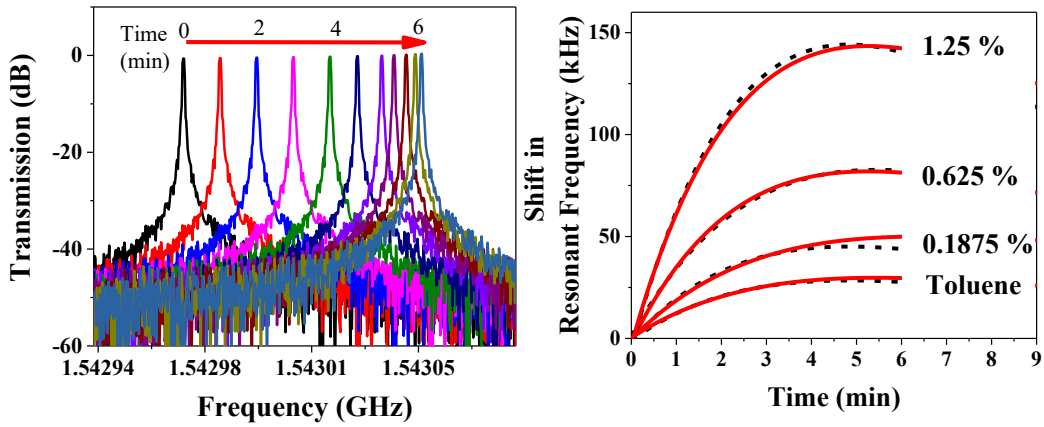

Fig. 3-12, (a) Transmission profile from the time based deposition in experiment. (b) Variation in resonant frequency for four samples. The solid and dotted lines represent two different measurements. Data is normalized to the starting time.

and finally this trend continues in larger scale to result in clusters that tend to deposit for their weight.

Following the same time line, S_{21} transmission responses of the sensor are shown in Fig. 3-12(a). Shifts in resonant frequencies are extracted after post processing the results and plotted in Fig. 3-12(b). Duplicate measurements were performed. As the particulates of Asphaltenes with higher permittivity deposits to the bottom of the glass container, leaving only liquids with lower permittivity in the sensor's sight, the effective dielectric constant is reduced, which results in shifting f_r upwards. The four different sample concentrations present quite distinctive profiles indicating the feasibility of quantifying the deposition after calibration.

3.2 Wireless communication in feedback-assisted active sensor [2]

In variety of applications such as pipelines, constructions, mining, *etc.*, the sensor is located in an enclosed area with no direct access. In field applications, the use of cabled devices creates problems such as increased phase noise or drifts with respect to thermal cycling, mechanical movement, or vibration [1-2]. In such applications, wireless communication within a mine, well takes a vital part of the appropriate operation of the underground facility. This communication capability is not only an enabling factor in the concept of safety [111], but also is beneficial to regular daily operations. Rapid, accurate and continuous flow of data from the sensor to outside world, would guarantee sooner and more accurate decision-making [112].

In harsh environments, where the surrounding medium impact is significant (i.e. extensively high temperature and pressure, existence of corrosive materials, etc.), processing the data and real time communication of the results, if not impossible is very difficult [113], [114]. Most of the present sensor such as photo-ion-detector for gas sensing [115], temperature, humidity sensors [116] as well as soil-water probe [117] use a digital display to communicate which is battery extensive. Wireless technology that can transfer raw data, could significantly benefit harsh environment sensing, eliminate the need to preprocessing unit and reduce the battery usage.

This work aims for high resolution wireless microwave sensing. To implement such configuration, two-port high-resolution sensor regenerated using active

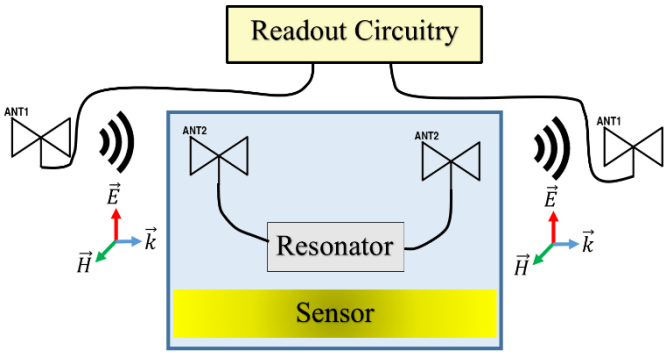

Fig. 3-13, Schematic of the sensor with wireless communication

feedback loop is connected to two wideband bow-tie slot antennas for wireless communication as shown in Fig. 3-13. The blue box represents the enclosure for the sensor while the outside antennas are used to communicate with the sensor. It has previously shown that the use of near field communication is suitable for sensor applications [118], [119]. Here, we show the possibility for *high-resolution wireless sensing* for close range communication. The goal is to enable high resolution sensing in non-accessible applications while minimizing the battery usage by eliminating the need to data processing at the sensing node.

This part is organized as follows: Section 3.2.1 presents the study of bow-tie antennas and the detailed analysis of the resonator with regenerative feedback loop in HFSS simulator. The integration and measured results along with detailed discussions are furnished in section 3.2.2. The experimental results for salt-water and liquid-chemical sensing are also presented. Section 3.2.3 concludes this chapter.

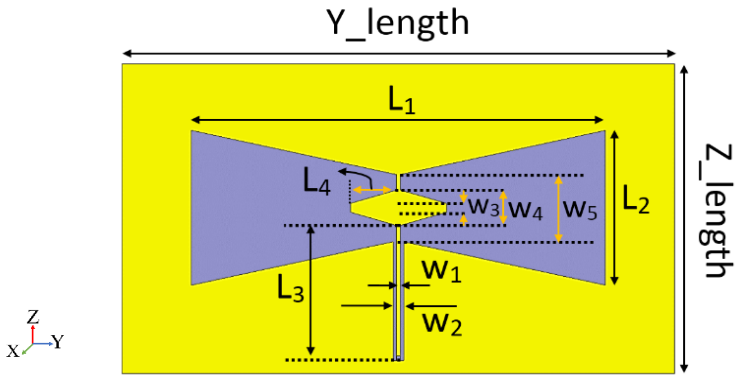

Fig. 3-14, Antenna Schematic with dimensions: Y_{length}=120, Z_{length}=70, L_1=90, L_2=35, L_3=30, L_4=10, W_1=0.8, W_2=2.4, W_3=2, W_4=8, W_5=15 (mm)

3.2.1 Simulation and Analysis

3.2.1.1 Antenna Design and Analysis:

Here, a CPW-Fed bowtie slot antenna is used to establish the wireless link between the readout device and sensing element with the following configuration. The slot profile on the antenna removes the need for a balun for current balance [120], [121] . In addition, relatively wideband operation of such structures enables sensing using frequency shift which is the base for microwave resonant based sensing.

The general schematic of the antenna is presented in Fig. 3-14. Design on low-dielectric- constant substrate (Rogers 5880 ($\varepsilon_r = 2.2, \tan(\delta) = 0.0009$)) enables the antenna to yield a high gain [122]. Fig. 3-15(a) illustrates reflection and matching of the antenna with mag(S11) = -15 dB and total gain in main lobe ($\theta = 90, \phi = 0$) to be 4.8 dB @ 1.41 GHz where is supposed to be the working region of the sensor. The ultra-wideband design (fractional bandwidth of 64 %) enables application of the antenna over a wide range of frequency shifts wherein matching

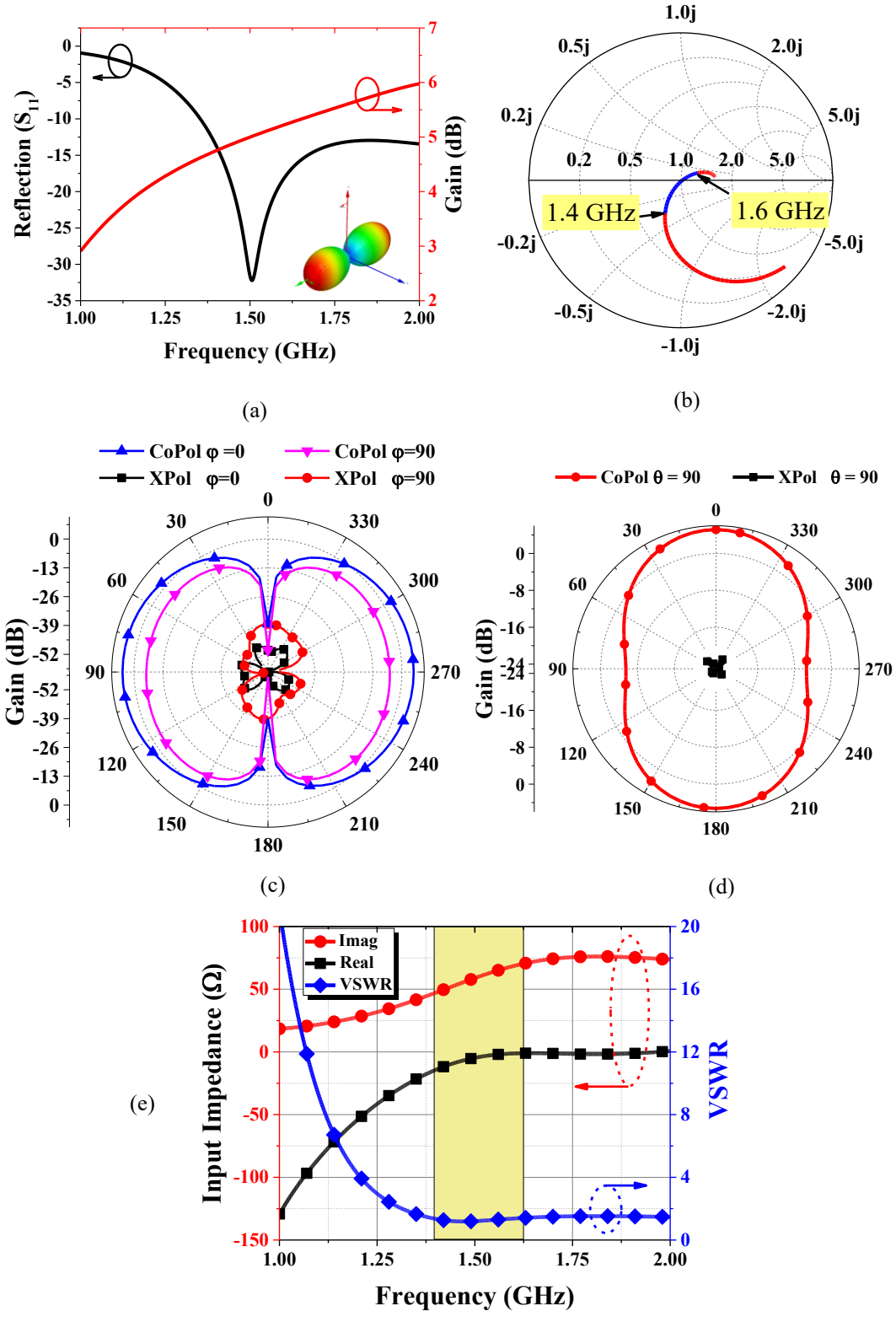

Fig. 3-15, (a) Reflection and Gain (b) Smith Chart and (c) Gain comparison in $\boldsymbol{\phi = 0}$ (XZ) and $\boldsymbol{\phi = 90}$ (YZ) planes and (d) $\boldsymbol{\theta = 90}$ (XY) plane (e) Input impedance and VSWR of the Antenna

and high gain still would remain [123]. This is specifically important in this application, as the frequency shift in sensor defines the dynamic range of the sensor. Its ultra-wide band realization as well as moderately high gain came at the cost of size.

As shown in Fig. 3-15(c) and (d), 5.1 dB gain for Co-polarization in $\phi = 0$ (XZ plane) with half-power-beam-width of 80 degree as main lobe, shows strong linearity compared with X-polarization in that plane with over 50 dB difference in co-pol-gain. This characteristic will be used in this project to reduce the cross coupling between the receive and transmit signals.

In Fig. 3-15(d) Co- and X-pol gain for H-Plane of the antenna ($\theta = 90$, XY plane) confirms large difference (over 25 dB in average for all directions), and reveals minor radiation in $\phi = 90$ as well. As a result, this design enables us to utilize linearly polarized signals for transmit and receive. Fig. 3-15(e) gives more comprehensive look into antenna's performance as input impedance of 48.4 - j11 Ω and voltage standing wave ratio (VSWR) of 1.3 @ 1.41 GHz. These properties are in good agreement with each other for an efficient radiation. In this study we plan to use two of these antennas, one inside the sensor enclosure and one outside (as shown in Fig. 3-13). Therefore, the two-antenna distance and the power transmission is important. Further study over mutual interaction of the two antennas in transmission, is done for different distances and illustrated in Fig. 3-16. Degraded level of communication where the distance gets larger is clearly quantified.

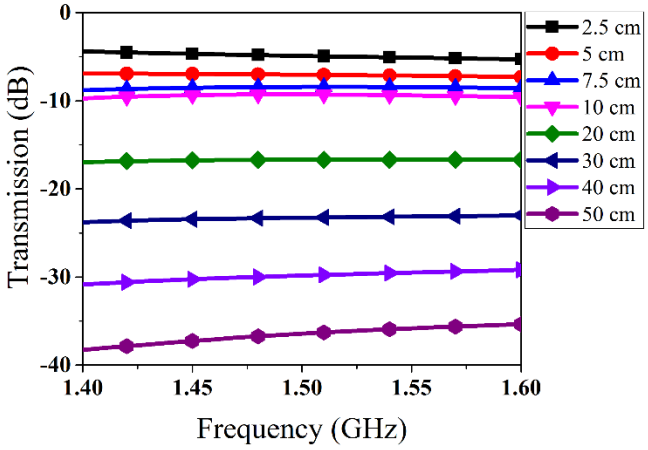

Fig. 3-16, Transmission of Antennas over distance

3.2.1.2 Resonator Analysis

The planar microwave sensor in this work is a meandered open-loop resonator (Fig. 3-17(a)) with initial quality factor of 104. To perform high resolution sensing, much higher quality factor is needed [77]. Based on the new approach of high-Q resonance implementation with details in [75] the passive resonator was armed with positive-feedback-loop to enhance its quality-factor substantially. This improvement in the sharpness of the resonances enables tracking of minute changes in ambient dielectric properties, including material detection in either bulk or concentrated form.

As the resonant frequency of the half-wavelength resonator is strongly linked to the inductive (L) and capacitive (C) constituents of resonator by $f_r = 1/2\pi\sqrt{LC}$ [124], any change in f_r could be a reflection of increase or decrease in C. Change in dielectric properties of environment would result in variation in sensors effective capacitance. Minimal variations in permittivity are detectable with the help of such a high Q-factor, as shown in Eq. (7), and consequently increases the sensor's readout resolution.

(a)

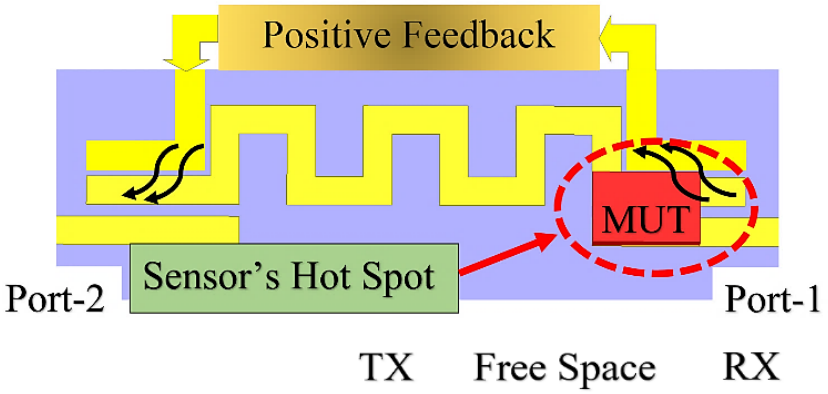

(b)

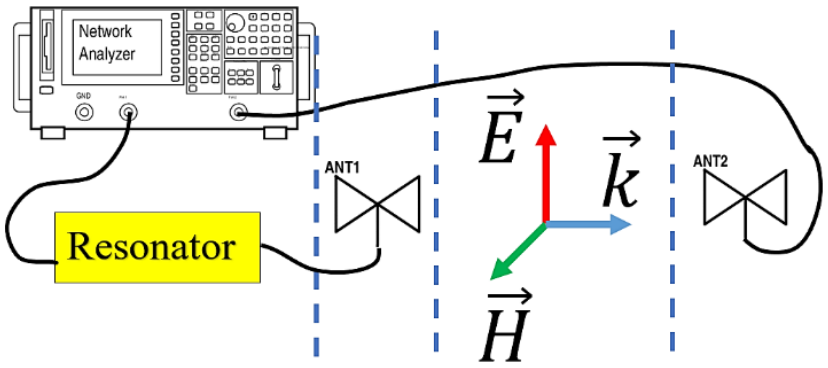

Fig. 3-17, (a) Schematic of core passive resonator, (b) Simulation-configuration accounting for effect of each antenna as well as intermediate medium in overall transfer-function of sensor's response

$$|\Delta\varepsilon_{min}| \propto \frac{\varepsilon_r}{V_{omax}Q}\sqrt{4kTBR} \qquad (7)$$

where k=1.38×10^{-23} $m^2kgs^{-2}k^{-1}$, T is the room temperature in Kelvin, B is the measured bandwidth, R is the resistivity of the device, ε_r' is the permittivity and Vomax is the maximum amplitude of the resonance profile. [69]

The transmission behavior of the sensor and its impact on the high-resolution sensing platform were studied based on a simulation on simplified configuration using finite-element-method in HFSS (considering only two antennas) as shown in Fig. 3-17(b). Please note that for simplicity of the simulations, only wireless communication link is considered. The positive feedback loop is modeled using a

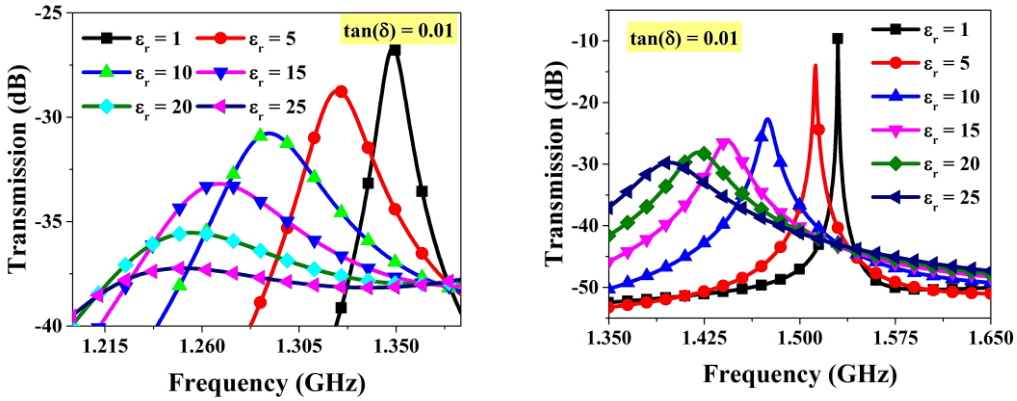

(a) (b)

Fig. 3-18, Transmission profile variation due to lossy analyte introduction in (a) passive and (b) active mode including antennas

Table 3-3

Quality Factor change comparison of active and passive sensor for sensor system including the antennas

ε_r	1	5	10	15	20	25
Q_{active}	3397	880	148	67	43	23
$Q_{passive}$	104	50	26	3.5	-	-

negative resistance. The sensor is connected to a transmitter that sends the data to the receiver (20 cm away), and the systems transmission behavior including the sensor and the two antennas are simulated.

To have the sensing profile, an analyte (MUT in Fig. 3-17(a)) is studied with $\tan(\delta) = 0.01$ and permittivity in the range of 5- 25 and illustrated in Fig. 3-18. Shifts in resonant frequency due to a change in dielectric properties of the sample are an indicator of each specific material. Passive sensor cannot keep up with larger changes in environment when the quality factor degrades drastically as $\varepsilon_r' > 15$, while the very the same sensor in feedback-assisted mode could compensate for

losses and the sensor's output could preserve its high Q profile. Changes of quality factor in Table 3-3 reveals a quality factor with orders of magnitude difference between the passive and active form of sensor while communicating through two antennas.

These large variations in f_r and maintenance in general profile or transmission, ensures the capability of high resolution microwave sensing in wireless fashion which enables its application in practical conditions with low accessibility to the sensing area/harsh environments.

3.2.2 Measurement and Results

3.2.2.1 Antenna's Characteristics

Four-identical bow-tie slot antennas were prepared in order to incorporate in data transmission between the sensor and the measuring device (Agilent 85052D - Vector Network Analyzer) in wireless fashion. Experimental results of antennas'

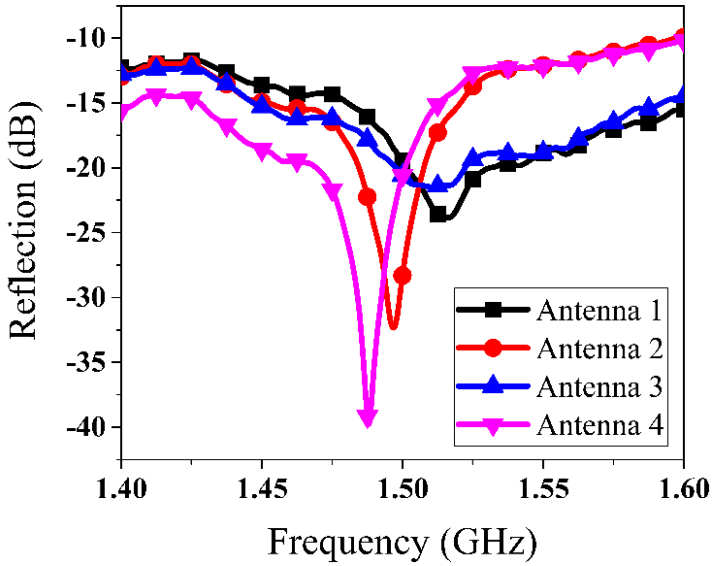

Fig. 3-19, Measurement results of reflection of individual antennas

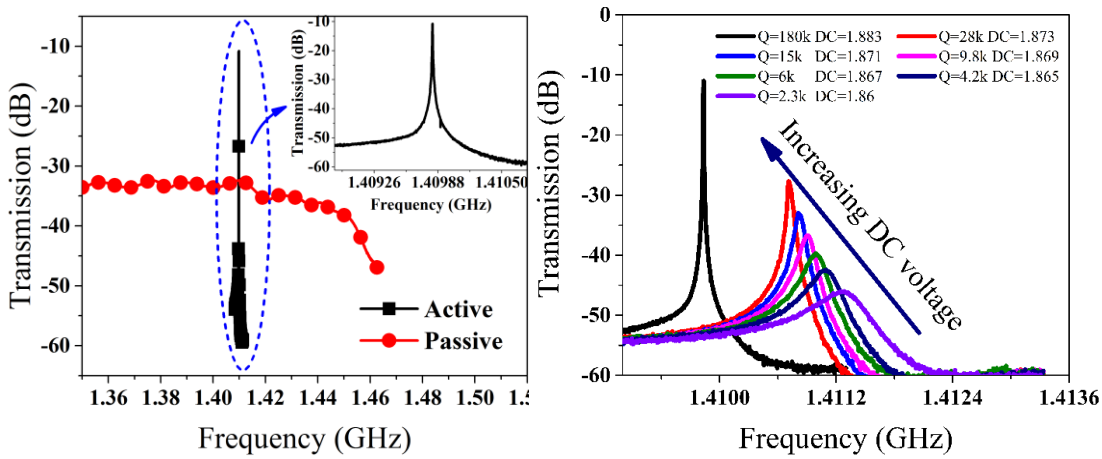

Fig. 3-20, (a) comparison between measured passive and active profiles of the sensor (b) quality factor adjustment of S_{21} profile using DC_bias voltage

reflection in Fig. 3-19 suggest good matching performance (below -10 dB) for all of them over sensor's operational frequency span (1.4-1.6 GHz).

3.2.2.2 Sensor's characteristics with Antennas

The results of fabricated sensor and its characteristics while connected to two sets of antennas (one set for transmitter and another for receiver) (Fig. 3-13) are presented here. The active-loop assisted positive feedback led to 5 orders of magnitude enhancement in transmission resonance sharpness, which reveals appreciably high quality factor of ~220 k @ ~1.4 GHz in comparison with the pseudo-flat transmission-response of sensor in passive form in the given narrow bandwidth (Fig. 3-20(a)). The control over strength of resonance and amplification level of resonant profile, can be achieved using the bias voltage of circuitry as depicted in Fig. 3-20(b).

Change in impedance of positive-feedback load on resonator while varying the bias voltage (as the S-parameters of active loop is directly linked to its DC-bias) turns into slight deviation in resonant frequency, while increasing the DC-bias

helps finding the optimal matching-impedance such that Q=180 k can be reached with $V_{bias} = 1.883$ V.

3.2.2.3 Chemical sensing at the sensor enclosure

Chemical materials are typical subject of interest for recognition in practice because of their high rate of daily application in industry. In an experiment some of those common chemicals, such as IPA, Methanol, Acetone, Ethanol, Acetone, and Water were tested. The fluid flow inside a 1/8" PTFE tube over the sensor where such a stable configuration helps to have repeatable measurements. In

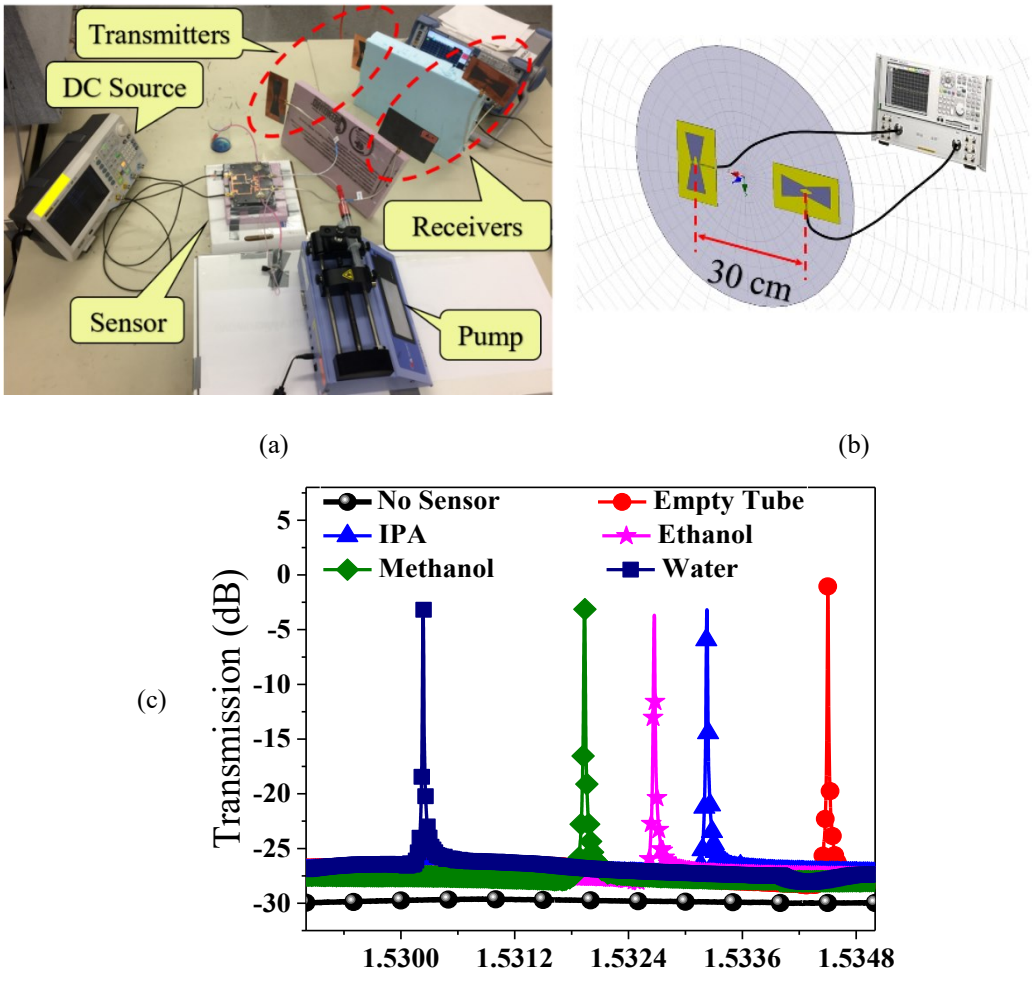

Fig. 3-21, (a) Material Detection Configuration (b) Antennas transmission as a reference and (c) Chemical material detection responses with antennas as transmission tools

addition, the temperature (T) and relative humidity (RH) are controlled constantly using another sensor and found to be T = 23.3 ℃ and RH = 11%, respectively. Chemicals were pumped inside the tube using syringe pumps as shown in Fig. 3-21(a). At first, only 2 of the antennas were connected to VNA in the same plane to extract the baseline (reference) for next steps with 30 cm center-to-center distance. As the antennas are linearly polarized, the transmitter antenna was rotated 90 deg (Fig. 3-21(b)) with respect to receiver to eliminate cross-coupling between them (see Fig. 3-15). The response is shown as the flat black line of -30 dB in Fig. 3-21(c) which implies no transmission. Afterwards, the two antennas connected to its input and output were placed 20 cm away from their pairs (connected to VNA). Transmission response of active sensor, with the empty tube fixed on it, shows a resonance @ 1.5345 GHz. The sharp response of sensor shifts downwards as the permittivity of materials (Isopropanol Acid IPA ($\varepsilon_r{}' = 17.9$, $\varepsilon_r{}'' = 17.5$, Ethanol (ε_r'=24,ε_r''=12), Methanol ($\varepsilon_r{}' = 30$, $\varepsilon_r{}'' = 8$), and Water (ε_r'=81, ε_r''=9.6)) inside the tube increases. Over 4 MHz variation is covering a wide range of materials (up to ε'_r = 81 of water). Considerably distinguished results show the high resolution of sensor in dealing with liquids, especially as the response of transmission for lossy media such as water, has not been degraded and the ultra-high quality factor was remained robust.

3.2.2.4 Salt Concentration Categorization

In this experiment, two of bow-tie slot antennas were connected to the sensor inside an enclosure and the other two to the vector network analyzer (representing a transmitter) outside of the enclosure for communicating with the sensor. The

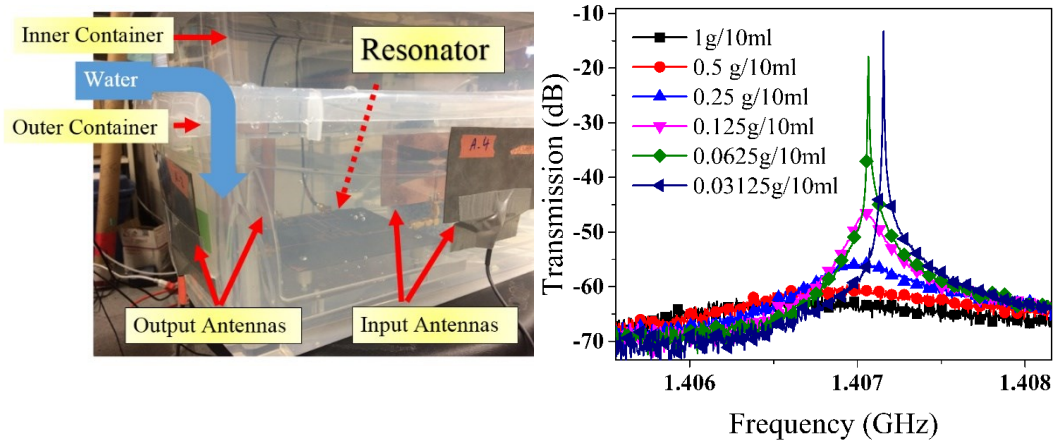

(a) (b)

Fig. 3-22, (a) Salt-Water wall experiment setup, (b) Salty-water concentration classification

sensor enclosure is located inside another larger plastic container within salt water to represent possible lossy environment in communication. Then the transceiver antennas are located outside of the larger plastic container as presented in Fig. 3-22(a).

A PTFE tube of 1/16'' is used to carry the saline solution over the sensor's hot spot with various magnitudes of salt inside it. The tube passes through the sensor hotspot for sensing. The change in solution's salt from 1g per 10 ml water down to low values of 0.03125 g per 10 ml water shows drop in both resonant frequency (~310 kHz) and quality factor (2 orders of magnitude), providing a wide sensing range for the resonator to distinguish intermediate concentrations. (Fig. 3-22(b)) Retrieving strong resonances could be achieved when the bias voltage of the sensor is adjusted such that the optimum feedback to the loop is provided.

3.2.3 Conclusion

We demonstrated that a high Q-factor high-resolution microwave resonator based sensor can be used to successfully detect and quantify the Asphaltene content of a set of model oils between 0.00125% (v:v) and 10% in noncontact fashion. A calibration curve is required to quantify the Asphaltene content of the sample. Time based measurement is also used to obtain independent information and measure time constant and permittivity in determining low concentrations of oil. It is also shown that such a system can detect and monitor the Asphaltene precipitation and deposition of a model oil when mixed with heptane in real time.

Moreover, it is shown that single high resolution microwave sensing can be performed wirelessly. The sensor's main core is a meander-shaped open-ended microstrip resonator with the regenerative feedback-loop. Wideband antennas at input and output of the resonator enable a wireless link between the microwave transmitter and the sensor in a non-accessible enclosure. In addition, the effect of high quality-factor on high resolution and precise measurement of different liquids and various concentration of salt-water is presented. Results depict 311 kHz variations on resonant frequency for a concentration range of 0.003125 – 0.1 g/ml and 3 order of magnitude drop in quality factor for the same range of salt-water concentration. Moreover, change in dielectric constant of common liquids (IPA, Acetone, Ethanol, Methanol and Water) is covered in 2.2 MHz resonant frequency shift with high precision of 4 kHz as measurements' error range. The proposed sensor can be used for sensing in non-accessible environment such as non metallic pipelines and mining applications.

Chapter 4

Dual Active Resonator and Its Applications

In this chapter, single active resonator is developed into dual active resonator and its enhanced functionality is shown in two sections as follows.

In the first part, environmental effects are studied and their impact on the final sensing characteristics are analyzed. The extraneous effect only due to unwanted variations of uncontrollable humidity change is monitored using a reference sensor and is removed with proper calibration technique. This method is explained with great detail in the paper entitled ”**Enhanced Q Double Resonant Active Sensor for Humidity and Moisture Effect Elimination**” [12].

Next, the dual active sensor is used in a unique configuration to evaluate the dispersion and diffusion coefficient of the suspended Nano-Particles in solvent liquid. For this purpose, two-window solution is chose and both of the dual active resonators are employed for detecting the dispersion coefficient of Asphaltene Nano-Particles inside n-Heptane as the precipitant element. The detailed experimental results are found in the paper, entitled: “**Dual Active Resonator for Dispersion Coefficient Measurement of Asphaltene Nano-Particles**” [In Press at IEEE Sensors Special Edition]

4.1 Enhanced-Q Double Resonant Active Sensor for Humidity and Moisture Effect Elimination [12]

Here, we report developing a new microwave sensor based on double high-Q uncoupled resonant loops, consisting of two regenerative feedback loops. The sensor exhibits two resonant peaks that can be tracked and used to linearly subtract the unwanted effects of humidity in microwave sensing measurements. In the proposed sensor, one of the resonant peaks are designed to be used as reference for only monitoring the sensing environment and the other one is responsible for changes in the sample under the test as well as sensing environment. The sensor design and fabrication including active feedback loop is explained next. It is followed by measured results and calibration details for humidity and moisture impact elimination. To our knowledge, this is the first time, that double resonant sensor utilizing regenerative feedback loop is designed and incorporated to eliminate the environmental impact in sensing.

4.1.1 Enhanced-Q Dual-Loop Active Sensor Design

The proposed sensor utilizes a passive part that is regenerated using active feedback loop as explained below.

4.1.1.1 Passive circuit design:

Two similar rectangular type SRR were designed at f_{r_1}=1.044 and f_{r_1} =1.148 GHz, on Rogers 5880 substrate. Each one of two SRRs coupled to transmission line (TL) is leading an exclusive resonant frequency while the mutual coupling is

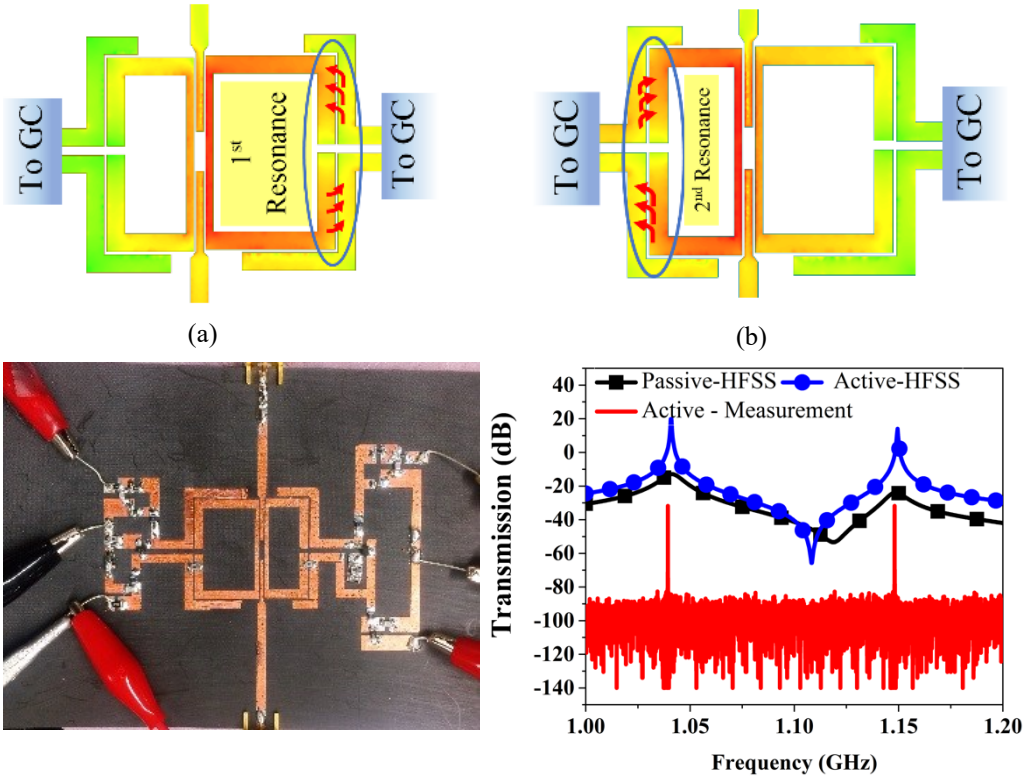

Fig. 4-1. Schematic of the sensor and relative surface current distribution depicted by arrows for 1st (a) and 2nd (b) resonances. (c) Comparison between active and passive mode of resonator. (d) fabricated sensor

minimized. Surface current distribution shown on Fig. 4-1(a, b) for the two resonant frequencies illustrate the corresponding loop. High level of miniaturizing could be achieved with simultaneous increase in equivalent capacitance and inductance of the SRR. Realization of lower resonances can be done using narrower strips where the current strength is maximal to enhance the inductance and wider strips where voltage is maximal to increase the capacitance [125].

4.1.1.2 Enhancing Q Using Active Feedback Loops

To increase the Q, two regenerative feedback loops, each consisting of a gain-controller (GC) circuitry is designed and added to the ring resonators as illustrated

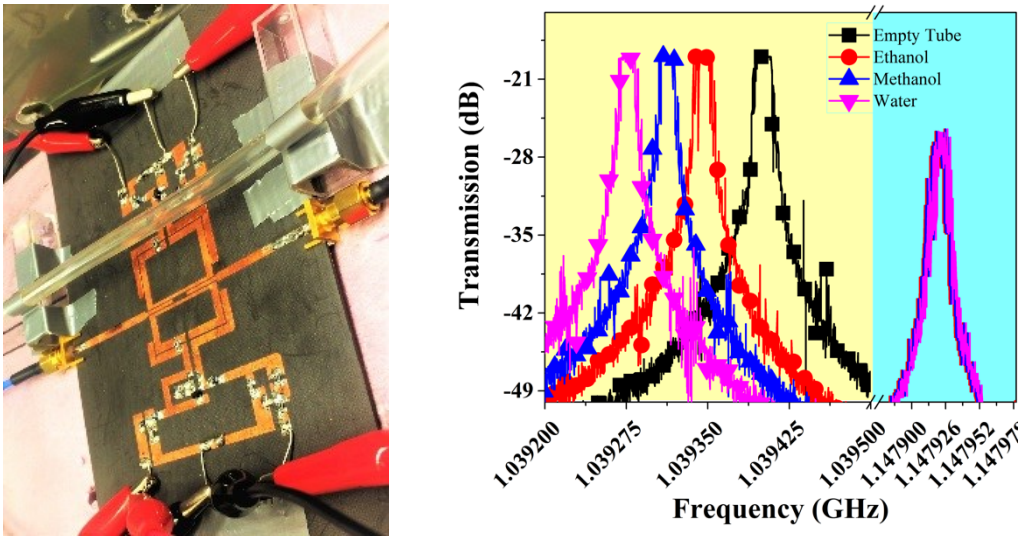

(a) (a)

Fig. 4-2 (a) Uncoupled resonances, (b) Experimental Configuration

in Fig. 4-1(a-b). The feedback loop compensates for the lost power of the circuit and enhances the quality factor [77]. Using such feedback loop, dual band ultra-high quality factor of 150k (at LF) and 210k (at UF) is designed. A comparison between the sensor's transmission response in both passive and active mode (Fig. 4-1(c)) in Full Wave simulation with HFSS shows a remarkable enhancement in quality factor (from 51 up to 150k and 54 up to 210k) which enables the sensor for highly accurate measurements where small variations require extreme sharpness in classifications.

4.1.1.3 Fabricated Sensor characterization

The proposed sensor has two uncoupled resonances exploited in sensing a material while changes in each resonance has no interaction with the other one. Fig. 4-2(a) shows the material sensing where the liquid flow is inside a PTFE tube of $^{1}/_{16}{}''$ diameter, with distance of 1 cm from sensor's surface over larger resonator

(Fig. 4-2(b)). It is clearly illustrated that by changing the material in the tube, the first resonant frequency shifts while the second one remains constant. This brings us to the conclusion that the second resonance variation can be used to calibrate the humidity and moisture impact out as explained in the next section.

4.1.2 Results and Discussion

Resonant frequencies of the sensor change when the effective permittivity of the environment (air or sand) undergoes a variation. Each resonator has been decoupled to represent exclusive behavior with respect to near-by ambient change. Relative humidity in air could change its permittivity [126], and similarly for underground sensing, variation in sand moisture could impact the sensor's results. The following will explain the material detection and linear subtractive method for both air humidity and sand moisture effect elimination.

4.1.2.1 Eliminating Humidity Effect and Linear Subtraction

Both of the two resonators respond to the environmental change in dielectric properties at the same time. Upper and lower resonant frequencies were recorded in presence of various RHs that exhibits infinitesimal effective variation in $\boldsymbol{\varepsilon_{r_{eff}}}$ (Fig. 4-3(a)). Because the resonators are designed to be uncoupled, the sensor has the ability to exploit the behavior of higher resonance (opted arbitrarily) in dealing with unwanted environmental effects such as humidity.

In order to cancel the humidity effect, the shifts in LF vs. UF are studied as calibration as shown in Fig. 4-3(b) where they show linear relation. During the measurement UF is used as a reference to eliminate the humidity effect on lower resonance accordingly. Residual sum of squares of LF for linear fittings of active and passive mode are 1.6e9 and 2.5e11 respectively. It is clear that the active sensor has more convergent behavior, due to the ultra-high quality factor of active mode.

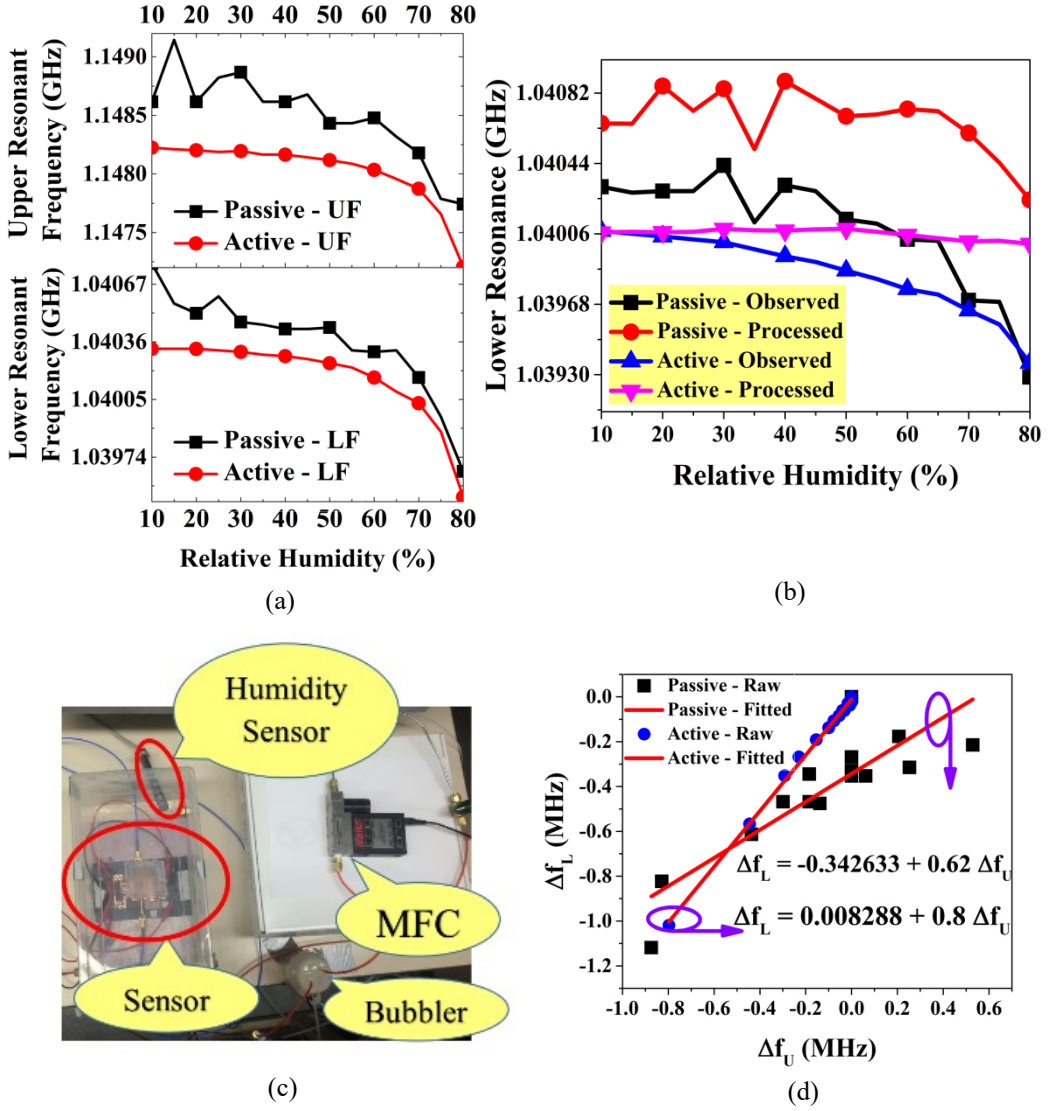

Fig. 4-3, (a) Humidity effect on both resonances in active and passive mode, (b) calibration curves, (c), (d) measured and processed frequencies

Experimental verification of the concept was done by tracking both upper and lower frequencies of the sensor in dealing with constant sample of water at 2-cm away the sensor's surface (Fig. 4-3(c)). Then the calibration data is used to make up the erroneous shifts originated from humidity, while the quality and quantity of material under the test was kept constant. The processed curve (Fig. 4-3(d)) shows considerably robust behavior in active sensor with mean square error (MSE) of 27k where the frequency noise is much less, while the curve in passive one, disappointingly shows much less capability in restoration after calibration with MSE of 169k. As a result, active sensor is a prerequisite for humidity-effect eliminating technique.

4.1.2.2 Eliminating Moisture Effect

When microwave sensors are used for underground microwave sensing and detection, the impact of the environmental inconsistency could be more significant. In this section, we illustrate that the proposed sensor can be used to eliminate such impacts. To show the concept, a schematic as shown in Fig. 4-4(a) is utilized that includes 3cm thick sand-cover with various moisture content (M %) with specific dielectric properties ($\varepsilon_r = 1.96208 + 0.4212M, \tan(\delta) = 0.06862 - 0.00313M$) [127] encapsulating a PTFE tube ($^1/_{16}{}''$ inner diameter) over the LF resonator. A finite-element method simulation suing HFSS© is performed while the tube carries materials with $\varepsilon_r = 10, 20, and\ 30$ and $tan(\delta) = 0.1$ where sand

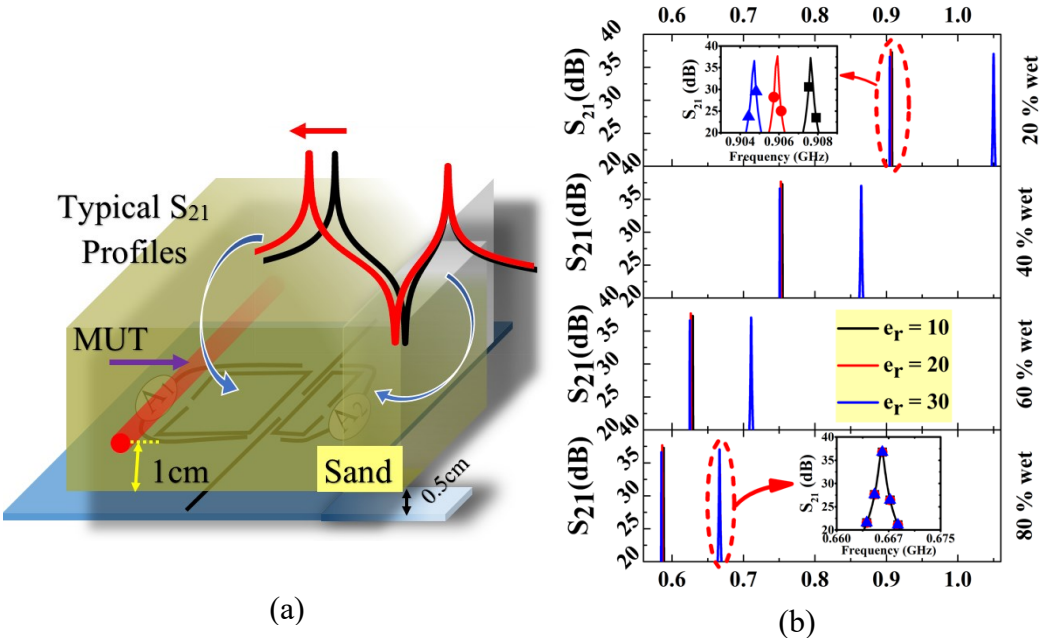

Fig. 4-4, (a) schematic of simulation , (b) modified view of frequency change based on humidity variation

moisture varies from 20% to 80% [127]. The sensor is 0.5cm elevated off the sensor's surface utilizing non-contact sensing feature of active sensors [75], [77], [128], [129]. From the results presented in Fig. 4-4(b), it is clear that the sand moisture can significantly impact the observed and readout frequency.

Experimental verification was done using the setup shown in Fig. 4-5(a) starting from dry sand covering the whole sensor. The change in environmental humidity is modeled using steps of 2ml water droplets that were spread uniformly over the sand and both upper and lower resonances were recorded. The materials under study, as ethanol, methanol and water were flowing inside a plastic tube over the resonator sensitive to the lower frequency and encapsulated in the middle of sand. For each measurement, the effective humidity of sand is changed and the materials are injected into the tube and the measured data was recorded. Raw data

for LF is presented in Fig. 4-5 illustrating a downshift of the resonant frequency for each sample by increasing the moisture content which is also expected from the simulation. It is clear that the moisture impact is significantly more that the sample variation and can easily influence the readout data.

To post-process the results using the second resonant peak of the sensor, the same technique as explained in section 4.1.2.1 is used. A calibration curve is extracted and the measuring results are calibrated. The results after calibration are presented in Fig. 4-5(b) depicting a robust behavior and a constant response for different sand moisture content.

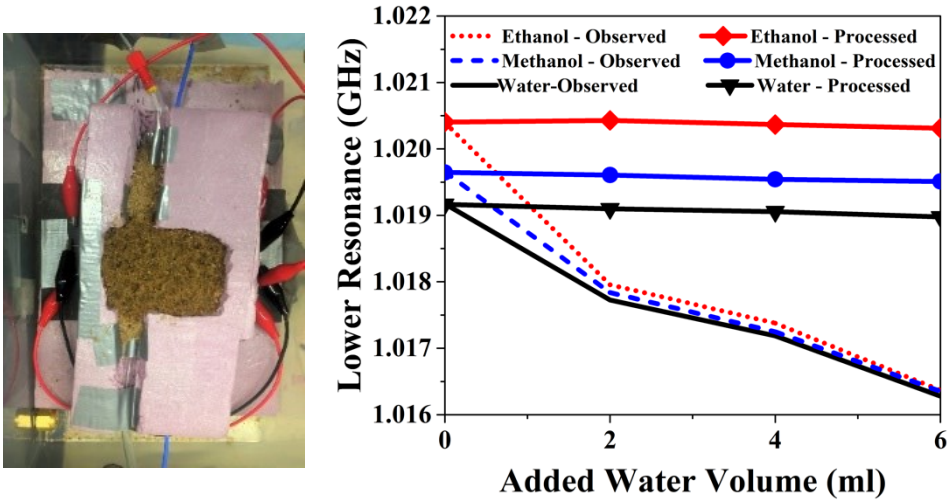

(a) (b)

Fig. 4-5, (a) experiment setup, (b) measured and processed data

4.2 Dispersion Coefficient Measurement of Nano-Particles [130]

Asphaltene is dissolvable compound in petroleum fluids, extracted as a result of precipitation from adding *n*-Heptane, *n*-Pentane, *etc.* Asphaltene particles are refractory, and can separate from crude oil due to abrupt variations in temperature, pressure, and composition, and may cause clogging in reservoirs and pipelines, which leads to extra maintenance expenses. These properties of Asphaltene affect the petroleum processing, from production to refining stages of oil. Moreover, in categorizing the porous and bulky phases of materials, it is necessary to obtain information about their physical size and shape [131], [132]. On larger scale, hydrodynamic properties, such as the diffusion coefficient, sedimentation velocity, and intrinsic viscosity are employed to determine the macroscopic characteristics of biological molecules in solution [133].

A thorough understanding of physical behavior of these Nano particles such as size, structure, diffusion, *etc.* is required to cope with *in-situ* deposition of Asphaltene in process equipment, reservoirs, *etc.*, and to optimize the processing unites accordingly [132]. Previously, several methods were used to identify the Asphaltene molecule flocculation, knowing that this information is site-specific and depend on the method of extraction. Leontaritis *et. al*.[134] have proposed methods to describe Asphaltene flocculation in concordance with Nellensteyn's view of crude oil as a colloidal system [135]. Recently Rajagopal *et. al.*[136] proposed polydisperse flocculation model to predict the size of Asphaltene particles.

Different techniques used for determining the particle size and flocculation of Asphaltene include fluorescence polarization [133], [137] while transmission of linearly polarized light through the material is analyzed. In addition, light scattering technique is mostly used, because its light beam doesn't destroy/ disturb the sample. The downside of these methods is the need for transparent communication between the light-emitter and the material under test that doesn't allow for opaque system. However, studies of photon correlation spectroscopy (PCS) adapted to opaque systems are published by Yudin *et. al.*[138], yet a very laborious and expensive method.

In all these models, it is emphasized that the average of particle size and diffusion coefficients strongly depend upon Asphaltene concentration and composition [139], [140].

In this chapter, we propose to use microwave sensing for such measurements in order to deal with opaque environment. In such technique there is no need for perpetual cleaning of sensing windows and maintenance expenses [141].

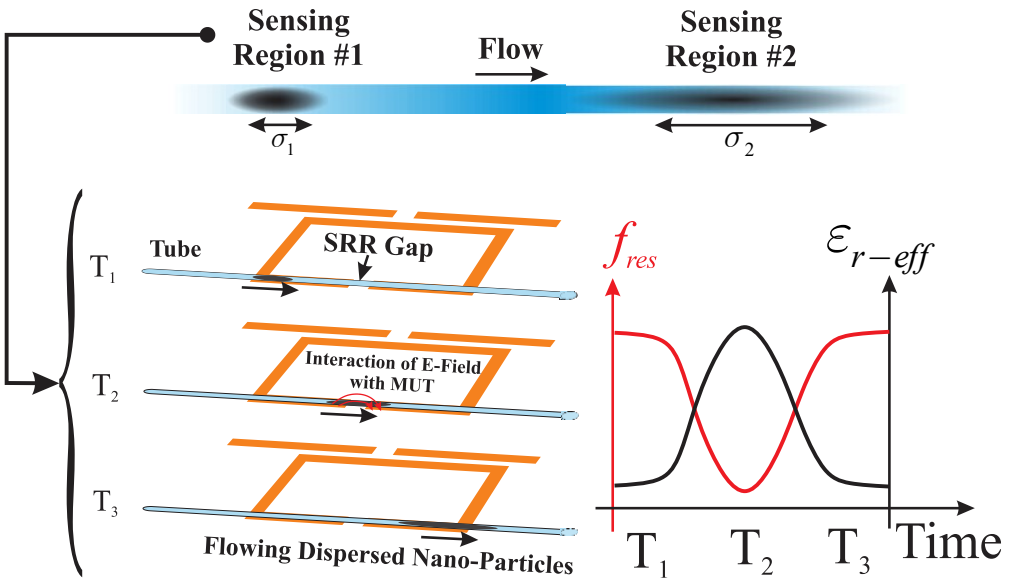

Fig. 4-6, Two-window solution of Asphaltene's dispersion in *n*-Heptane using split ring resonators

Since the resonant frequency of the sensor is strongly dependent on the environmental permittivity variations, it is used to characterize the materials' permittivity. A microwave resonator with two resonant frequencies is developed to measure the dispersion coefficient according to the concept presented in Fig. 4-6. Both resonators are armed with active feedback loop creating extra high Q resonant profiles. The sharp resonances of dual active sensor in this study are used to monitor the physical properties of Asphaltene when a sample of oil (Asphaltene-in-Toluene) is mixed with a precipitant element (*n*-Heptane here). Extraction of the diffusion and dispersion coefficients of Asphaltene from Taylor-Aris dispersion analysis [142] requires two windows to monitor the mixture's flow as shown in Fig. 4-7. Each one of SRR-based dual active resonators acts as a single sensor in monitoring the fluid in a unique configuration. The dispersion coefficient is calculated from the shifts in the resonance frequencies of the two resonators. When

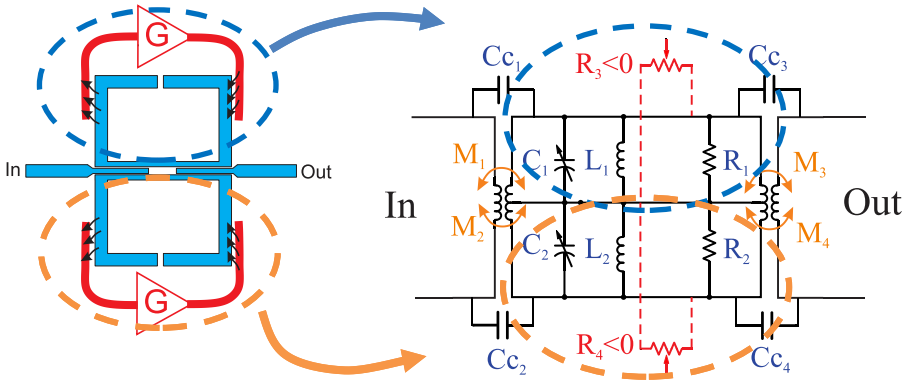

Fig. 4-7, Electric circuit equivalent of dual active resonator

short plug of model oil is injected into flowing *n*-Heptane, the localized effective permittivity during the time with precipitation, resulting into two time-based profiles that are distinctly different.

4.2.1 Theory of Measurements

The diffusion of liquid-based solutions can be determined using the information at two states of the flow during the transmission. Once the spread of the solute could be realized at a certain location, it should be repeated in another known location such that the combination of these two measurements give enough information about the diffusibility of the solute inside the solution. An extensive method that explains the whole scenario in this regards is called two-window solution, which is based on Taylor dispersion analysis given in the Appendix A. In summary, the diffusion coefficient k can be computed from the following expression:

$$k = \frac{u^2(\sigma_2^2 - \sigma_2^2)}{2(t_2 - t_1)} \tag{7}$$

where $\sigma, u, and\ t$ are Gaussian-variance, average speed, and the timings of the two successive measurements during the spreading in flow.

Each sensor consists of an SRR that is an electrically small resonator in folded configuration to achieve a compact size. The resonance frequency (f_r) of the SRR, which depends on the electrical length of the microstrip line, is highly impacted by variations in ambient effective dielectric constant (ε'_{r_eff}) as follows [141]:

$$f_r = \frac{1}{\sqrt{\varepsilon_0 \varepsilon'_{r\_eff} \mu_0}} \frac{1}{2l} \tag{8}$$

where l is the length of the resonator, and ε_0, μ_0 are permittivity and permeability of vacuum, respectively.

A finite sample of Asphaltene-in-Toluene is injected as an impulse into the ever-flowing HPLC grade *n*-Heptane (C_7), and started into precipitation and dispersion. A mixture of several species (solutions, suspensions, electrolyte, *etc.*) represent mixed properties of its constituents. For one, Asphaltene is Nano-colloidal suspensions of crude oil in toluene. First, dielectric properties of only oil sample is discussed. Real and imaginary part of the dielectric constant in a suspension can be calculated if the induced dipole for suspended inclusion is known based on Delacey and White theory as follows [143]:

$$\boldsymbol{\varepsilon'(\omega) = \varepsilon'_s + 3\phi\varepsilon'_s \left[C_1(\omega) - \frac{K^\infty}{\omega\varepsilon_0\varepsilon'_s} C_2(\omega)\right]} \tag{9}$$

$$\varepsilon''(\omega) = 3\phi\varepsilon'_s \left[\frac{K^\infty}{\omega\varepsilon_0\varepsilon'_s}\big(C_1(\omega) - C_1(0)\big) + C_2(\omega)\right] \tag{10}$$

where ϕ is the volume fraction of solids, ε'_s and K^∞ are dielectric constant and DC conductivity of the host medium, and C_1 and C_2 are the real and imaginary of

induced dipole coefficient (for Asphaltene can be found in [14]), respectively. Here, not only the permittivity of the inclusions and the host medium should be considered separately, but also the volume of liquid that is being substituted by solid particulates is of great importance. It should be noted that reducing the external inclusion in the mixture (with high ε_r') decreases the effective (and inhomogeneous) permittivity of the mixture.

Next, the dielectric constant for the mixture of several fluids (here toluene and heptane) should be determined. For single fluid, the dielectric constant is related to its polarization per unit volume, p, as follows [144], [145]:

$$p = \frac{(\varepsilon - 1)(2\varepsilon + 1)}{9\varepsilon} \tag{11}$$

and for mixture of several fluids, with constant temperature and pressure during mixing, Oster's rule [146] applies in evaluating the polarization of the mixture. Having said that, polar-nonpolar mixture of toluene-heptane would need to account for the change of the correlation between neighboring molecules due to mixing, then, leads to the following mixing rule [146]:

$$p_m = \frac{\sum_i^n \sum_j^n x_i x_j (vp)_{ij}}{\sum_{i=1}^n x_i v_i} \tag{12}$$

where

$$(\boldsymbol{vp})_{\boldsymbol{ij}} = \frac{\mathbf{1}}{\mathbf{2}}\left(\boldsymbol{v_i p_i} + \boldsymbol{v_j p_j}\right)\left(\mathbf{1} + \boldsymbol{k_{ij}}\right) \tag{13}$$

and k_{ij} is a parameter determined from the dielectric constant data for the binary system *i-j*, and x_i, x_j are mole fraction of component *i,j* and p_i, p_j are polarization of pure component *i,j*.

Therefore, it is expected that by monitoring the resonance frequency of the sensor, affected by the permittivity variation in the liquid, one can characterize the mixture using the Gaussian type profiles in the response as shown in Fig. 4-6. In this paper, monitoring such mixtures is done using high quality factor active microwave sensor that is able to instantly follow the variations in the environment, *i.e.* the mixture under test, in a non-contact mode. The inverse-square relationship between ε'_{r-eff} and f_r of Eq. (8) is depicted in Fig. 4-6 over time. In presence of the precipitated Asphaltene Nano particles, each one of the active resonators will experience a downshift in f_r due to increased ε'_{r-eff}, while a reasonable physical separation between them would result in different profiles of downshift that ultimately help resolving Eq. (7).

4.2.2 Dual Resonant High Quality Factor Sensor Analysis

4.2.2.1 Simulation

Planar resonator sensors are privileged of non-contact sensing due to their microstrip structure, allowing electromagnetic power to radiate into space and penetrate into the desired objects. Conventional passive sensors have been used in sensing applications for the past two decades, however, their low resolution, due to low-to-moderate quality factor, would restrain getting into sensing minute variations in highly sensitive measurements. Recently, this issue has been successfully addressed with the advent of active resonators as a means used for increasing the quality factor drastically by removing the loss of the sensor [2], [12],

[69], [70]. Introduction of active feedback loop around the passive resonator is embodiment of negative resistance.

Two-window solution of the problem, needs two sensors mounted in distance from each other, hence a dual resonator is designed with identical resonators in parallel as shown in Fig. 4-6 with geometrically different sizes to achieve slightly different resonance frequencies. The electric circuit model of each SRR is a parallel RLC network, where R, L, and C are resistance, inductance and the capacitance of the sensor, respectively. Single transmission line as input and output of both resonators, is coupled with electrically (denoted as C_{c1}, C_{c2}) and magnetically (denoted as M_1 and M_2) as shown in Fig. 4-7. This model is verified by Ansys Electronics (HFSS) in passive mode as shown in Fig. 4-8(a) with two resonances at 1.03, 1.149 GHz. The two resonances correspond to the two microstrip resonators with lengths of 78 and 66 mm that both have the same gap of 1 mm and are located in 0.4 mm proximity of I/O transmission lines. All widths measure 2.4 mm, except the coupled region with 1mm thickness, to have the best matching and excitation of SRRs, respectively. The electric field distribution over the surface of the resonator is shown in Fig. 4-8(b-c) at resonances. It shows that the gaps host maximum electric energy concentration, whose perturbation would affect the resonance frequency more significantly than other places, hence this area is chosen for sensing purposes. In addition, a typical enhancement of quality factor is sought after using the active feedback loop in HFSS (Fig. 4-8(a)), which shows remarkable improvement in the sharpness of the transmission profile. The reason for utilizing active circuitry in the resonator design is to overcome the moderate quality factor

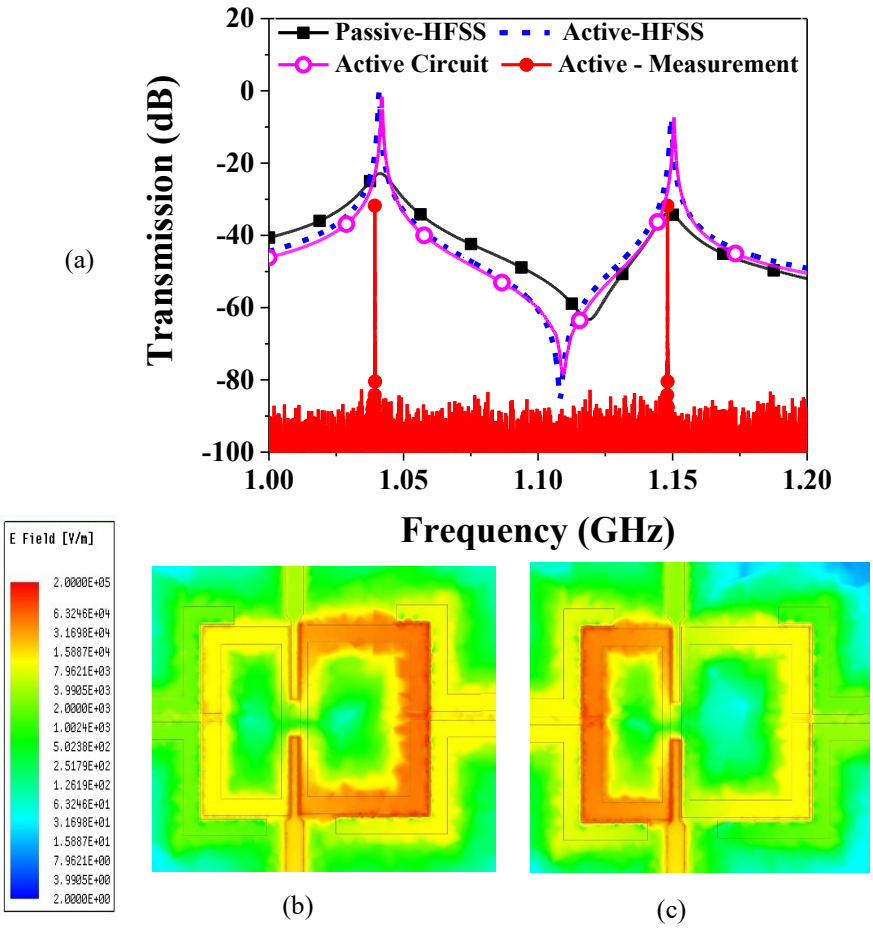

Fig. 4-8, (a) simulation of dual resonator in HFSS and its confirmation with ADS in Circuit model, comparison of active and passive mode or resonators, and active resonator measurement, (b) E-field distribution at f_L= 1.03GHz, (c) E-field distribution at f_H= 1.149GHz

of *Q=200* that become a setback in very sensitive experiments, including detection of minute variations in permittivity values, sensing extremely small volumes of sample under test, distant sensing in non-contact mode, *etc.* Simulations confirm that the quality factor could be enhanced over 3k in microstrip technology that improves the resolution of main resonance frequency by orders of magnitude. Please note that the active circuit is responsible to compensate the losses in the system (from many sources such as dielectric loss, conductor loss, radiation,

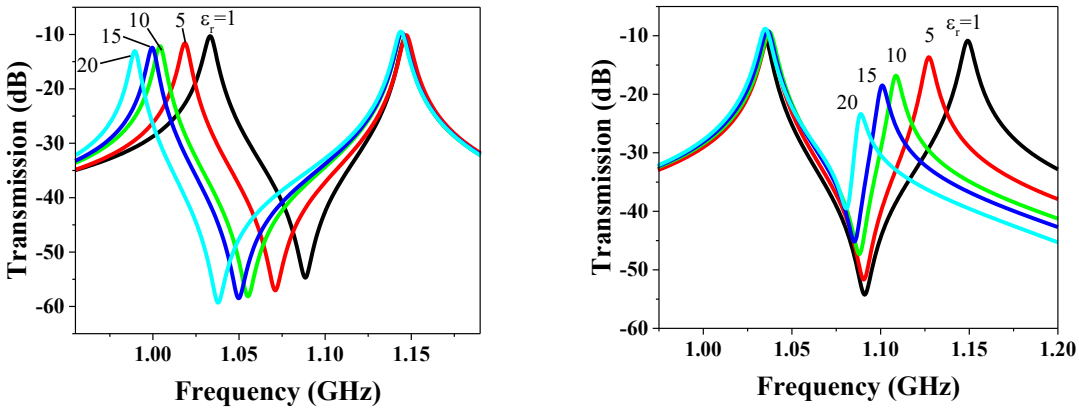

Fig. 4-9, Independent Sensing on the resonators, with MUT on SRR with (a) f_L and (b) f_H

mismatching, *etc.*) in a controlled manner, such that with introduction of any lossy environment to the sensor's vicinity, it can be re-adjusted to maintain its ultra-high quality factor. To this end, a gain-controller unit is designed using a transistor as an amplifier that provide arbitrary negative resistance for the SRR. Simulation of the active circuit using circuit model of Fig. 4-6 is shown in Fig. 4-8(a), which is in great agreement with HFSS results in both predicting the peaks and the notches.

Independent Sensing- The SRRs possess highly sensitive regions around the gaps, distinguishable in Fig. 4-8(b-c), which are best for sensing applications. The gaps are located away from the input/output transmission lines to have independent regions for sensing, as can be observed by comparing the E-field distribution in the resonant and non-resonant SRRs. Moreover, a simulation of the dual resonator (passive) is conducted in HFSS with a cubic material of size $4\times 2.4\times 2\, mm^3$, identically located on the gaps, to examine the resultant variations in resonant frequencies. Relative permittivity values cover the range of 1-20 as shown in Fig.

4-9(a-b). It is evident that the change in the resonances are independent, since the gaps are far away from each other.

4.2.2.2 Fabrication

The planar sensor is fabricated similar to the schematic of simulations on 0.8 mm thick Rogers5880 substrates with $\varepsilon_r' = 2.2, tan(\delta) = 0.0009$ (5(a)). The transmission lines are etched from a patterned substrate using etching bath of aluminum persulfate (see Fig. 4-10(a)).

The gain controller in active circuitry is composed of a low-noise transistor NE68033 as an amplifier and its gain is controlled by its driving voltage, hence the

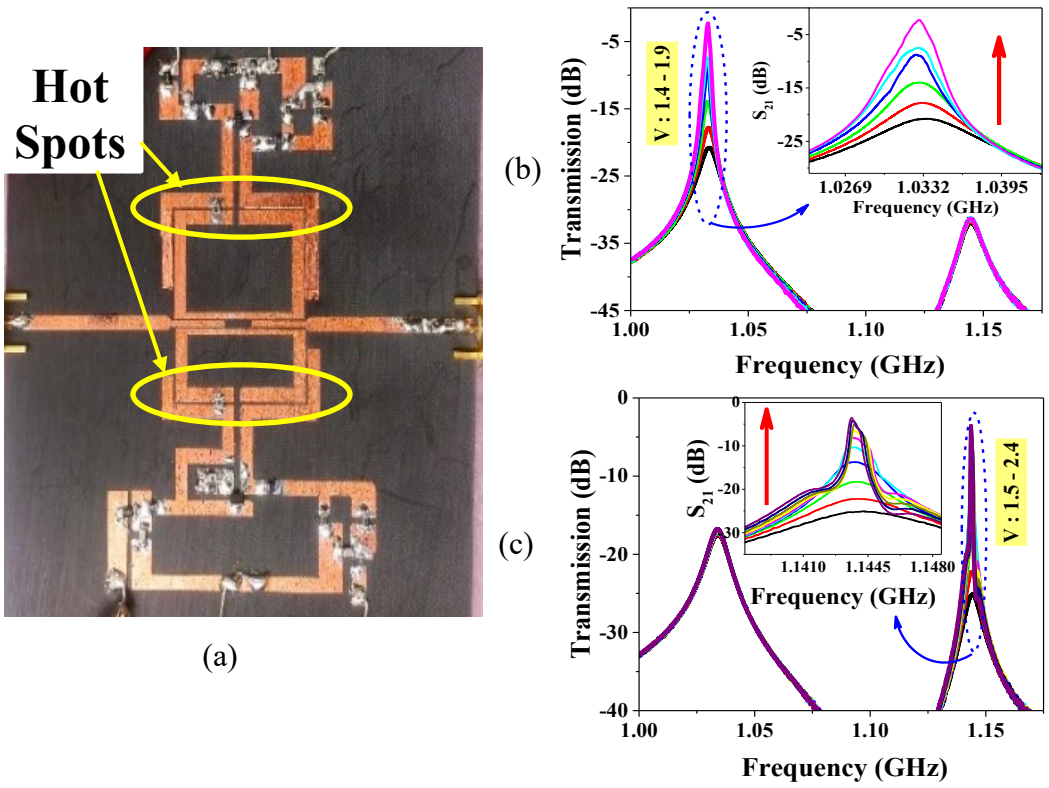

Fig. 4-10, Fabricated sensor, (b) Quality factor improvement in f_L, (c) Quality factor improvement in f_H

collector current. The resonant frequency of the operation considers the gain limitations of the transistor (suitable for less than 3 GHz), and is arbitrarily chosen to be at ~1GHz for better frequency domain stability of the sensor. Fig. 4-10(b-c) demonstrates change in the transmission profiles of the resonators when the driving voltage V is varied with 0.1 V increments. Controllable sharpness in the inset of S_{21} profile confirms its behavior as an active resonator, which arbitrarily compensates loss of the sensor. Having said that, the improvement in the resolution is only on single resonator to affirm their independent functionality.

Considering the independent behavior of the SRRs, the sensor is used to quantify the dispersion factor of Asphaltene in *n*-Heptane as follows.

4.2.3 Dispersion Characterizing Results

The fabricated dual active resonator has two main hotspots, each on a different and uncoupled SRR. These sensing regions are two windows needed for the two-window solution discussed in section 4.2.1. In order to have repeatable and more accurate response of sensing, a microfluidic PTFE tube with inner radius of 0.8 mm is used to carry the fluids. Schematic of the tube's configuration over the SRRs is shown in Fig. 4-11(a). Since the effective permittivity of the sensor depends on the relative position of the tube on it, hence the tube is designed and attached permanently to the surface of the sensor, based on which that next measurements and calibration will take place. The tube is extended enough after the first SRR to provide a reasonable distance in time for the resonators to identify two considerably different Gaussian profiles as shown in Fig. 4-6.

Two syringe pumps are utilized to inject the fluids, one continuously pumping the *n*-Heptane, and the other, infusing short pulses of Asphaltene-in-Toluene. The two fluids join in a *T* intersection and start to pass through the tube following the ever-flowing *n*-Heptane fluid. The Asphaltene as presumably considered to be the part of crude oil dissolved in toluene experiences a different state when mixing with the non-polar *n*-Heptane, since the latter behaves as precipitant element. Therefore, the Nano particles are extracted from the solvent, and start fluctuating due to their highly polarized nature and mutual interactions. The small grains stick together and form larger Nano-aggregates of Asphaltene, and continues to develop into clusters of larger dimensions. This extraction process is a time-based phenomenon that is happening while the Asphaltene infusion is in flow by the host fluid (*n*-Heptane). Direct result of the continuous flow is the *spread* of the infusion along the carrying capillary to form a Gaussian type spatial profile according to Taylor's dispersion

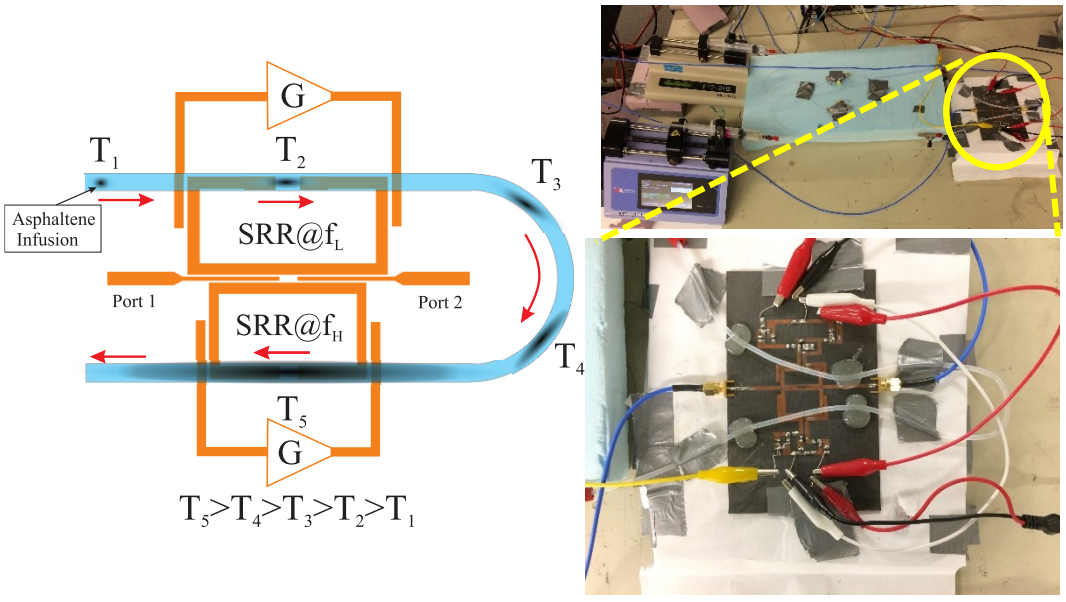

Fig. 4-11, Schematic of the , and (b) experimental test setup for dispersion characterization

analysis [142]. Timings of T_1-T_5 are conceptually depicting the variations in the Gaussian profile during the flow as shown in Fig. 4-11(a). It is visually clear that the second SRR meets the Asphaltene infusion with larger spread-width and less central concentration. Since the two SRRs are independent in sensing paradigm, the variations in the frequency response of the individual resonators account only for the permittivity-fluctuations in their vicinity and not being impacted by the other resonator or permittivity variations elsewhere, as confirmed by Fig. 4-9.

Permittivity of the Asphaltene-in-Toluene liquid is modified by the concentration of Asphaltene (with permittivity of $\sim$5[105]) in volumetric content of toluene (with permittivity of $\sim$2.4 [147]), hence larger concentrations would result in higher dielectric constants of the suspension.

In fluidic view of permittivity variation in this experiment, the whole process is comprised of the following steps. First, the axial spread of the solute along the direction of the flow is known as *convection*, which its continuity results in an asymmetric concentration distribution of the solute over the length of the capillary. While, *diffusion* is considered to be the transfer of the solute molecules from higher to lower concentration regions. The high concentration of molecules at the capillary center with respect to its walls leads to radial diffusion. This effect in combination with convection, allowing the injected Asphaltene to distribute symmetrically, is known as *Taylor Dispersion*, whereas accounting for additional assumption of axial diffusion is suggesting Taylor-Aris dispersion analysis.

The flow rate for the host medium is 1.75 mm^2/sec inside the microfluidic capillary, and is kept constant during the experiment (Fig. 4-10(b)). The two SRRs

of dual active resonators are in high-resolution mode to detect the variations in the permittivity with high accuracy (see red line in Fig. 4-8(a)). Several samples of Asphaltene-in-Toluene, within a wide range of concentrations of 0.000625, 0.004375, 0.025, 0.1875, 0.625 (% v:v) Asphaltene : Toluene are prepared and measured. It should be noted that the length of the tube is designed large enough to have distinct variations during the flow, such that the SRR with f_L monitors the flow firstly (*T2*), and the second one with f_H follows it around 100 seconds later as 2nd window (*T5*) using a data recording rate of 5 seconds with LabVIEW program. Diffusion and dispersion of the samples are analyzed using Taylor-Aris dispersion. For lower concentrations, the effective permittivity of oil-sample is less different from the host *n*-Heptane, however, the small size of clusters being formed after

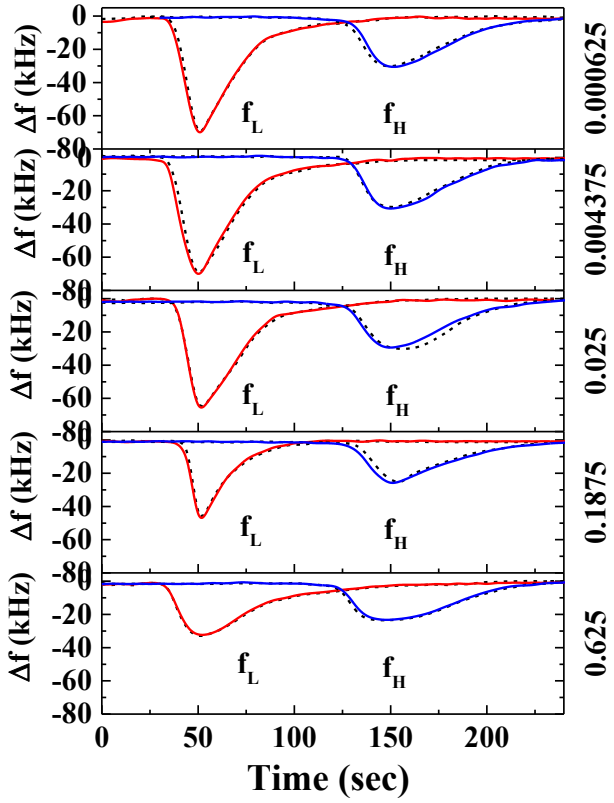

Fig. 4-12, Resonance frequency shifts of dual active sensor in two distinct spots of tube with 100 seconds difference

precipitation is found not suitable for axial convection, thus tend to inhabit in the areas close to the wall allowing for the host fluid to flow. In this case, the effective permittivity variation due to infusion of oil-sample would seem large and the frequency of resonance considerably shifts to lower values as shown in Fig. 4-12. On the other hand, larger clusters as a result of higher concentration in oil-sample,

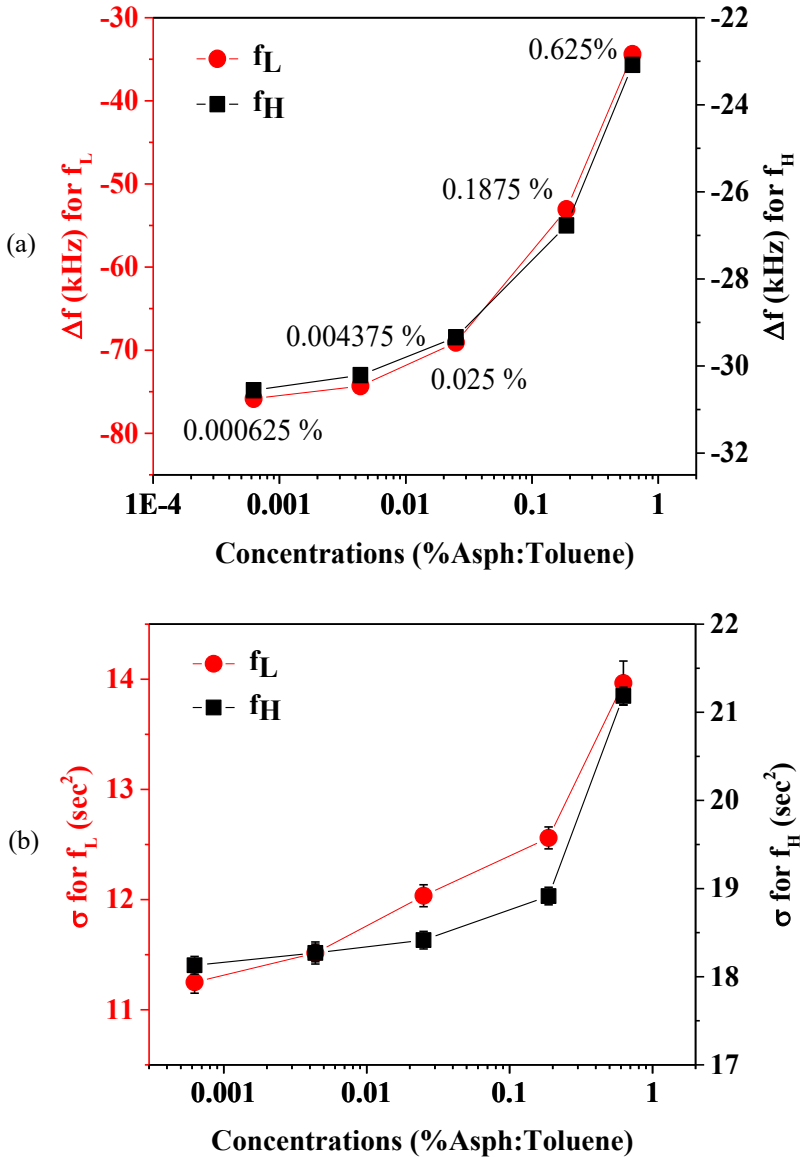

Fig. 4-13, (a) maximum frequency shift and (b) variances of the profiles shown in Fig. 4-12

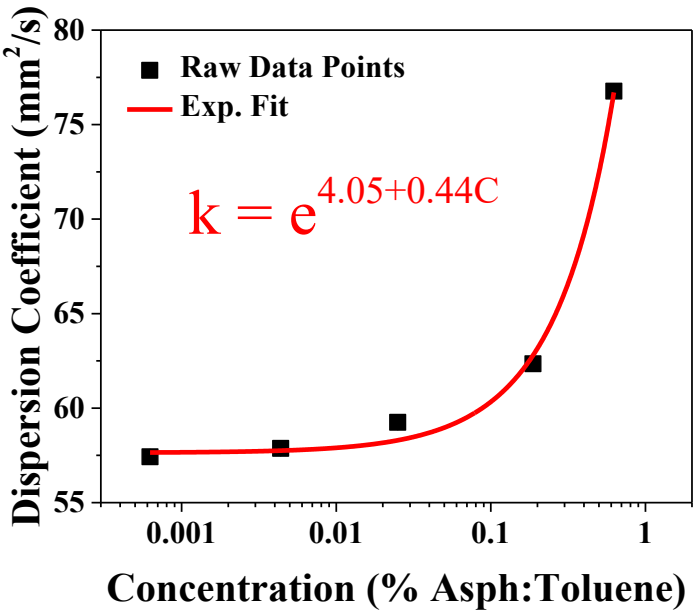

Figure 4-14, Dispersion coefficient of the Taylor-Aris Analysis

would be easily flushed by the host flow not to block the stream, hence these vastly spreading samples cause f_r to undergo less variation (see Fig. 4-6). The maximum change in f_r is extracted for each sample on a single SRR and plotted in a logarithmic scale to present the whole range of concentrations in Fig. 4-13(a). It is shown that the higher the concentration the less the changes in the resonance frequency, as expected due to fast dispersion in the host liquid. This graph can also be a representative of the concentration characterization for the samples. In addition, mapping Gaussian profiles with the downshifts of resonance frequency enables us classify them using their spread-width that can be evaluated by their corresponding variances (σ^2). It is evident that the 2nd sensor can visualize the spread in a wider bandwidth since the time spent for the core of the Asphaltene infusion to pass from the 1st sensor to reach the 2nd is almost 100 seconds, long enough to allow for the dispersion and diffusion to happen. Exploring Fig. 4-12 one

can find the general decrease in maximum shifts of f_r for 2nd SRR (blue line f_H) compared with the corresponding ones in 1st SRR (red line f_L) in each sample oil, which shows that dispersion is a time-based phenomenon and gradually lowers the concentration of oil sample at its center, pushing it outwards. Larger values of variances (Fig. 4-13(b)) and frequency shifts for samples with higher concentrations, are consistently expected as discussed. The dashed lines in Fig. 4-12 show repetition of the test, which implies a repeatable experiment and the acquired data is reliable.

The dispersion of Asphaltene in *n*-Heptane can be evaluated using Eq. (7) and the data for the variances in Fig. 4-12 as plotted in Figure 4-14. It represents that samples with higher concentrations of Asphaltene disperse more in the flow, as expected, and it has a consistent trend for the whole range of concentrations. The experimental points are fitted with an exponential expression with R^2=0.99:

$$k = e^{4.05+0.44C}\ [mm^2/s] \qquad (14)$$

where C is the concentration of sample oil in toluene. Using this data and the viscosity information of the sample (not conducted in this work) one can find the hydrodynamic radii of the Asphaltene molecules in the sample using Eq. (7).

In order to verify the validity of the Eq. (7) in this analysis the following conditions should hold as follow [148]:

i) Longitudinal molecular diffusion must be negligible compared with the dispersive effect:

$$D \ll \frac{r^2u^2}{12D}$$

ii) $\left(\frac{r^2 U}{D}\frac{1}{x}\right)$ must be small

Combining (i) , (ii) to be satisfied simultaneously it can be shown that [148] :

$\frac{2x}{r} \gg \frac{2ur}{D} \gg 6.9$

which in our case $x{\sim}350\,mm, r = 0.8\,mm, u = 1.78\frac{mm^2}{s}$ (see Eq. (4)). The diffusion coefficient *D*, extracted from Fig. 4-13, is in the range of [5.2 - 7] $10^{-4} mm^2/sec$, in great agreement with typical values in the literature [133]. With these value for D, $\frac{2x}{r} = 875$, and $\frac{2ur}{D}$>4000 that validates the experiment.

4.2.4 Conclusion

This chapter summarizes our developments on double resonant microwave sensor. Two specific application of that is highlighted for moisture and liquid measurements.

Initially, a new double uncoupled resonators that are backed by two gain-controller circuitry in order to achieve a very high quality factor response. Two resonant frequency peaks with quality factors of 150K and 210K are measured and their uncoupled behavior is examined. Extremely high quality factor of such sensors enables non-contact measurement, which in return makes them susceptible to the environmental condition such as moisture or humidity. It has been illustrated that using double resonant structure, these unwanted parameters' influence can be cancelled and the effect of the sample under test monitored accurately.

In the second part of the chapter, dispersion coefficient of Asphaltene Nano-Particles is explored using dual active resonator sensor as a two window solution.

Two SRRs are used in parallel as the sensing elements that can independently monitor the flowing fluids inside a capillary. Mixing the Asphaltene-in-Toluene samples with *n*-Heptane as the precipitant element, helps the Asphaltene Nanoparticles to exit from the solvent and gradually disperse along the host flow with Gaussian asymmetric distribution. This physical change in the mixture impacts on the effective local permittivity since Asphaltene is high in ε_r compared with *n*-Heptane. The carrying capillary is designed long enough to pass both sensors with considerable time difference such that each SRR records the variation in the permittivity of samples in two distinctly difference Gaussian profiles. Employing Taylor-Aris dispersion analysis, the dispersion coefficient of Asphaltene samples are extracted that can be later combined with the viscosity information of samples to extract the hydrodynamic radii of Asphaltene Nano particles.

Chapter 5

Compelling Impact of Mixing Behavior of Active Sensors on Sensitivity Enhancement

In this chapter, the sensitivity of microwave planar sensors are considered to be the main attention. Single side access of the sensor to MUT reduces its sensitivity, and it gets worse as the distance between them increases. For active microwave sensors to compete with other existing technologies such as electrochemistry, the sensitivity should be improved [11], [48], [149]. Despite active microwave sensor's excellent potential in dealing with so many fine sensing paradigms, significant improvement in its sensitivity remains, yet, a moot point in the literature.

In order to compensate for this short-coming in planar sensors, mixing behavior of oscillators are proposed, for the first time, such that the intermodulation of the signals from the sensor and another reference signal, results in multiplying the variations in the MUT. The magnification of minute changes in the concentrations is depicted in a novel sensor accompanied with a wireless communication scheme. The detailed information about this is given in the paper,

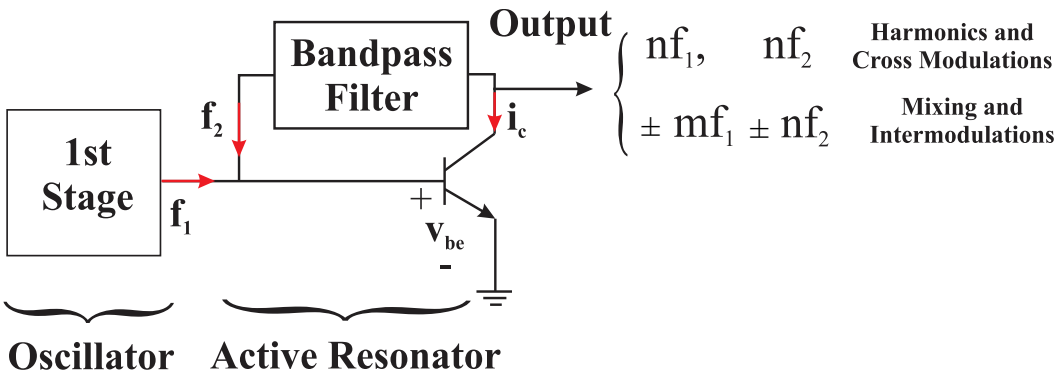

Fig. 5-1, Mixing/Intermodulation using double stage Active Resonator

entitled: "**Compelling Impact of Intermodulation Products of Regenerative Active Resonators on Sensitivity**". [In Press at IMS2017, Honolulu, Hawaii].

5.1 Sensitivity Enhancement Using Intermodulation Products

Here, we propose a new approach to enhance the sensitivity for multiple times. It is shown that using intermodulation (IM) products of two tones, thanks to the transistor's nonlinearity (Fig. 5-1), one can achieve significantly larger sensitivities.

Combination of a two tones (one from sensing element, another is arbitrarily fixed) produces intermodulation products that *multiples* the variations in frequency of the sensor (Δf), just as nΔf, n: 2, 3, …. It is shown that regenerative active resonators have the capability of producing such intermodulation products.

This chapter presents the design and measured data for a two-stage sensor, including sensing oscillator and an active resonator. Since sensors are highly utilized for growing market of Internet of Things (IoT), the proposed sensor is

integrated with a pair of antennas and wirelessly communicated. It is shown that the suggested design has significantly higher sensitivity than conventional type of DSRR-based elements. This chapter starts with the principle of operation (Sec. 5.2), continues with sensing results and explanation in Sec. 5.3. and concluded in Sec. 5.4.

5.2 Principle of IM products as a Novel Tool for Enhancing the Sensitivity

For the configuration shown in Fig. 5-1, assume that the exiting signal of the first stage is $A_1\cos(\omega_1 t)$, where $\omega = 2\pi f_1$. The second stage is an active resonator at f_2 with a compensating feedback loop [2], [12], [150]. For lower gains of the feedback loop, the insertion loss due to the circuit and the environment is compensated with increasing the quality factor. As the gain further increased, along with enhancing loaded Q of the circuit, an oscillatory tone is also added to the output [151], which is at f_2 as $A_2\cos(\omega_2 t)$. Impact of these waveforms at the output current of the 2nd stage (Fig. 5-1), i_c, is expressed as follows:

$$i_C(AC) = I_S\left(e^{qv_{be}/\eta KT} - 1\right) \tag{15}$$

where $I_S, q, \eta, K, and\ T$ are device saturation current (A), electric charge (1.602×10^{-19}C), ideality factor ($1 < \eta < 2$), Boltzmann's constant (1.38×10^{-23}J/K), and temperature (K), respectively, and

$$v_{be} = A_1\cos(\omega_1 t) + A_2\cos(\omega_2 t) \tag{16}$$

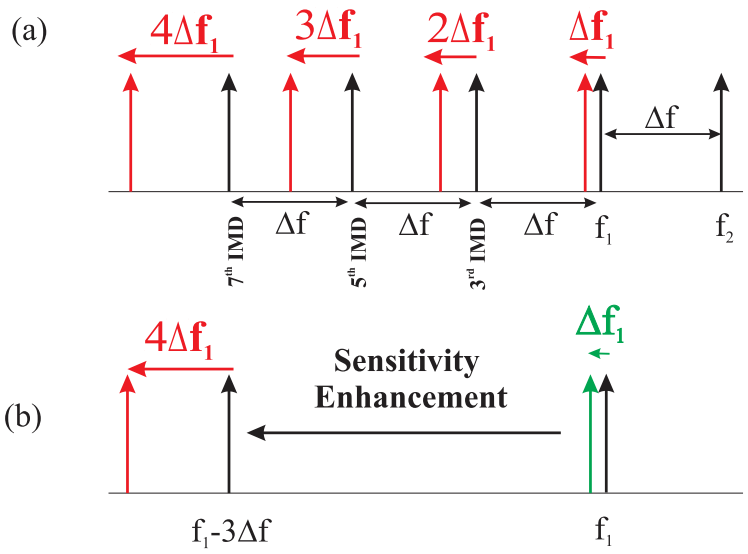

Fig. 5-2, IM products of two stages (b) Increased sensitivity at 7th IM (red) compared with main oscillating frequency (green)

Taylor expansion of the exponential term can be written as follows:

$$e^{v_{be}/V_T} = \sum_{n=0}^{\infty} \frac{1}{V_T{}^n n!} \left(A_1 cos(\omega_1 t) + A_2 cos(\omega_2 t) \right)^n \tag{17}$$

which implies that higher order components of $\omega_1 \& \omega_2$, called "cross/inter-modulation", will be generated due to non-linearity of the transistor. Equation. 17 is composed of:

$$v_{be}^n = \sum_{k=1}^{n} \binom{n}{k} \left(A_1 cos(\omega_1 t) \right)^k \left(A_2 cos(\omega_2 t) \right)^{n-k} \tag{18}$$

These higher order by-products of $\cos^k(\omega_1 t)\cos^{n-k}(\omega_2 t)$ include the frequency components of $\cos(\pm k\omega_1 \pm (n-k)\omega_2)$ t. In other words, some of the IM components are located at $2f_1 - f_2 = f_1 - \Delta f, 3f_1 - 2\Delta f = f_1 - 2, 4f_1 - 3f_2 = f_1 - 3\Delta f$, …, where $\Delta f = f_2 - f_1$ (see Fig. 5-2(a)). Whereas these components cause distortion in communication application, are found interestingly appealing for sensing applications. This is due to the fact that the variations in the sensing frequency (f_1) is magnified as $2\Delta f_1, 3\Delta f_1, and\ 4\Delta f_1, \ldots$, so that the first

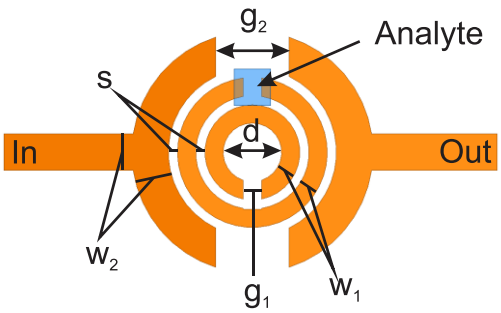

Fig. 5-3, DSRR as sensing element with dimensions in [mm]: d=3.2, g_1=1, g_2=4, s=0.5, w_1=1, w_2=2

stage (as sensing element) is shifting only as Δf_1 (green in Fig. 5-2(b)), while the 7th IM is changing by $4\Delta f_1$(red in Fig. 5-2(b)), a behavior that reflects a compelling impact on sensitivity due to mixing behavior of 2nd stage.

5.3 Theory and Analysis

5.3.1 Optimized Sensing Element – Sensitivity Aspect

The core of the microwave sensor is a DSRR (Fig. 5-3) that can be modeled as a parallel RLC (R: resistance, L: inductance, C: capacitance) with corresponding frequency of resonance at $f_{res} = 1/2\pi\sqrt{LC}$. Thus, it is evident that since the capacitance is a function of the effective permittivity of the surrounding medium, namely, $C = f(\varepsilon_{r\_eff})$, the changes in the resonant frequency depends on the relative variations of the medium.

The effort has been made to initially optimize the passive resonator sensitivity as a standalone component. This major is achieved in two steps: firstly, the sensing element is designed on a low $\varepsilon_r = 2.2$ of Rogers 5880 with $tan\delta = 0.0009$; secondly, the operating frequency is intended to be at higher frequency to have smaller resonant element for a given samples size, hence 5 GHz is chosen to be the

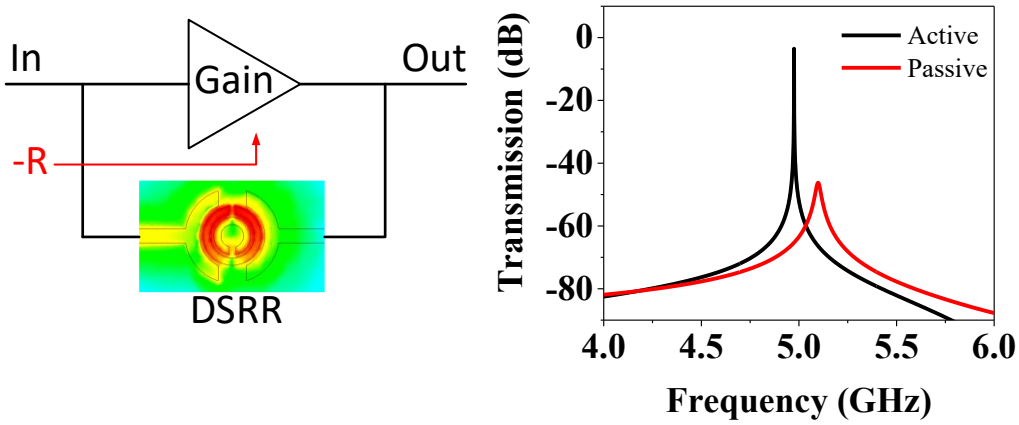

(a) (b)

Fig. 5-4, (a) Conceptual Active Resonator with loss-compensation schematic (b) Quality factor improvement in Active Resonator

highest frequency of active sensors ever (to the best of authors' knowledge). DSRR is then optimally designed with respect to the dimensions of gap, widths, and spacing between the rings to have highest sensitivity for any given sample.

5.3.2 Employing positive feedback loop

A positive feedback loop is assisting the passive resonator (Fig. 5-4(a)) to compensate for all sources of loss (dielectric loss, conductor loss, radiation, *etc.*). Fig. 5-4(b) shows that improvement in the quality factor as the main achievement of the positive feedback loop that can enhance the quality factor by orders of magnitude. This design constitutes the second stage shown in Fig. 5-1 as mixer. Similar design in one port configuration is utilized, with a gain high enough, to satisfy oscillating condition and utilized as our sensing source.

5.3.3 Double stage sensor:

Developed structure is comprised of two similar designs as presented in (Fig. 5-5(a)). The oscillating tone at the first stage is ~200 MHz different from that of

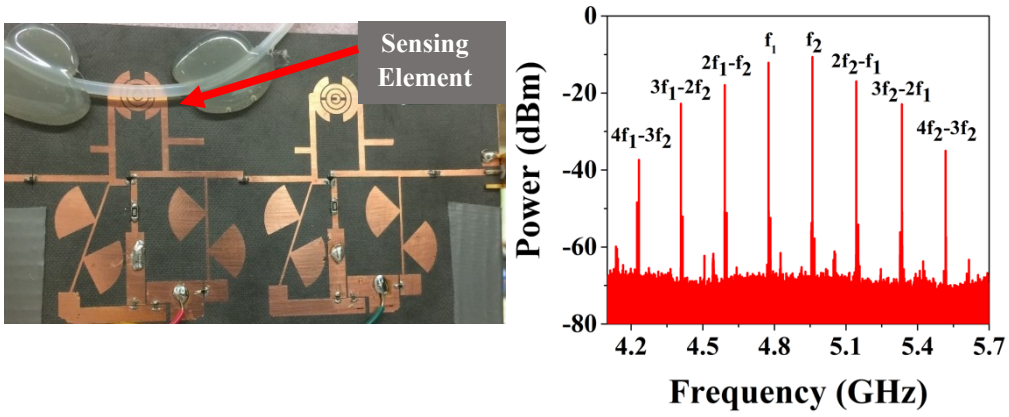

(a) (b)

Fig. 5-5, (a) Fabricated Sensor (b) IM products of f_1 and f_2 in spectrum analyzer

the second stage. The tones from the two stages are interacted at the transistor of 2nd stage. High power nature of the tones (f_1, f_2) helps efficient excitation of transistor for its nonlinear behavior, their IM (3rd, 5th, and 7th) [151]–[154] is shown in Fig. 5-5(b) measured by spectrum analyzer.

Wireless Communication in readout circuit- Amplification feature of the two stages in a regenerative feedback loop fashion, provides enough power for the exiting signal to be transmitted wirelessly, such that this availability at 5 GHz is preparing the sensor to join a larger network in a realm of IoT (Fig. 5-7(a)).

The antennas should be wideband to cover the frequency span of the 'variations in profile'. These features can be easily explored in a compact bowtie slot antenna (more information at [155]) that is shown in Fig. 5-7(b-c) with ultra-wideband fractional bandwidth of 60 %. The gain of the antenna is 6 dBi at 5 GHz (not shown for brevity). Linearity of this omnidirectional antenna in polarization is also investigated to confirm that it can be stablished in a way to prevent extraneous interference from environment.

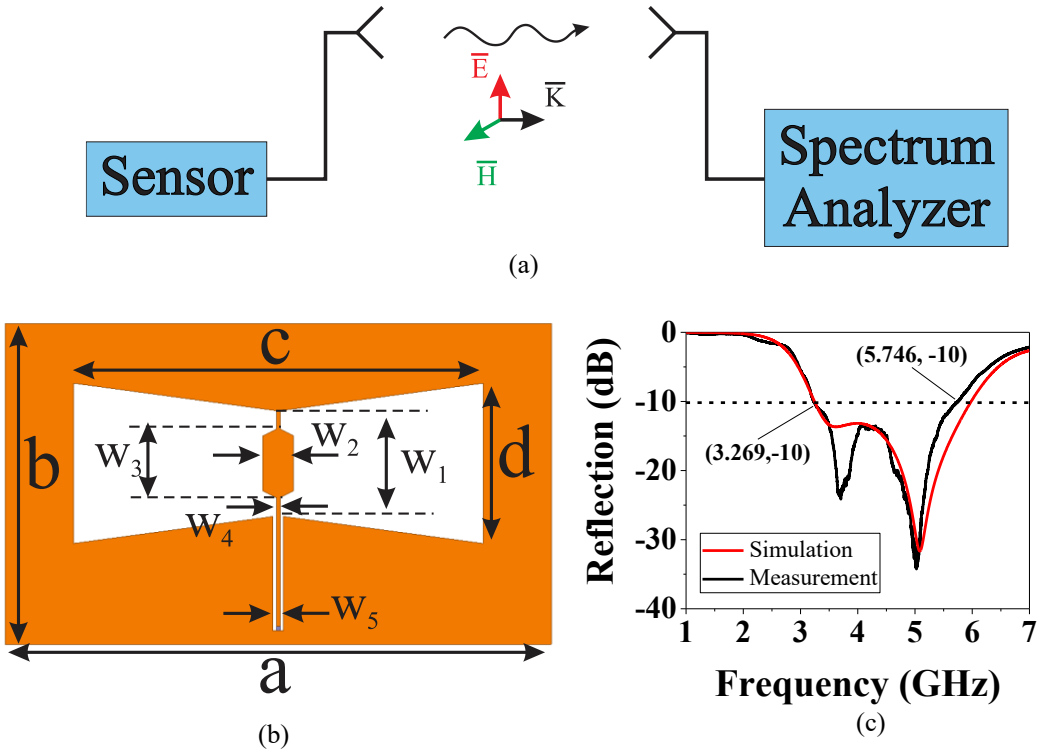

Fig. 5-6, (a)Wireless communication with antenna integration (b) bowtie slot antenna with dimensions in [mm]: a=50, b=30, c=38, d=12.8, w1=10, w2=3, w3=8.5, w4=0.35, w5=1 (c) simulated and measured reflection of bowtie slot

Liquid Sensing -The sensing setup for lossy liquids is obtained by integrating all of the abovementioned pivotal steps. A 1/8'' PTFE tube is placed over the gap of first DSRR (f_1) as sensitive region, allowing to liquid volumes, as small as 40 μL to be characterized in a microfluidic fashion Fig. 5-7(a). The resonant frequency of the sensor is recorded at the main frequency and its IM products, when exposed to Toluene, Methanol, IPA, and Water. The results are compared as shown in Fig. 5-7(b) that shows its compelling impact on sensitivity enhancement, where each IM component provides better sensitivity for higher orders $\_2\Delta f, 3\Delta f, 4\Delta f$ at 3rd, 5th, and 7th IM, respectively. Also, the noteworthy point is the readout stability at different IM products of Fig. 4-7(b). The time-based measurements over 1-min are

(a)

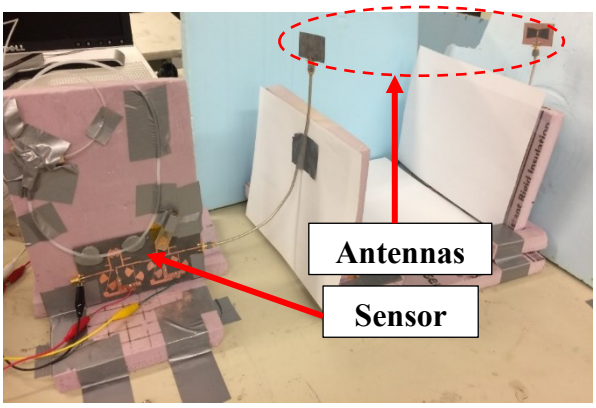

(b)

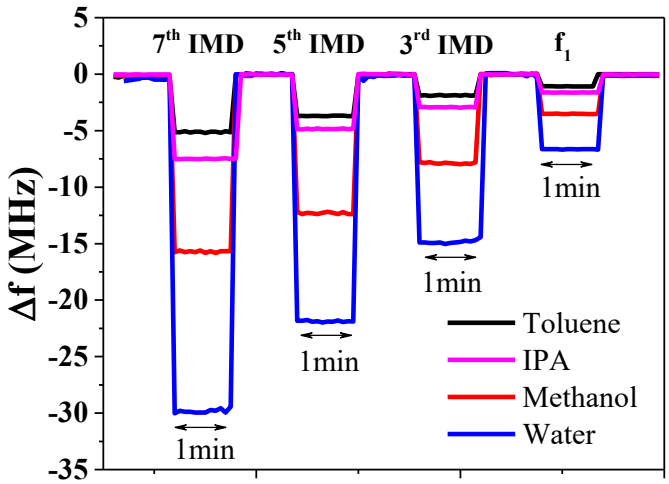

Fig. 5-7, (a) Measurement setup (b) Material characterization using 3rd, 5th, and 7th IM products, with improved sensitivity in each state

provided to prove the same stability of resultant 7th IM regardless of the enhanced sensitivity.

5.4 Conclusion

In this chapter, a unique technique is introduced to help increase the sensitivity in active sensors. Two-stages sensor with DSRRs as sensing elements combined with active feedback loops are cascaded (f_1, f_2) and their IM is exploited in a unique configuration. The higher-order IM products are shown to have significantly high sensitivity. Moreover, enough amplification of power in this setup allows for

wireless transmission of the data in readout section. Material characterization is shown over toluene, IPA, methanol, and water that 4-fold enhancement in sensitivity is achieved using 7^{th} IM product. This technique can also be employed in fine sensing applications such as biomedical and gas sensing that require very sensitive setup.

Chapter 6

Conclusions and Future Work

In this chapter, the main findings of the thesis are summarized and suggestions for future work are presented.

6.1 Thesis conclusions and contributions

This thesis started with the passive planar sensor for material characterization and its applications in industry as well as biomedical/pharmaceutical fields. The conclusions and contributions are as following:

Designing an ultra high Q resonator as sensing platform and illustrating its enabling application in highly sensitive measurement conditions on oil/sand industry in Chapter 3.

- Embedding two pairs of ultra-wideband slot bow-tie antenna for wireless communication of the sensor in active mode in Chapter 3.
- Developing single active resonator into “dual active resonator” and its application in removing the extraneous environmental impact such as humidity in sensing results in Chapter 4.
- Employing the ‘dual active resonator’ in a two-window solution for evaluating the dispersion coefficient of suspended solids in solvent liquids in Chapter 4.

- Developing the sensor into mixer design and incorporating the intermodulation products as the sensing signals with drastically enhanced sensitivity in Chapter 5.

6.2 Suggestions for future work

The suggestions for extending and modifying this research are as follows:

- In chapters 3, the design of highly stable sensor in time with low phase-noise for sensitive measurements
- In chapter 3, modifying the antenna size with no degradation in the performance, in terms of gain, and bandwidth.
- In chapter 4, employing the dual active resonator to be expanded into multi-resonator, a structure that each individual resonator could be devoted to separate MUT sensing.
- In chapter 4, employing the dual resonator using single transistor to have equal noise effect on the frequency instability of the sensor.
- In chapter 5, developing the IM products for highly stable mixers for extremely sensitive applications. Increasing the range of IM-order for higher sensitivity.
- In chapter 5, employing active resonator as the sensing element to improve frequency stability of the intermodulation products.
- Employing all of these ideas in IC-design and CMOS technology for highly integrated functionality without performance loss.

References

[1] M. Abdolrazzaghi, M. H. Zarifi, M. Daneshmand, and C. F. A. Floquet, "Contactless asphaltene solid particle deposition monitoring using active microwave resonators," in *SENSORS, 2016 IEEE*, 2016, pp. 1–3.

[2] M. Abdolrazzaghi, M. H. Zarifi, and M. Daneshmand, "Wireless Communication in Feedback-Assisted Active Sensors," *IEEE Sens. J.*, vol. 16, no. 22, pp. 8151–8157, Nov. 2016.

[3] *Remote Sensing Note*. Japan Association on Remote Sensing, 1993.

[4] K. Venugopalan and N. Agrawal, "Applications of Microwave Sensors in Medicines," in *World Congress on Medical Physics and Biomedical Engineering, September 7 - 12, 2009, Munich, Germany SE - 2*, vol. 25/11, O. Dössel and W. Schlegel, Eds. Springer Berlin Heidelberg, 2009, pp. 6–8.

[5] A. Sohrabi, P. M. Shaibani, M. H. Zarifi, M. Daneshmand, and T. Thundat, "A novel technique for rapid vapor detection using swelling polymer covered microstrip ring resonator," *IEEE MTT-S Int. Microw. Symp. Dig.*, pp. 1–4, 2014.

[6] J. Naqui, C. Damm, A. Wiens, R. Jakoby, L. Lijuan Su, and F. Martin, "Transmission lines loaded with pairs of magnetically coupled stepped impedance resonators (SIRs): Modeling and application to microwave sensors," in *2014 IEEE MTT-S International Microwave Symposium (IMS2014)*, 2014, pp. 1–4.

[7] J. Naqui, L. Su, J. Mata, and F. Martín, “Analysis of transmission lines loaded with pairs of coupled resonant elements and application to sensors,” *J. Magn. Magn. Mater.*, vol. 383, pp. 144–151, 2015.

[8] A. Ebrahimi, W. Withayachumnankul, S. F. Al-Sarawi, and D. Abbott, “Microwave microfluidic sensor for determination of glucose concentration in water,” in *Microwave Symposium (MMS), 2015 IEEE 15th Mediterranean*, 2015, pp. 1–3.

[9] Y. Zhao, Y. Li, B. Pan, S.-H. Kim, Z. Liu, M. M. Tentzeris, J. Papapolymerou, and M. G. Allen, “RF evanescent-mode cavity resonator for passive wireless sensor applications,” *Sensors Actuators A Phys.*, vol. 161, no. 1–2, pp. 322–328, Jun. 2010.

[10] S. Vashist, “A review of microcantilevers for sensing applications,” *J. Nanotechnol.*, vol. 3, no. June, pp. 1–15, 2007.

[11] M. Abdolrazzaghi, A. Abdolali, and S. Hashemy, “Improvements in DNA Biosensors Using Joint Split Ring Resonators Coupled with Thin Film Microstrip Line.,” *Appl. Comput. Electromagn. Soc. J.*, vol. 31, no. 2, pp. 126–131, 2016.

[12] M. Abdolrazzaghi and M. Daneshmand, “Enhanced Q double resonant active sensor for humidity and moisture effect elimination,” in *2016 IEEE MTT-S International Microwave Symposium (IMS)*, 2016, pp. 1–3.

[13] M. H. Zarifi, P. Shariaty, M. Abdolrazzaghi, Z. Hashisho, and M. Daneshmand, “Particle size characterization using a high resolution planar resonator sensor in a lossy medium,” *Sensors Actuators, B Chem.*, vol. 234,

2016.

[14] M. H. Zarifi, S. Farsinezhad, M. Abdolrazzaghi, M. Daneshmand, and K. Shankar, “Selective microwave sensors exploiting the interaction of analytes with trap states in TiO 2 nanotube arrays,” *Nanoscale*, vol. 8, no. 14, pp. 7466–7473, 2016.

[15] M. H. Zarifi, S. Farsinezhad, B. D. Wiltshire, M. Abdorrazaghi, Najia Mahdi, P. Kar, M. Daneshmand, and K. Shankar, “Effect of phosphonate monolayer adsorbate on the microwave photoresponse of TiO 2 nanotube membranes mounted on a planar double ring resonator,” *Nanotechnology*, vol. 27, no. 37, p. 375201, Sep. 2016.

[16] M. H. Zarifi, A. Mohammadpour, S. Farsinezhad, B. D. Wiltshire, M. Nosrati, A. M. Askar, M. Daneshmand, and K. Shankar, “Time-Resolved Microwave Photoconductivity (TRMC) Using Planar Microwave Resonators: Application to the Study of Long-Lived Charge Pairs in Photoexcited Titania Nanotube Arrays,” *J. Phys. Chem. C*, p. 150615093503007, Jun. 2015.

[17] H. Zangl, A. Fuchs, and T. Bretterklieber, “Non-invasive measurements of fluids by means of capacitive sensors,” *e i Elektrotechnik und Informationstechnik*, vol. 126, no. 1–2, pp. 8–12, Feb. 2009.

[18] B. Kumar, G. Rajita, and N. Mandal, “A Review on Capacitive-Type Sensor for Measurement of Height of Liquid Level,” *Meas. Control*, vol. 47, no. 7, pp. 219–224, Sep. 2014.

[19] L. Umar, “Smart level sensor based on thermal resistance measurement with

self calibration," in *2010 International Conference on Autonomous and Intelligent Systems, AIS 2010*, 2010, pp. 1–5.

[20] Q.-Y. Ren, L.-F. Wang, and Q.-A. Huang, "A New Method for Real-Time Measuring the Temperature-Dependent Dielectric Constant of the Silicone Oil," *IEEE Sens. J.*, vol. 16, no. 24, pp. 8792–8797, Dec. 2016.

[21] G. Galindo-Romera, F. Javier Herraiz-Martinez, M. Gil, J. J. Martinez-Martinez, and D. Segovia-Vargas, "Submersible Printed Split-Ring Resonator-Based Sensor for Thin-Film Detection and Permittivity Characterization," *IEEE Sens. J.*, vol. 16, no. 10, pp. 3587–3596, May 2016.

[22] M. Abdolrazzaghi, M. H. Zarifi, and M. Daneshmand, "Sensitivity enhancement of split ring resonator based liquid sensors," in *2016 IEEE SENSORS*, 2016.

[23] A. K. Jha and M. J. Akhtar, "SIW cavity based RF sensor for dielectric characterization of liquids," in *2014 IEEE Conference on Antenna Measurements & Applications (CAMA)*, 2014, pp. 1–4.

[24] A. W. Kraszewski and S. O. Nelson, "Resonant-cavity perturbation measurement for mass determination of the perturbing object," in *Conference Proceedings. 10th Anniversary. IMTC/94. Advanced Technologies in I & M. 1994 IEEE Instrumentation and Measurement Technolgy Conference (Cat. No.94CH3424-9)*, pp. 1261–1264.

[25] U. Raveendranath, J. Jacob, and K. T. Mathew, "Complex permittivity measurement of liquids with coaxial cavity resonators using a perturbation technique," *Electron. Lett.*, vol. 32, no. 11, p. 988, 1996.

[26] K. Loizou, E. Koutroulis, D. Zalikas, and G. Liontas, “A low-cost sensor based on Time-Domain Reflectometry for water level monitoring in environmental applications,” in *2015 IEEE 15th International Conference on Environment and Electrical Engineering (EEEIC)*, 2015, pp. 261–266.

[27] A. V Dormidontov and Y. V. Prokopenko, “Sensor for two-resonator refractometer,” in *2013 International Kharkov Symposium on Physics and Engineering of Microwaves, Millimeter and Submillimeter Waves*, 2013, pp. 543–545.

[28] C. P. Nemarich, “Time domain reflectometry liquid level sensors,” *IEEE Instrum. Meas. Mag.*, vol. 4, no. 4, pp. 40–44, 2001.

[29] Weixuan Jing, Fan Zhou, Lujia Chen, Zhuangde Jiang, Lingling Niu, Bing Wang, and Han Qi, “Characterization of Au ring microelectrode with cyclic voltammetry and AC impedance spectroscopy,” in *2013 IEEE International Symposium on Assembly and Manufacturing (ISAM)*, 2013, pp. 125–127.

[30] K. Tiwari, B. Tudu, R. Bandhopadhya, and A. Chatterjee, “Discrimination of monofloral honey using cyclic voltammetry,” in *2012 3rd National Conference on Emerging Trends and Applications in Computer Science*, 2012, pp. 132–136.

[31] B. C. Wadell, *Transmission line design handbook*. Artech House, 1991.

[32] J. Hinojosa, “S-parameter broad-band measurements on-microstrip and fast extraction of the substrate intrinsic properties,” *IEEE Microw. Wirel. Components Lett.*, vol. 11, no. 7, pp. 305–307, Jul. 2001.

[33] P. Queffelec, P. Gelin, J. Gieraltowski, and J. Loaec, “A microstrip device

for the broad band simultaneous measurement of complex permeability and permittivity," *IEEE Trans. Magn.*, vol. 30, no. 2, pp. 224–231, Mar. 1994.

[34] G. R. Facer, D. A. Notterman, and L. L. Sohn, "Dielectric spectroscopy for bioanalysis: From 40 Hz to 26.5 GHz in a microfabricated wave guide," *Appl. Phys. Lett.*, vol. 78, no. 7, pp. 996–998, Feb. 2001.

[35] A. Raj, W. S. Holmes, and S. R. Judah, "Wide bandwidth measurement of complex permittivity of liquids using coplanar lines," *IEEE Trans. Instrum. Meas.*, vol. 50, no. 4, pp. 905–909, 2001.

[36] S. S. Stuchly and C. E. Bassey, "Microwave coplanar sensors for dielectric measurements," *Meas. Sci. Technol.*, vol. 9, no. 8, pp. 1324–1329, Aug. 1998.

[37] U. Raveendranath, S. Bijukumar, and K. T. Mathew, "Broadband coaxial cavity resonator for complex permittivity measurements of liquids," *IEEE Trans. Instrum. Meas.*, vol. 49, no. 6, pp. 1305–1312, 2000.

[38] R. A. Waldron, "Perturbation theory of resonant cavities," *Proc. IEE Part C Monogr.*, vol. 107, no. 12, p. 272, 1960.

[39] A. W. Kraszewski and S. O. Nelson, "Observations on resonant cavity perturbation by dielectric objects," *ARS Repr. Collect.*, 1992.

[40] N. Haase and A. F. Jacob, "Substrate-Integrated Half-Mode Resonant Near-Field Sensor for Liquid Characterization," *Eur. Microw. Conf.*, pp. 310–313, 2013.

[41] K. Saeed, R. D. Pollard, and I. C. Hunter, "Substrate Integrated Waveguide Cavity Resonators for Complex Permittivity Characterization of Materials,"

IEEE Trans. Microw. Theory Tech., vol. 56, no. 10, pp. 2340–2347, Oct. 2008.

[42] V. V. Varadan, R. D. Hollinger, D. K. Ghodgaonkar, and V. K. Varadan, "Free-space, broadband measurements of high-temperature, complex dielectric properties at microwave frequencies," *IEEE Trans. Instrum. Meas.*, vol. 40, no. 5, pp. 842–846, 1991.

[43] G. Ekinci, A. D. Yalcinkaya, G. Dundar, and H. Torun, "Split-Ring Resonator-Based Strain Sensor on Flexible Substrates for Glaucoma Detection," *J. Phys. Conf. Ser.*, vol. 757, no. 1, p. 12019, Oct. 2016.

[44] X.-C. Zhu, W. Hong, K. Wu, H.-J. Tang, Z.-C. Hao, and H.-X. Zhou, "Characterization of substrate material using complementary split ring resonators at terahertz frequencies," in *2013 IEEE International Wireless Symposium (IWS)*, 2013, pp. 1–4.

[45] B. Wang, J. Long, and K. H. Teo, "Multi-Channel Capacitive Sensor Arrays," *Sensors*, vol. 16, no. 2, p. 150, 2016.

[46] K. Grenier, D. Dubuc, P.-E. Poleni, M. Kumemura, H. Toshiyoshi, T. Fujii, and H. Fujita, "Integrated Broadband Microwave and Microfluidic Sensor Dedicated to Bioengineering," *IEEE Trans. Microw. Theory Tech.*, vol. 57, no. 12, pp. 3246–3253, Dec. 2009.

[47] A. K. Horestani, C. Fumeaux, S. F. Al-Sarawi, and D. Abbott, "Displacement Sensor Based on Diamond-Shaped Tapered Split Ring Resonator," *IEEE Sens. J.*, vol. 13, no. 4, pp. 1153–1160, Apr. 2013.

[48] A. Ebrahimi, W. Withayachumnankul, S. Al-Sarawi, and D. Abbott, "High-

Sensitivity Metamaterial-Inspired Sensor for Microfluidic Dielectric Characterization," *IEEE Sens. J.*, vol. 14, no. 5, pp. 1345–1351, May 2014.

[49] H.-J. Lee, H.-S. Lee, K.-H. Yoo, and J.-G. Yook, "DNA sensing using split-ring resonator alone at microwave regime," *J. Appl. Phys.*, vol. 108, no. 1, p. 14908, 2010.

[50] H.-J. Lee, J.-H. Lee, S. Choi, I.-S. Jang, J.-S. Choi, and H.-I. Jung, "Asymmetric split-ring resonator-based biosensor for detection of label-free stress biomarkers," *Appl. Phys. Lett.*, vol. 103, no. 5, p. 53702, 2013.

[51] H.-J. Lee, J.-H. Lee, and H.-I. Jung, "A symmetric metamaterial element-based RF biosensor for rapid and label-free detection," *Appl. Phys. Lett.*, vol. 99, no. 16, p. 163703, 2011.

[52] D. J. Rowe, S. Al-Malki, A. A. Abduljabar, A. Porch, D. A. Barrow, and C. J. Allender, "Improved Split-Ring Resonator for Microfluidic Sensing," *IEEE Trans. Microw. Theory Tech.*, vol. 62, no. 3, pp. 689–699, Mar. 2014.

[53] B. Kapilevich and B. Litvak, "Optimized Microwave Sensor for Online Concentration Measurements of Binary Liquid Mixtures," *IEEE Sens. J.*, vol. 11, no. 10, pp. 2611–2616, Oct. 2011.

[54] C.-S. Lee and C.-L. Yang, "Thickness and Permittivity Measurement in Multi-Layered Dielectric Structures Using Complementary Split-Ring Resonators," *IEEE Sens. J.*, vol. 14, no. 3, pp. 695–700, Mar. 2014.

[55] M. S. Boybay and O. M. Ramahi, "Material Characterization Using Complementary Split-Ring Resonators," *IEEE Trans. Instrum. Meas.*, pp. 1–9, 2012.

[56] J. Naqui, “On the Symmetry Properties of Resonator-Loaded Transmission Lines,” in *Symmetry Properties in Transmission Lines Loaded with Electrically Small Resonators*, Springer, 2016, pp. 73–124.

[57] G. Biffi Gentili, G. Avitabile, M. Cerretelli, C. Riminesi, and N. Sottani, “Microwave permittivity measurements through cross-shaped ring sensors,” in *2nd ISA/IEEE Sensors for Industry Conference,* pp. 208–211.

[58] E. Fratticcioli, M. Dionigi, and R. Sorrentino, “A Simple and Low-Cost Measurement System for the Complex Permittivity Characterization of Materials,” *IEEE Trans. Instrum. Meas.*, vol. 53, no. 4, pp. 1071–1077, Aug. 2004.

[59] E. Fratticcioli, M. Dionigi, and R. Sorrentino, “A planar resonant sensor for the complex permittivity characterization of materials,” in *IEEE MTT-S International Microwave Symposium Digest (Cat. No.02CH37278)*, 2002.

[60] J. Skulski and B. A. Galwas, “Planar resonator sensor for moisture measurements,” in *12th International Conference on Microwaves and Radar. MIKON-98. Conference Proceedings (IEEE Cat. No.98EX195)*, 1998.

[61] K. Saeed, M. F., M. B., and I. C., “Planar Microwave Sensors for Complex Permittivity Characterization of Materials and Their Applications,” in *Applied Measurement Systems*, InTech, 2012.

[62] J. Abdulnour, C. Akyel, and Ke Wu, “A generic approach for permittivity measurement of dielectric materials using a discontinuity in a rectangular waveguide or a microstrip line,” *IEEE Trans. Microw. Theory Tech.*, vol. 43,

no. 5, pp. 1060–1066, May 1995.

[63] N. Meyne, C. Cammin, and A. F. Jacob, “Accuracy enhancement of a split-ring resonator liquid sensor using dielectric resonator coupling,” in *2014 20th International Conference on Microwaves, Radar and Wireless Communications (MIKON)*, 2014.

[64] U. Schwerthoeffer, R. Weigel, and D. Kissinger, *Microwave Conference (GeMIC), 2014 German : date 10-12 March 2014.* Aachen, Germany: VDE, 2014.

[65] A. A. Abduljabar, D. J. Rowe, A. Porch, and D. A. Barrow, “Novel Microwave Microfluidic Sensor Using a Microstrip Split-Ring Resonator,” *IEEE Trans. Microw. Theory Tech.*, vol. 62, no. 3, pp. 679–688, Mar. 2014.

[66] T. Chretiennot, D. Dubuc, and K. Grenier, “A Microwave and Microfluidic Planar Resonator for Efficient and Accurate Complex Permittivity Characterization of Aqueous Solutions,” *IEEE Trans. Microw. Theory Tech.*, vol. 61, no. 2, pp. 972–978, Feb. 2013.

[67] P. A. Bernard and J. M. Gautray, “Measurement of dielectric constant using a microstrip ring resonator,” *IEEE Trans. Microw. Theory Tech.*, vol. 39, no. 3, pp. 592–595, Mar. 1991.

[68] M. Bogosanovich, “Microstrip patch sensor for measurement of the permittivity of homogeneous dielectric materials,” *IEEE Trans. Instrum. Meas.*, vol. 49, no. 5, pp. 1144–1148, 2000.

[69] M. H. Zarifi, T. Thundat, and M. Daneshmand, “High resolution microwave microstrip resonator for sensing applications,” *Sensors Actuators A Phys.*,

vol. 233, pp. 224–230, 2015.

[70] M. Abdolrazzaghi, M. H. Zarifi, W. Pedrycz, and M. Daneshmand, “Robust Ultra-High Resolution Microwave Planar Sensor Using Fuzzy Neural Network Approach,” *IEEE Sens. J.*, vol. 17, no. 2, pp. 323–332, 2017.

[71] M. Abdolrazzaghi, M. H. Zarifi, and M. Daneshmand, “Sensitivity enhancement of split ring resonator based liquid sensors,” in *SENSORS, 2016 IEEE*, 2016.

[72] E. H. Armstrong, “Some recent developments in the audion receiver,” *Proc. IEEE*, vol. 51, no. 8, pp. 1083–1097, 1963.

[73] R. Boudot and E. Rubiola, “Phase noise in RF and microwave amplifiers,” *IEEE Trans. Ultrason. Ferroelectr. Freq. Control*, vol. 59, no. 12, pp. 2613–2624, Dec. 2012.

[74] M. Abdolrazzaghi, M; Zarifi, M. .; Floquet, C. F.; Daneshmand, “Contactless Asphaltene Solid Particle Deposition Monitoring Using Active Microwave Resonators,” in *IEEE Sensors Conference*, 2016.

[75] M. H. Zarifi, M. Fayaz, J. Goldthorp, M. Abdolrazzaghi, Z. Hashisho, and M. Daneshmand, “Microbead-assisted high resolution microwave planar ring resonator for organic-vapor sensing,” *Appl. Phys. Lett.*, vol. 106, no. 6, p. 62903, Feb. 2015.

[76] M. H. Zarifi and M. Daneshmand, “Liquid sensing in aquatic environment using high quality planar microwave resonator,” *Sensors Actuators B Chem.*, vol. 225, pp. 517–521, 2016.

[77] M. H. Zarifi and M. Daneshmand, “Non-contact liquid sensing using high

resolution microwave microstrip resonator," in *2015 IEEE MTT-S International Microwave Symposium*, 2015, pp. 1–4.

[78] M. H. Zarifi, A. Mohammadpour, S. Farsinezhad, B. D. Wiltshire, M. Nosrati, A. M. Askar, M. Daneshmand, and K. Shankar, "Time-Resolved Microwave Photoconductivity (TRMC) Using Planar Microwave Resonators: Application to the Study of Long-Lived Charge Pairs in Photoexcited Titania Nanotube Arrays," *J. Phys. Chem. C*, p. 150615093503007, Jun. 2015.

[79] M.-F. Joubert, S. A. Kazanskii, Y. Guyot, J.-C. Gâcon, and C. Pédrini, "Microwave study of photoconductivity induced by laser pulses in rare-earth-doped dielectric crystals," *Phys. Rev. B*, vol. 69, no. 16, p. 165217, Apr. 2004.

[80] M. H. Zarifi, P. Shariaty, M. Abdolrazzaghi, Z. Hashisho, and M. Daneshmand, "Particle size characterization using a high resolution planar resonator sensor in a lossy medium," *Sensors Actuators B Chem.*, vol. 234, pp. 332–337, 2016.

[81] M. H. Zarifi, P. Shariaty, Z. Hashisho, and M. Daneshmand, "A non-contact microwave sensor for monitoring the interaction of zeolite 13X with CO 2 and CH 4 in gaseous streams," *Sensors Actuators B Chem.*, vol. 238, pp. 1240–1247, Jan. 2017.

[82] W. N. Frenier, M. Ziauddin, and R. Venkatesan, *Organic Deposits in Oil and Gas Production*. .

[83] E. Y. Sheu, "Petroleum AsphalteneProperties, Characterization, and Issues,"

Energy & Fuels, vol. 16, no. 1, pp. 74–82, Jan. 2002.

[84] A. D.-12 S. T. M. for D. of A. (Heptane I. in C. P. and Petroleum, "ASTM D6560," *ASTM Int. West Conshohocken, PA,* 2012.

[85] A. K. M. Jamaluddin, J. Creek, C. S. Kabir, J. D. McFadden, D. D'Cruz, M. T. Joseph, N. Joshi, and B. Ross, "A Comparison of Various Laboratory Techniques to Measure Thermodynamic Asphaltene Instability," in *SPE Asia Pacific Improved Oil Recovery Conference*, 2001.

[86] Y. Ruiz-Morales, X. Wu, and O. C. Mullins, "Electronic absorption edge of crude oils and asphaltenes analyzed by molecular orbital calculations with optical spectroscopy," *Energy & fuels*, vol. 21, no. 2, pp. 944–952, 2007.

[87] O. C. Mullins, S. S. Betancourt, M. E. Cribbs, F. X. Dubost, J. L. Creek, A. B. Andrews, and L. Venkataramanan, "The colloidal structure of crude oil and the structure of oil reservoirs," *Energy & Fuels*, vol. 21, no. 5, pp. 2785–2794, 2007.

[88] M.-J. T. M. Ching, A. E. Pomerantz, A. B. Andrews, P. Dryden, R. Schroeder, O. C. Mullins, and C. Harrison, "On the nanofiltration of asphaltene solutions, crude oils, and emulsions," *Energy & Fuels*, vol. 24, no. 9, pp. 5028–5037, 2010.

[89] M. H. Schneider, V. J. Sieben, A. M. Kharrat, and F. Mostowfi, "Measurement of Asphaltenes Using Optical Spectroscopy on a Microfluidic Platform," *Anal. Chem.*, vol. 85, no. 10, pp. 5153–5160, May 2013.

[90] M. Schueler, C. Mandel, M. Puentes, and R. Jakoby, "Metamaterial Inspired Microwave Sensors," *IEEE Microw. Mag.*, vol. 13, no. 2, pp. 57–68, Mar.

2012.

[91] A. P. Gregory and R. N. Clarke, “A review of RF and microwave techniques for dielectric measurements on polar liquids,” *IEEE Trans. Dielectr. Electr. Insul.*, vol. 13, no. 4, pp. 727–743, Aug. 2006.

[92] K. Staszek, A. Rydosz, E. Maciak, K. Wincza, and S. Gruszczynski, “Six-port microwave system for volatile organic compounds detection,” *Sensors Actuators B Chem.*, 2017.

[93] A. Rydosz, E. Maciak, K. Wincza, and S. Gruszczynski, “Microwave-based sensors with phthalocyanine films for acetone, ethanol and methanol detection,” *Sensors Actuators B Chem.*, vol. 237, pp. 876–886, 2016.

[94] W. Withayachumnankul, K. Jaruwongrungsee, A. Tuantranont, C. Fumeaux, and D. Abbott, “Metamaterial-based microfluidic sensor for dielectric characterization,” *Sensors Actuators A Phys.*, vol. 189, pp. 233–237, 2013.

[95] A. A. Abduljabar, D. J. Rowe, A. Porch, and D. A. Barrow, “Novel Microwave Microfluidic Sensor Using a Microstrip Split-Ring Resonator,” *IEEE Trans. Microw. Theory Tech.*, vol. 62, no. 3, pp. 679–688, Mar. 2014.

[96] A. Abduljabar, X. Xin Yang, D. Barrow, and A. Porch, “Microstrip split ring resonator for microsphere detection and characterization,” in *2015 IEEE MTT-S International Microwave Symposium*, 2015, pp. 1–4.

[97] J. Naqui and F. Martin, “Transmission Lines Loaded With Bisymmetric Resonators and Their Application to Angular Displacement and Velocity Sensors,” *IEEE Trans. Microw. Theory Tech.*, vol. 61, no. 12, pp. 4700–4713, Dec. 2013.

[98] I. Rusni, A. Ismail, A. Alhawari, M. Hamidon, and N. Yusof, “An Aligned-Gap and Centered-Gap Rectangular Multiple Split Ring Resonator for Dielectric Sensing Applications,” *Sensors*, vol. 14, no. 7, pp. 13134–13148, Jul. 2014.

[99] H.-J. Lee, H.-S. Lee, K.-H. Yoo, and J.-G. Yook, “DNA sensing using split-ring resonator alone at microwave regime,” *J. Appl. Phys.*, vol. 108, no. 1, p. 14908, Jul. 2010.

[100] A. K. Horestani, C. Fumeaux, S. F. Al-Sarawi, and D. Abbott, “Displacement Sensor Based on Diamond-Shaped Tapered Split Ring Resonator,” *IEEE Sens. J.*, vol. 13, no. 4, pp. 1153–1160, Apr. 2013.

[101] G. Galindo-Romera, F. Javier Herraiz-Martinez, M. Gil, J. J. Martinez-Martinez, and D. Segovia-Vargas, “Submersible Printed Split-Ring Resonator-Based Sensor for Thin-Film Detection and Permittivity Characterization,” *IEEE Sens. J.*, vol. 16, no. 10, pp. 3587–3596, May 2016.

[102] M. S. Boybay and O. M. Ramahi, “Material Characterization Using Complementary Split-Ring Resonators,” *IEEE Trans. Instrum. Meas.*, vol. 61, no. 11, pp. 3039–3046, Nov. 2012.

[103] C.-S. Lee and C.-L. Yang, “Thickness and Permittivity Measurement in Multi-Layered Dielectric Structures Using Complementary Split-Ring Resonators,” *IEEE Sens. J.*, vol. 14, no. 3, pp. 695–700, Mar. 2014.

[104] R. 2016 ANSOFT HFSS® Academic Research, “ANSOFT HFSS® Academic Research, Release 2016.” .

[105] I. N. Evdokimov and A. P. Losev, “Electrical conductivity and dielectric

properties of solid asphaltenes," *Energy and Fuels*, vol. 24, no. 7, p. 3959, 2010.

[106] "National Instruments Website.," *http://www.ni.com/labview/*. [Online]. Available: http://www.ni.com/labview/.

[107] M. L. Jiménez, F. J. Arroyo, J. van Turnhout, and A. V Delgado, "Analysis of the dielectric permittivity of suspensions by means of the logarithmic derivative of its real part.," *J. Colloid Interface Sci.*, vol. 249, no. 2, pp. 327–35, May 2002.

[108] L. Goual and A. Firoozabadi, "Measuring asphaltenes and resins, and dipole moment in petroleum fluids," *AIChE J.*, vol. 48, no. 11, pp. 2646–2663, Nov. 2002.

[109] M. V. Gandhi and B. D. Thompson, *Smart Materials and Structures*. CRC Press (Jan. 1 1998), 1998.

[110] F. P. Lees, *Some Data on the Failure Modes of Instruments in the Chemical Plant Environment*. The Chemical Engineer, 1973.

[111] A. Parker, "Chemical Sensor Is All Wires, No Batteries," *Sci. Technol. Rev.*, 2012.

[112] M. F. Acevedo, *Real-Time Environmental Monitoring: Sensors and Systems*. CRC Press, 2015.

[113] C. M. Pereira, M. S. Mattice, and R. C. Testa, "<title>Intelligent sensing and wireless communications in harsh environments</title>," 2000, pp. 194–203.

[114] L.-Y. G. W. Hunter, P. G. Neudeck, G. M. Beheim, and G. E. Ponchak,

Chen, “HIGH TEMPERATURE WIRELESS COMMUNICATION AND ELECTRONICS FOR HARSH ENVIRONMENT APPLICATIONS.”

[115] “PID Technology.” [Online]. Available: http://www.crowcon.com/uk/products/portables/gas-pro-pid.html.

[116] “Wireless Digital Humidity and Temperature Monitor.” [Online]. Available: https://www.lowes.ca/acurite_m13334.html.

[117] “Soil Moisture Sensor.” [Online]. Available: http://www.delta-t.co.uk/product-display.asp?id=ML3 Product&div=Soil Science.

[118] C. A. Opperman and G. P. Hancke, “Near Field Communication in Smart Sensing Applications.”

[119] E. Strömmer, M. Hillukkala, and A. Ylisaukko-oja, “Wireless Sensor and Actor Networks: IFIP WG 6.8 First International Conference on Wireless Sensor and Actor Networks, WSAN’07, Albacete, Spain, September 24--26, 2007,” L. Orozco-Barbosa, T. Olivares, R. Casado, and A. Bermúdez, Eds. Boston, MA: Springer US, 2007, pp. 131–142.

[120] Yu-De Lin and Syh-Nan Tsai, “Coplanar waveguide-fed uniplanar bow-tie antenna,” *IEEE Trans. Antennas Propag.*, vol. 45, no. 2, pp. 305–306, 1997.

[121] E. A. Soliman, S. Brebels, P. Delmotte, G. A. E. Vandenbosch, and E. Beyne, “Bow-tie slot antenna fed by CPW,” *Electron. Lett.*, vol. 35, no. 7, p. 514, 1999.

[122] W. Wiesbeck, G. Adamiuk, and C. Sturm, “Basic Properties and Design Principles of UWB Antennas,” *Proc. IEEE*, vol. 97, no. 2, pp. 372–385, Feb. 2009.

[123] L. A. Berge, M. T. Reich, and B. D. Braaten, “A compact dual-band bow-tie slot antenna for 900-MHz and 2400-MHz ISM bands,” *Antennas Wirel. Propag. Lett. IEEE*, vol. 10, pp. 1385–1388, 2011.

[124] C. A. Balanis, *Antenna Theory: Analysis and Design*. Wiley, 2016.

[125] A. K. Horestani, C. Fumeaux, S. F. Al-Sarawi, and D. Abbott, “Split Ring Resonators With Tapered Strip Width for Wider Bandwidth and Enhanced Resonance,” *IEEE Microw. Wirel. Components Lett.*, vol. 22, no. 9, pp. 450–452, Sep. 2012.

[126] J. M. Choi and T. W. Kim, “Humidity Sensor Using an Air Capacitor,” *Trans. Electr. Electron. Mater.*, vol. 14, no. 4, pp. 182–186, Aug. 2013.

[127] C. Liu, L. Zhang, J. Peng, C. Srinivasakannan, B. Liu, H. Xia, J. Zhou, and L. Xu, “Temperature and moisture dependence of the dielectric properties of silica sand.,” *J. Microw. Power Electromagn. Energy*, vol. 47, no. 3, pp. 199–209, 2013.

[128] M. H. Zarifi, M. Rahimi, M. Daneshmand, and T. Thundat, “Microwave ring resonator-based non-contact interface sensor for oil sands applications,” *Sensors Actuators B Chem.*, vol. 224, pp. 632–639, Mar. 2016.

[129] M. H. Zarifi, S. Farsinezhad, K. Shankar, and M. Daneshmand, “Liquid Sensing Using Active Feedback Assisted Planar Microwave Resonator,” *IEEE Microw. Wirel. Components Lett.*, vol. 25, no. 9, pp. 621–623, Sep. 2015.

[130] M. Abdolrazzaghi and M. Daneshmand, “Dual Active Resonator for Dispersion Coefficient Measurement of Asphaltene Nano-Particles,” *IEEE*

Sens. J., pp. 1–1, 2017.

[131] H. A. Scheraga and L. Mandelkern, "Consideration of the Hydrodynamic Properties of Proteins [1,2]," *J. Am. Chem. Soc.*, vol. 75, no. 1, pp. 179–184, Jan. 1953.

[132] R. E. Baltus and J. L. Andersen, "Comparison of g.p.c. elution characteristics and diffusion coefficients of asphaltenes," *Fuel*, vol. 63, no. 4, pp. 530–535, Apr. 1984.

[133] V. J. Wargadalam, K. Norinaga, and M. Iino, "Size and shape of a coal asphaltene studied by viscosity and diffusion coefficient measurements," *Fuel*, vol. 81, no. 11–12, pp. 1403–1407, Jul. 2002.

[134] K. J. Leontaritis and G. A. Mansoori, "Asphaltene Flocculation During Oil Production and Processing: A Thermodynamic Collodial Model," in *SPE International Symposium on Oilfield Chemistry*, 1987.

[135] D. Lesueur, "The colloidal structure of bitumen: Consequences on the rheology and on the mechanisms of bitumen modification," *Adv. Colloid Interface Sci.*, vol. 145, no. 1–2, pp. 42–82, Jan. 2009.

[136] K. Rajagopal and S. M. C. Silva, "An experimental study of asphaltene particle sizes in n-heptane-toluene mixtures by light scattering," *Brazilian J. Chem. Eng.*, vol. 21, no. 4, pp. 601–609, Dec. 2004.

[137] H. G. and and O. C. Mullins*, "Molecular Size and Structure of Asphaltenes from Various Sources," 2000.

[138] M. A. Anisimov, I. K. Yudin, V. Nikitin, G. Nikolaenko, A. Chernoutsan, H. Toulhoat, D. Frot, and Y. Briolant, "Asphaltene Aggregation in

Hydrocarbon Solutions Studied by Photon Correlation Spectroscopy," *J. Phys. Chem.*, vol. 99, no. 23, pp. 9576–9580, Jun. 1995.

[139] J.-A. Östlund, M. Nydén, I. H. Auflem, and J. Sjöblom, "Interactions between Asphaltenes and Naphthenic Acids," *Energy & Fuels*, vol. 17, no. 1, pp. 113–119, Jan. 2003.

[140] E. Durand, M. Clemancey, J.-M. Lancelin, J. Verstraete, D. Espinat, and A.-A. Quoineaud, "Aggregation States of Asphaltenes: Evidence of Two Chemical Behaviors by ^{1}H Diffusion-Ordered Spectroscopy Nuclear Magnetic Resonance," *J. Phys. Chem. C*, vol. 113, no. 36, pp. 16266–16276, Sep. 2009.

[141] D. M. Pozar, "Microwave Engineering 3e." Wiley Interscience, 2005.

[142] M. S. Bello, R. Rezzonico, and P. G. Righetti, "Use of Taylor-Aris Dispersion for Measurement of a Solute Diffusion Coefficient in Thin Capillaries," *Science (80-.).*, vol. 266, no. 5186, pp. 773–776, Nov. 1994.

[143] M. L. Jiménez, F. J. Arroyo, J. Van Turnhout, and A. V Delgado, "Analysis of the dielectric permittivity of suspensions by means of the logarithmic derivative of its real part," *J. Colloid Interface Sci.*, vol. 249, no. 2, pp. 327–335, 2002.

[144] J. G. Kirkwood, "The Dielectric Polarization of Polar Liquids," *J. Chem. Phys.*, vol. 7, no. 10, pp. 911–919, Oct. 1939.

[145] J. Wyman, "Polarization and Dielectric Constant of Liquids," *J. Am. Chem. Soc.*, vol. 58, no. 8, pp. 1482–1486, Aug. 1936.

[146] G. OSTER, "The dielectric properties of liquid mixtures.," *J. Am. Chem.*

Soc., vol. 68, no. 10, pp. 2036–41, Oct. 1946.

[147] A. A. Maryott and F. Buckley, *Table of dielectric constants and electric dipole moments of substances in the gaseous state*, vol. 537. US Department of Commerce, National Bureau of Standards, 1953.

[148] G. Taylor, "Conditions under Which Dispersion of a Solute in a Stream of Solvent can be Used to Measure Molecular Diffusion," *Proc. R. Soc. A Math. Phys. Eng. Sci.*, vol. 225, no. 1163, pp. 473–477, Sep. 1954.

[149] K. K. Joshi and R. D. Pollard, "Sensitivity analysis and experimental investigation of microstrip resonator technique for the in-process moisture/permittivity measurement of petrochemicals and emulsions of crude oil and water," in *Microwave Symposium Digest, 2006. IEEE MTT-S International*, 2006.

[150] M. Nick and A. Mortazawi, "Low Phase-Noise Planar Oscillators Based on Low-Noise Active Resonators," *IEEE Transactions on Microwave Theory and Techniques*, vol. 58, no. 5. pp. 1133–1139, 2010.

[151] J. L. Bohorquez, A. P. Chandrakasan, and J. L. Dawson, "Frequency-Domain Analysis of Super-Regenerative Amplifiers," *IEEE Trans. Microw. Theory Tech.*, vol. 57, no. 12, pp. 2882–2894, Dec. 2009.

[152] E. A. Keehr and A. Hajimiri, "Successive Regeneration and Adaptive Cancellation of Higher Order Intermodulation Products in RF Receivers," *IEEE Trans. Microw. Theory Tech.*, vol. 59, no. 5, pp. 1379–1396, May 2011.

[153] F. X. Moncunill-Geniz, P. Pala-Schonwalder, and O. Mas-Casals, "A

generic approach to the theory of superregenerative reception," *IEEE Trans. Circuits Syst. I Regul. Pap.*, vol. 52, no. 1, pp. 54–70, Jan. 2005.

[154] A. Tang and M.-C. F. Chang, "Inter-Modulated Regenerative CMOS Receivers Operating at 349 and 495 GHz for THz Imaging Applications," *IEEE Trans. Terahertz Sci. Technol.*, vol. 3, no. 2, pp. 134–140, Mar. 2013.

[155] L. A. Berge, M. T. Reich, and B. D. Braaten, "A compact dual-band bow-tie slot antenna for 900-MHz and 2400-MHz ISM bands," *Antennas Wirel. Propag. Lett. IEEE*, vol. 10, pp. 1385–1388, 2011.

[156] P. Atkins and J. De Paula, *Physical Chemistry*, 8th ed. Oxford, 2006.

[157] "https://en.wikipedia.org/wiki/Radio_receiver." .

[158] M. Nick, "New Q-Enhanced Planar Resonators for Low Phase-Noise Radio Frequency Oscillators," 2011.

Appendix A Diffusion Coefficient

Theoretical Extraction

The diffusibility of any solute-in-solvent system is inversely related to the diffusion coefficient of the solute. The dispersion can be represented based on time elapsed during disposition of the solute in the flow as follows [142]:

$$\frac{dC}{dt} = k\frac{d^2C}{dx^2} \tag{19}$$

where C is the solute concentration across the capillary diameter, and k is the dispersion coefficient, which is related to diffusion coefficient (D) as follows:

$$k = \frac{r^2u^2}{48D} + D \tag{20}$$

where r is the capillary radius and u is the mean speed of the fluid flow.

The hydrodynamic radius (R_h) of Asphaltene molecules can be determined using the following inverse relationship by Stokes' law [156]:

$$\boldsymbol{R_h = \frac{k_B T}{6\pi\eta D}} \tag{21}$$

where $k_B, T,$ and η are Boltzmann constant ($1.38e^{-23}$ [$m^2kgs^{-2}K^{-1}$]), temperature, and the solvent viscosity, respectively.

The concentration profile in time (t) and location (x) dependent form can be expressed as:

$$C \propto C_0\sqrt{\frac{t_0}{t}}e^{-\frac{u^2(t-t_0)^2}{4kt}} \propto C_0 e^{-\frac{(t-t_0)^2}{2\,\sigma^2}} \tag{22}$$

where $t_0 = x/u$ is the resident time (the time of peak/dip in Gaussian profile) and k can be evaluated as:

$$\boldsymbol{k = \frac{u^2\sigma^2}{2t_0}} \tag{23}$$

The assumption in the Eq. (23) is the infinitesimally small inclusion of the solute at $x=0$ and $t=0$. In order to avoid the complexities of approximating the initial status, the evolution of the dispersion along the capillary is exploited with monitoring two points as shown in Fig. 4-6, which leads to a set of data as $\{t_1, \sigma_1\}$ and $\{t_2, \sigma_2\}$. The dispersion coefficient then can be calculated from a two-window solution as follows:

$$\boldsymbol{k = \frac{u^2\sigma_1^2}{2t_1} = \frac{u^2\sigma_2^2}{2t_2} = \frac{u^2(\sigma_2^2 - \sigma_2^2)}{2(t_2 - t_1)}} \tag{24}$$

Therefore, the sensing is all about determining the spread of the solute inclusion over time that is done using dual microwave planar resonators in this work.

Appendix B Publication List (As of September 2017)

Patent:

U.S. Provisional Patent Application Serial No. 62/514,233

Title: A Method of Using Intermodulation Products for Sensitivity Enhancement of Microwave Sensors,

Inventors: **Abdolrazzaghi, M.**, Daneshmand, M.

Journal Papers:

1. **Abdolrazzaghi, M.**, *et. al. (tentative)*, "Multi-material level sensing", Under Preparation
2. **Abdolrazzaghi, M.**, *et. al. (tentative)*, "pH sensing using open complementary split ring resonator based sensor in microwave regime", Under Preparation.
3. **Abdolrazzaghi, M.**, Daneshmand, M., "Intermodulation Product technique on drastically sensitivity enhancement" Under Preparation
4. Zarifi, M., **Abdolrazzaghi, M.**, Abbasi, Z., Daneshmand, M., "Flow meter in microwave frequencies using active resonators", Under Preparation
5. **Abdolrazzaghi, M.**, Daneshmand, M., Iyer. A. K., "Strongly Enhanced Sensitivity in Planar Microwave Sensors Based on Metamaterial coupling", July 2017, Submitted to IEEE Transactions on Microwave Theory and Techniques

6. **Abdolrazzaghi, M.**, Daneshmand, M. "Dual Active Resonator for Dispersion Coefficient Measurement of Asphaltene Nano-Particles", In Press, Invited Paper to Special Issue of IEEE sensors Journal
7. **Abdolrazzaghi, M.**, Zarifi, M. H., Floquet, C. F. A, and Daneshmand, M. "Contactless Asphaltene Detection Using an Active Planar Microwave Resonator Sensor", Energy Fuels, 2017, Just Accepted Manuscript, DOI: 10.1021.
8. **Abdolrazzaghi, M.**, Zarifi, M. H., Daneshmand, M., "High Resolution Wireless Chemical Sensing Using Microwave Active Resonator" in IEEE Sensors Journal, 2016, vol.PP, no.99, pp.1-1
9. **Abdolrazzaghi, M.**, M. H. Zarifi; W. Pedrycz; M. Daneshmand, "Fault-Tolerant Ultra-High Resolution Microwave Planar Sensor using Fuzzy Neural Network Approach," in IEEE Sensors Journal , vol.PP, no.99, pp.1-1
10. Zarifi M. H., Sameir Deif, **Abdolrazzaghi, M.**, C. Bertie, R. Dennis, Amyotte, M., Vahabisani N., Zaher. H., Chen. W., and Daneshmand. M., "A Microwave Ring Resonator Sensor for Early Detection of Breaches in Pipeline Coatings", IEEE Transactions on Industrial Electronics (2017)
11. Zarifi, MH., Gholidoost A, **Abdolrazzaghi, M**., Shariaty, P., Hashisho, Z., and Daneshmand, M. "Sensitivity enhancement in planar microwave active-resonator using metal organic framework for CO 2 detection." Sensors and Actuators B: Chemical (2017).
12. Fayaz, M. ; Zarifi, M. H.; **Abdolrazzaghi, M.** ; Shariaty, P.; Hashisho, Z.; Daneshmand, M., "A Novel Technique to Determine the Adsorption Capacity and Breakthrough Time of Adsorbents Using a Non-contact High Resolution Microwave Resonator Sensor" Environmental Science Technology 2017 51 (1), 427-435

13. Zarifi, M. H., Farsinezhad, S., **Abdolrazzaghi, M.**, Daneshmand, M., Shankar, K. (2016). "Selective microwave sensors exploiting the interaction of analytes with trap states in TiO 2 nanotube arrays". Nanoscale, 8(14), 7466-7473.
14. Zarifi, M. H., Shariaty, P., **Abdolrazzaghi, M.**, Hashisho, Z., Daneshmand, M. (2016). "Particle size characterization using a high resolution planar resonator sensor in a lossy medium". Sensors and Actuators B: Chemical, 234, 332-337.
15. Zarifi, M. H., Fayaz, M., Goldthorp, J., **Abdolrazzaghi, M.**, Hashisho, Z., Daneshmand, M. (2015). "Microbead-assisted high resolution microwave planar ring resonator for organic-vapor sensing". Applied Physics Letters, 106(6), 062903.
16. Zarifi, M. H., Farsinezhad, S., Wiltshire, B. D., **Abdorrazaghi, M.**, Mahdi, N., Kar, P., Daneshmand, M. Shankar, K. (2016). "Effect of phosphonate monolayer adsorbate on the microwave photoresponse of TiO2 nanotube membranes mounted on a planar double ring resonator". Nanotechnology, 27(37), 375201.13)

Conference Papers:

1. **Abdolrazzaghi, M.**, Daneshmand, M., “Compelling Impact of Intermodulation Products of Regenerative Active Resonators on Sensitivity" Accepted in IMS 2017, Honolulu, Hawaii
2. **Abdolrazzaghi, M.**, Daneshmand, M. (2016, May). "Enhanced Q double resonant active sensor for humidity and moisture effect elimination". In 2016 IEEE MTT-S International Microwave Symposium (IMS) (pp. 1-3). IEEE. Invited for Best Student Competition

3. **Abdolrazzaghi. M.**, Zarifi, M. H., Daneshmand. M., "Sensitivity enhancement of split ring resonator based liquid sensors." In SENSORS, 2016 IEEE, pp. 1-3. IEEE, 2016
4. **Abdolrazzaghi. M.**, Zarifi. M. H., Floquet C. F., Daneshmand. M., "Contactless Asphaltene Solid Particle Deposition Monitoring Using Active Microwave Resonators" In SENSORS, 2016 IEEE, pp. 1-3. IEEE, 2016. Invited for Best Student Competition.
5. **Abdolrazzaghi, M.**, Abdolali, A., Daneshmand, M. (2015, July). "Highly sensitive miniaturized bio-sensor using 2-layer double split ring resonators". In 2015 IEEE International Symposium on Antennas and Propagation USNC/URSI National Radio Science Meeting (pp. 736-737). IEEE.
6. Sharafadinzadeh. N., **Abdolrazzaghi. M.**, and Daneshmand. M., "Highly Sensitive Microwave Split Ring Resonator Sensor Using Gap Extension for Glucose Sensing," accepted in IEEE-MTTs International Microwave Workshop Series on Advanced Materials and Process (IMWS-AMP), Sept. 2017